Probing the mechanisms of substrate selectivity of VcINDY, the model divalent anion symporter (DASS) transporter

Cristina Fàbregas Bellavista

KENT ID: 1990288

A thesis submitted to the Biosciences School of the University of Kent

MSc-Research in Cell Biology

December 2020

Supervisor: Christopher Mulligan

University of **Kent**

DECLARATION

No part of this thesis has been submitted in support of an application for any degree or qualification of the University of Kent or, any other University or Institute of learning.

Cristina Fàbregas

December 2020

ACKNOWLEDGMENTS

Firstly, I would like to thank my supervisor Dr. Christopher Mulligan for his continued guidance and support throughout this project. I would also like to acknowledge my laboratory colleagues for their help in the laboratory, and teaching me their previous expertise, with gratitude.

Finally, I would like to thank my family for their support and to bring me the opportunity to study abroad and carry out this Master of Research.

CONTENTS

CHAPTER 1: INTRODUCTION

CHAPTER 2: MATERIALS AND METHODS

CHAPTER 3: RESULTS

CHAPTER 4: DISCUSSION

- **DASS:** Divalent Anion/Sodium Symporter.

- **NaC:** Na^+-carboxylate co-transporters.

- **NaDC1:** Na^+-dependent Dicarboxylate symporter1.

- **NaDC3:** Na^+-dependent Dicarboxylate symporter3.

- **NaCT:** Na^+-dependent Citrate Transporter.

- **NaS:** Na^+-sulphate co-transporters.

- **NaS1:** Na^+-dependent Sulphate symporter1.

- **NaS2:** Na^+-dependent Sulphate symporter2.

- **INDY:** I'm Not Dead Yet.

- **VcINDY:** *Vibrio Cholerae* I'm Not Dead Yet (a divalent anion/sodium symporter from *Vibrio cholerae*).

- **LaINDY:** *Lactobacillus acidophilus* I'm Not Dead Yet (a divalent anion/sodium co-transporter from *Lactobacillus acidophilus*).

- **DrINDY:** *Drosophila Melanogaster* I'm Not Dead Yet (a divalent anion/sodium symporter from *Drosophila Melanogaster*).

- **Gltp$_{th}$:** Glutamate transporter from *Pyrococcus horikoshii.*

- **Gltp$_{tk}$:** Glutamate transporter from *Thermococcus kodakarensis.*

- **SdcS:** Sodium-dependent dicarboxylate transporter from *Staphylococcus aureus*

- **DDM:** n-dodecyl-β-D-maltoside.

- **CPM:** CPM (7-Diethylamino-3-(4'-Maleimidylphenyl)-4-Methylcoumarin).

- **OFS:** outward-facing state (conformation of the transporter with the binding-site facing the extracellular medium).

- **IFS:** inward-facing state (conformation of the transporter with the binding-site facing the cytosolic medium).

ABSTRACT

DASS transporters can behold accountant for their metabolic regulation relevance in many species. Alterations of DASS transporters affect fat storage, energy balance and lifespan. Hence, DASS proteins have been identified as a potential therapeutic target, especially members of the human family SLC13. Here, by using VcINDY (*I'm not dead yet*) from *Vibrio cholerae* as a model for DASS transporters, we have investigated the relevance of specific amino acids to explain DASS transport mechanism, substrate binding and, cation binding events.

By measuring ligand-protein interactions with a thermostability-based approach, our data provide a better understating of VcINDY preference for C4-dicarboxylate and a promising idea of binding-site related amino acids roles in the notification of VcINDY's apo state. The interplay of oligomerization and scaffold residues in substrate binding has been revealed accordingly to the elevator-type mechanism of VcINDY for the first time, while the importance of amino acids involved in the conserved SNT family motif has been further corroborated in the ligand's chain-length filter. Besides, sodium binding has been identified as a requisite for allowing substrate binding. There seems to exist a role of cation binding forces in readjusting essential amino acid positions for a suitable substrate-binding site. Finally, differences in substrate selectivity due to the binding of Li^+ and Na^+ have been identified.

CHAPTER 1: INTRODUCTION

1.1. INTRODUCTION TO THE DASS PROTEINS

1.1.1. SECONDARY ACTIVE TRANSPORTERS

Biological membranes can be impermeable to some molecules and ions relevant to cell survival. The essential process of transporting these important solutes across biological membranes is carried out by protein transporters (Bosshart and Fotiadis, 2019).

In bacteria, these transporters can be classified into primary active transporters, channels, or secondary transporters. Secondary transporters can be uniporters, symporters, or antiporters (Bosshart and Fotiadis, 2019). The last two are characterised as being active transporters, which means they couple the movement of a specific solute using other molecules' existent electrochemical gradient. Another characteristic of secondary active transporters is their structure; Secondary transporters have shown to own some structural folding in their structure. The presence of disconnected transmembrane helices (TM) and pseudo-symmetries are common hallmarks on them (Shi, 2013).

These related folds in structure allow secondary transporters to acquire different conformations necessary to transport substrates throughout membranes. Therefore, a minimum of two distinguished conformation states is required for a protein to follow an alternating-access mechanism, consisting of two conformations changing over modulating substrate accessibility to one side of the other of the membrane (Jardetzky, 1966)(Bosshart and Fotiadis, 2019).

To date, there are three different types of altering-access transport mechanisms described according to crystal structures. The first is the rocker-switch mechanism, where two domains of the protein move against each other, allowing access to the binding site to both cytoplasm and extracellular medium (Yan, 2013)(Karpowich, N. K. *et al.*, 2008). Another type is called the rocking-bundle mechanism in which one domain shifts against the other (Forrest and Rudnick, 2010). Finally, the last one is the elevator mechanism.

This mechanism has been more recently identified in the glutamate-transporter homolog Glt_{Ph} and suggested for VcINDY (Drew and Boudker, 2016)(Mulligan et al., 2016). In both transporters, substrates are carried vertically across the membrane bound to a mobile domain, which is at the same time anchored at a fixed domain into the membrane, acting as a lift.

VcINDY belongs to the divalent anion/Na^+ symporter (DASS) family, which is included in the Ion Transporter (IT) superfamily (Prakash *et al.*, 2003). It has been suggested that members of these families could use an elevator-type mechanism, as some proteins from both families share similar architecture, such as AbgT with VcINDY (Vergara-jaque *et al.*, 2012). However, phylogenetic studies of IT and DASS proteins have shown huge and sequence diverse families found in all domains of life (Chen et al., 2011). Hence, despite the potential probability of a widespread elevator-type mechanism among IT and DASS members, more studies are necessary since mammalian homologs of the characterised VcINDY could have therapeutic potential (Bergeron *et al.*, 2013)(Colas *et al.*, 2016).

1.1.2. COMPREHENSIVE TRANSPORT OF DASS PROTEINS

Members from the DASS family are conserved from bacteria to humans. The reason behind its ubiquitous expression is found in its functional relevance (Pajor, 1999). Hence, DASS transporters have been preserved in highly active metabolic locations (Lu, 2019)(Pajor, 1999). Prokaryotic proteins from bacteria are found in cytoplasmatic membranes, whereas, in vertebrate species, these proteins are found in an array of essential tissues and organs (Bergeron *et al.*, 2013).

In general, DASS transporters couple the free energy generated from an electrochemical Na^+ or H^+ gradient to transport organic anions against its concentration gradient (Markovich, 2012) (Pajor, 2014) (Prakash *et al.*, 2003). Bacterial DASS uptake two or more Na^+ ions to transport C_4-dicarboxylates and eukaryotic mammal proteins co-transport sulphates or Krebs cycle intermediates together with two, three or more Na^+ ions (Pajor, 1999). The stoichiometry of the cation-anion coupling ratio experimentally determined is, on average, 3:1. Thus, one positive charge is transferred across the cell membrane per cycle, considering the solutes are commonly divalent (Bergeron *et al.*, 2013).

Almost all members share an electrogenic and Na^+-dependent transport mechanism. However, some members of invertebrate species, such as the fruit fly, are Na^+-independent (Inoue *et al.*, 2002). There are likewise divergences in kinetic properties and substrate selectivity since these transporters have widespread substrate specificities. Studies in isolated cells and membrane vesicles of close relatives showed a disparity of functional traits when observing substrate affinity, substrate specificity, and sensitivity to lithium inhibition (*Table 1.0*)(Pajor, 1999).

FUNCTIONAL CHARACTERISTICS OF DASS FAMILY MEMBERS

Protein	Substrate	Substrate Km	Strong Transport inhibitors	Counterion identification	Electrogenic transport	References
VcINDY	Succinate	1 uM	Malate Fumarate Oxaloacetate Tricarballylate	Na$^+$ Li$^+$	Yes	(Mulligan *et al.,* 2014)
DrINDY	Succinate Citrate Pyruvate	Succinate: ~40 uM Citrate: 105 uM	a-KG Fumarate Glutarate Citrate	*Cation independent*	No	(Knauf *et al.,* 2002) (Inoue, 2002)
SdcS	Succinate divalent succinate Fumarate Malate	Succinate: 12 ± 1.9 uM Divalent succinate: 6.6 ± 0.75 uM Malate: 8.1 ± 0.4 uM Fumarate: 15 ± 0.54 uM	Fumarate Malate Oxaloacetate	Na+ Li$^+$	No	(Hall et al., 2005-2007) (Pajor *et al.,* 2007) (Pajor *et al.,* 2013),
SdcF	Succinate a-KG	Succinate: 8 ± 1 uM	Malate Fumarate Tartrate Oxaloacetate Aspartate	Na+ Li$^+$	No	(Pajor et al., 2013)
SdcL	Succinate Fumarate Malat	Succiante: 5.2 uM Malate: 6.4 uM	Oxaloacetate aspartate a-KG	Na$^+$	-	(Strickler,2009)
rNaS1	Sulfate Thiosulfate Selenate	Sulfate: 93 ± 30 uM Selenate: 580 ± 90 uM Thiosulfate: 84 ± 9 uM	-	Na$^+$	Yes	(Busch, 1994)
rNaS2	Sulfate	380 ± 10 uM (sulfate)	Selenate Thiosulfate Phosphate Oxalate	Na$^+$	Yes	(Dawson, 2005)
rNaDC1	Succinate Citrate Fumarate Malate a-KG oxaloacetate	Succinate: 640 ± 10 uM	-	Na$^+$ K$^+$ *Li$^+$ can inhibit transport.*	Yes	(Chen, 1998),
rNaDC3	Succinate	2 ± 0.1 uM	Fumarate Malate a-KG Citrate Aspartate	Na$^+$ Li$^+$	Yes	(Kekuda, 1999)
rNaCT	Succinate Pyruvate Citrate (pH 7 optimum)	Citrate: 18 ± 4 uM	Succinate Malate Fumarate a-KG	Na$^+$	Yes	(Inoue, 2002).

Table 1.0: **Summarized functional variances within relative DASS transporters**.

Table representing DASS transporters differences in substrate affinity, substrate specificity and cation dependence. Overall, DASS transporters can carry organic dicarboxylates of the Krebs cycle, sulfate and phosphate. To date, a few related proteins have been characterised throughout different studies. The best characterised are summarized here. Information taken from different papers (see references column).

1.1.3. A COMMON MARK TO MOST DASS TRANSPORTERS

The overall architecture of the proteins is likely conserved (Lu, 2019). As a case in point, the number of transmembrane helixes (TMs) in the SLC13 family is between 8 and 13 when observed by hydropathy and similarity plots (Markovich *et al.*, 2004). There is also some conservation in the length of the N-terminal and C-terminal regions but in a lower manner (Markovich, 2012).

Variation is found when comparing protein sequences. However, amino acids in critical positions for transport and substrate-binding seem to maintain their similarity among members (Mancusso et al., 2012). Especially, three amino acids, Serine-Asparagine-Threonine (SNT), located in the protein's binding site, have been found reasonably conserved over many species (*Figure 1.1*). They are described to create the SNT motif, which seems to be crucial for substrate transport specificity (Mancusso *et al.*, 2012).

Among INDY homologue proteins from various species, this motif is more preserved at the N-terminal (HP1) than the C-terminal (HP2), as represented in *Figure 1.1* (Vergara-jaque et al., 2012). The visible variation is always on the 3rd amino acid, wherein some species present an Alanine, Valine or Proline instead of Threonine (SNT/A/V/P).
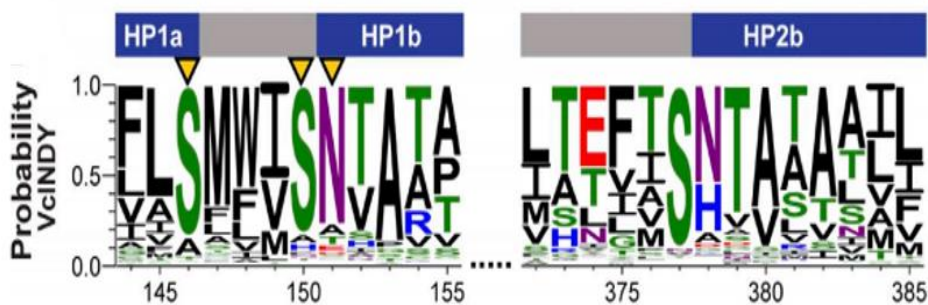
***Figure 1.1:* Sequence logo of key motifs in homologues of VcINDY.**

Image from a multiple sequence alignment of homologs of VcINDY. The positions of the most conserved amino acids in the bacterial protein are N151, T152 and S150. Secondary structures are indicated by colours: blue (helix) and grey (loops). Interestingly, around the binding site amino acids' characteristics are conserved since the same chemical properties pattern has been seen for the amino acid in respective positions among homologues of INDY. Residues involve in sodium binding are marked with yellow triangles. Taken and adapted from (Vergara-jaque *et al.*, 2012).

1.2. SLC13 MAMMALIAN FAMILY

1.2.1. A SMALL FAMILY INSIDE DASS TRANSPORTERS

The mammalian proteins are grouped into one small family. Proteins encoded from the SLC13 gene are 572 to 627 amino acids long. In humans, this family is known as the SLC13 gene family. SLC13 only consists of five sodium-coupled transporters SLC13A1 (NaS1), SLC13A2 (NaDC1), SLC13A3 (NaDC3), SLC13A4 (NaS2), SLC13A5 (NaCT). They are all membrane proteins of 8-13 transmembrane domains (TMDs)(Markovich *et al.*, 2004). They share approximately 40-50% identical protein sequences (Markovich *et al.*, 2004).

Due to different anions substrate specificities, two groups of SLC13 transporters can be outlined: Na^+-sulphate (NaS) co-transporters, with a tetra-oxyanions preference (sulfate, selenate and thiosulfate) and, Na^+-carboxylate (NaC) cotrans-porters with a preference for C_4-dicarboxylate or C_6-tricarboxylate Krebs cycle intermediates (Bergeron *et al.*, 2013).

1.2.2. PHYSIOLOGICAL ROLES AND RELEVANCE OF SLC13

TRANSPORTERS

NaS transporters uptake inorganic sulfate from the circulation. They participate in the regulation of sulfate conjugation of various molecules in the placenta, kidney and intestine (Birkenfeld *et al.*, 2011). The loss of NaS1 certainly disturbs sulfate homeostasis by causing hyposulfatemia. The KO mouse for this gene (mNaS1) displays different phenotypes ranging from reduced detoxification capacity to altered gastrointestinal function and spontaneous seizures. It also

reduces fertility and postnatal growth (Dawson, Steane and Markovich, 2005)(Lee *et al.*, 2007)(Markovich and Aronson, 2007)(Markovich, 2012). NaS2 is expressed at the placenta, where it possibly facilitates sulfate transference from the mother to the fetus (Girard *et al.*, 1999). It has also been found in the brain, heart, thymus, liver and tonsils, where its role has yet to be determined (Birkenfeld *et al.*, 2011).

NaC transporters are equally important for their physiological role. They are mainly located in the kidney to prevent stone formation (Bergeron et al., 2013). NaDC1 is the main contributor to the Krebs cycle intermediates absorbency in the proximal tubule (up to 65%) and the intestine. Therefore, the mNaDC1 mouse knockout (KO) gene shows increased urinary excretion of different compounds due to kidney failure re-absorption (Ho *et al.*, 2007).

The mRNA of NaDC3 is present in the brain, kidney, placenta, pancreas, eye and optic nerve, where it participates in regulating the oxidative metabolism (Inoue et al., 2002)(Markovich *et al.*, 2004). NaDC3 also contributes to the synthesis of cholesterol and fatty acids in hepatocytes and neurons (Chen *et al.*, 1999). It is believed that NaDC3 has a role in the regulation of cellular senescence, hypertension and type-2 diabetes (Simino *et al.*, 2011)(Langefeld *et al.*, 2008)(Kallo, 2014).

Finally, NaCT is involved in energetic metabolic pathways, and it is mainly found in the liver. It participates in the absorption of cytosolic citrate across the plasma membrane. NaCT transports citrate for mitochondrial Krebs cycle, fatty acid synthesis, cholesterol synthesis, gluconeogenesis and glycolysis (Bergeron *et al.*,

2013). NaCT transporters' expression has become of high interest since the disruption of NaCT activity in liver cancer cells ceases their proliferation (Li *et al.*, 2017).

1.3. DISCOVERY OF THE LONGEVITY GENE

1.3.1. GENE KNOCK-OUT STUDIES

Orthologues of NaCT with similar physiological relevance have been reported in prokaryotes and eukaryotes (Lu, 2019). In 2000, a longevity study using adult *Drosophila melanogaster* identified mutations in a gene resulting in a phenotype resembling caloric restriction without reducing food intake. These mutations resulted in a doubling of the mean lifespan duration of the fly (*Figure 1.2-A*) (Rogina and Helfand, 2013). In another model organism, *Caenorhabditis elegans,* deletion of the gene homolog ceNAC-2 concluded in the same outcome (*Figure 1.2-B*) (Fei *et al.*, 2004).
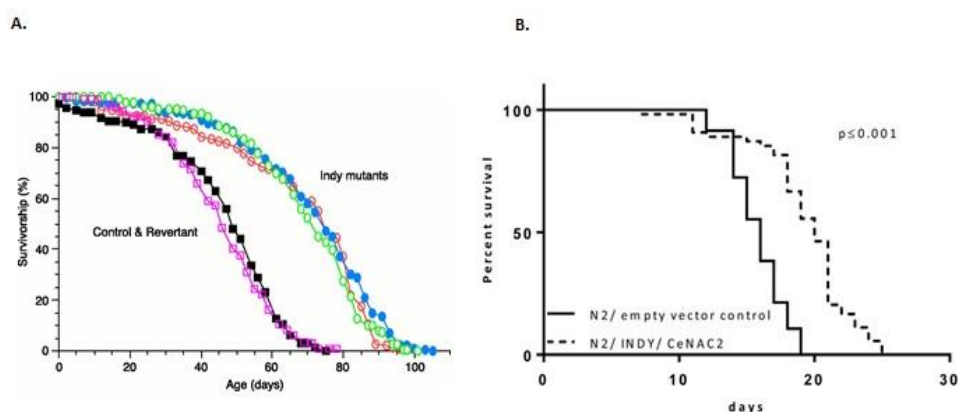
Figure 1.2: **Indy Knockdown effect in longevity.**

Increase in both scenarios of the organisms' lifespan when INDY is knockdown. **A)** Survival curve of Indy knockdown mutant vs wild type *Drosophila melanogaster*. Taken from (Rogina and Helfand, 2013) **B)** Survival curve of N2 (*wt*) grown *C. elegans* fed *E. coli* harbouring an empty vector control vs INDY/CeNAC2 siRNA. Taken from (Fei *et al.*, 2004).

To date, several lines of evidence suggest that decreased *indy* gene expression extends the lifespan of various eukaryotes (Knauf *et al.*, 2006). As a result, SLC13A5/NaCT is known by *I'm Not Dead Yet* (INDY)(Willmes *et al.*, 2018).

The mammalian mouse gene (mINDY), which encodes for sodium–dicarboxylate co-transporter, has also been studied. Thus, knockout of the m*indy* gene mimics caloric restriction and protects against age-related insulin resistance and adiposity when fed with a high-fat diet (Birkenfeld *et al.*, 2011). Unique phenotypes of reduced lipid synthesis and elevated lipid oxidation rates were shown when whole KO mouse models were fed with fats compared to controls. Thus, it has been suggested that the nutritional state mediates mINDY's transcriptional regulation throughout epigenetic mechanisms (Willmes and Birkenfeld, 2013).

1.3.2. LIABILITY OF A PROMISING THERAPEUTIC APPROACH

As seen above, DASS proteins can be accounted for their relevance in metabolic regulation in light of their psychopathological effects when alteration of DASS function is present. Specifically, considering the beneficial effects of reducing INDY's transport activity has on metabolism and longevity, INDY has been highlighted as a potential therapeutic target (Kekuda *et al.*, 1999)(Pajor, 2006). Studies ranging from prokaryotes and lower organisms to mammals proved that reducing INDY expression could help treat metabolic disease and age-related diseases (Willmes *et al.*, 2018). In fact, it has been argued that mINDY could have therapeutic potential in humans for the treatment of kidney stones, neurological disorders, type II diabetes, non-alcoholic fatty liver disease (NAFLD) and obesity (Birkenfeld *et al.*, 2011).

Yet only a few chemical compounds with the ability to inhibit mINDY/NaCT transport have been reported. Most of the inhibitors found so far exhibit poor ADME (absorption, distribution, metabolism, excretion) properties *in vivo* experiments. Two compounds named 2 and 4a were described as possible pharmacological inhibitors for mINDY/NaCT with low-affinity (*Supplementary Figure 6.1.1*). However, their inhibition effect is dependent on the absence of citrate and the protein conformational state (Willmes *et al.*, 2018).

1.4. I'M NOT DEAD YET FROM *Vibrio Cholerae*

1.4.1. THE CRYSTAL STRUCTURES OF A DASS TRANSPORTER

Bacterial SLC13 homologs can be overexpressed and purified easily to cast new light on the potential function and structure of SLC13 family members. VcINDY, a homolog of the mammalian SLC13 transporters, has brought some information of relevance to light regarding this advantage.

VcINDY is a sodium-succinate secondary active transporter from *Vibrio cholerae*. Until very recently, VcINDY was the only member of the DASS family from which high-resolution crystal structures were published (Mancusso *et al.*, 2012)(Nie *et al.*, 2017)(Sauer *et al.*, 2020).

DASS members present a related secondary protein structure to VcINDY, which could indicate a common elevator-type transport mechanism in the DASS family (Mulligan et al., 2014). Besides, VcINDY shares 36–38 % amino acid sequence identity with human SLC13 transporters (Schlessinger *et al.*, 2014)(Colas, Schlessinger and Pajor, 2017). Consequently, VcINDY can fully act as a structural model for the DASS family as shown by DASS proteins sequence alignment with

VcINDY *(Figure 1.3)*. In the same alignment, the positions of the amino acids selected for this study are marked to attain a better structural comprehension of each residue within the family. The relevance of some mutated residues for they key position in the transporter's structure is discussed in Chapter 4, according to the results found.

(Figure continues on next page)

Figure 1.3: **Amino acid sequence alignment of VcINDY and its homologues.**
Secondary structures of the protein from the knowledge of the 2012 Crystal structure are marked above the sequence alignment. The SNT motifs are marked in dots, the second and third dots from the HPin are N151 and T152. Other amino acids described in this project are pointed out with arrows: red (D319), light blue (I96), light green (F100), brown (V66), orange (T67), dark green (S290), yellow (S200), dark blue (V322) pink (F326) and purple (T421).

1.4.2. THE MOLECULAR STRUCTURE OF VcINDY

The molecular structure of VcINDY was reported in 2012 for the first time in high-resolution. This crystal structure (PDB 4F35) had a 3.2 Å resolution of the transporter with the substrate facing the cytoplasm, which is known to be the inward-facing conformation of the protein (Mancusso et al., 2012). It also revealed the homodimeric transporter architecture together with one sodium ion bound and one citrate-bound molecule. Thus, only one Na+-binding site was observed, so the second sodium binding-site was just predicted without successful structural evidence (Mancusso et al., 2012).

On account of the moderate structural evidence found on the 3.2 Å structure, a second crystal X-ray of VcINDY was reported in 2017 at a resolution of 2.8 Å (*Figure 1.4*). This current structure (PDB 5UL7) showed succinate bound to VcINDY and a second Na^+-binding site as predicted (Nie *et al.*, 2017).
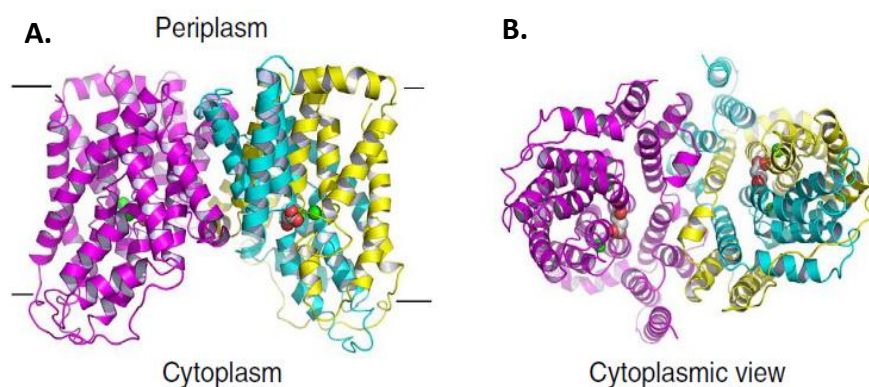
Figure 1.4: **The 2.8 Å crystal structure of VcINDY.**

A) View of the protein from the plasma membrane plane in the inward-face conformation. **B)** View of the protein from the top. In both representations, one protomer is coloured magenta and the other blue and yellow. The structure allows observation of the Na^+ ions (green) bound to the protein and succinate is represented by red spheres. Taken from (Nie et al., 2017)

VcINDY is a homodimeric protein consisting of 462 amino acids and 11 transmembrane helices (TM1-TM11) in each protomer. The N- terminal consists of TM2 to TM6 and it is found in the cytosol, while C-terminal, formed by TM7-TM11, is in the extracellular space. The two chain ends, N- and C-terminal, share approximately 26% amino acid sequence identity (Mancusso *et al.*, 2012). The protein shape from the membrane plane resembles an "M" with a concave aqueous depression that reaches the membrane's midpoint. Transmembrane alfa-helixes TM4, TM5, TM9 and TM10 are segmented into two or even three divisions (Mancusso *et al.*, 2012). These divisions allow secondary structural regions to play dominant mechanical roles in transport (Mulligan *et al.*, 2016).

1.4.2.1. Secondary structural structures in VcINDY

The H4c domain forms an interfacial helix, which is related to the other H9c interfacial helix in the VcINDY structure (Mancusso *et al.*, 2012). One recent study pointed out the importance of positive charge distribution in the H4c domain on SLC13 transporters (Khamasyi *et al.,* 2020). Positively charged amino acids from H4c seem the interact with hydrophobic residues of HPin, allowing the movement of HPin during transport while H4c stays motionless. Moreover, some particular amino acids in H4c are suggested to participate in protein-protein interactions. All together gives H4c, and perhaps H9c, control of the cellular metabolite transport (Khamasyi *et al.,* 2020).

Besides the two interfacial helices (H4c and H9c), further secondary structures are the intra-helical loops generated as a result of the TM5 and TM10 fragments. The loops connect in the middle of the membrane heading to the depression towards the cytoplasm (*Figure 1.5*) (Nie *et al.*, 2017).
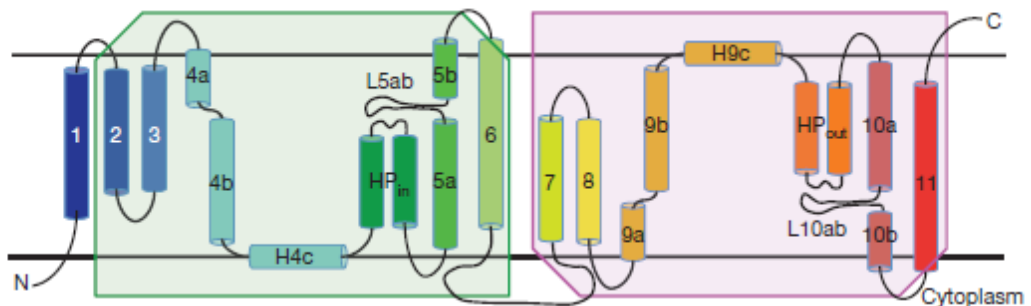
***Figure 1.5*: VcINDY protein scheme of one protomer.**

VcINDY protomer owns 11 α -transmembranes. Transmembrane alfa-helixes TM4, TM5, TM9 and TM10 are segmented. The loops 5a-b and 10a-b are formed by 8 amino acids. TM2–6 and TM7–11 blocks (green and red boxes, respectively) are related by inverted amino acid repetitions. Taken from (Mancusso *et al.,* 2012).

1.4.2.2. Protein domains in VcINDY

The protein structure is classified by domains according to their location and function of the parts. Each protomer has a transport domain, a scaffold domain and an oligomerization domain (*Figure 1.6-A*) (Mancusso *et al.*, 2012).

The scaffold domain holds the union between the two protomers of the dimmer and is formed by TM1, TM2, TM4c, TM7 and TM9c. Importantly, the transport domain is responsible for moving back and forth across the lipid bilayer. It is formed for TM5a-b, TM6, TM10a-b, TM11 and two secondary structures called HP1 (HPin) and HP2 (HPout). They are two re-entrant helix-turn-helix hairpins (HP) formed by inter-helical loops found in both protomers.

HPin is connected to the membrane by H4c in the cytosolic site and by the TM5 loop. In a similar way, HPout communicates to the extracellular site connected to H9c to the membrane (Mancusso *et al.*, 2012).

The oligomerization domain of the protein generates the interface between the two protomers. Connection occurs between TM3, TM4a and TM9b from one protomer with TM4b, TM8 and TM9a of the other protomer. In addition, the first part of the protein is related in sequence and structure to the second half.

Each protomer is composed of an inverted repeated structure following what is known as inverse twofold symmetry. This symmetry, together with the little differences in the structure of the repeats, allowed the outward-facing state's prediction by reverse-swap modelling studies (*Figure 1.6-B*) (Mulligan et al., 2014) (Mulligan et al., 2016).
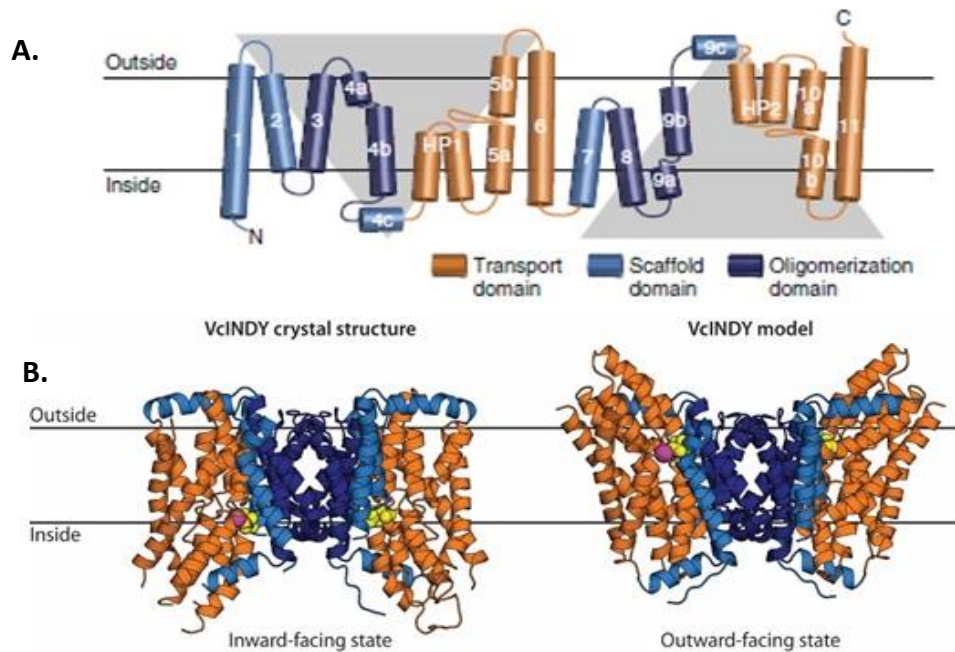
Figure 1.6: **Structure of the VcINDY protein in its two known conformational states.**

A) View of the one protomer and its domains: Transport domain (orange), scaffold domain (light blue) and oligomerization domain (dark blue). **B)** The two protein's conformations. At the right the inward-facing state with the substrate facing the cytoplasm of the cell (from the crystal structure of Mancusso *et al.,* 2012). On the contrary, at the left, is the outward-facing state model of the protein predicted by computational approaches. Taken and adapted image from (Mulligan *et al.,* 2016)

1.4.2.3.   Sodium-Binding sites

In *Nie et al.* crystal structure, both Na^+-binding sites were characterized and named Na1 and Na2. In Mancusso et al., only one sodium was presented in the crystallized protein, located in the space between HPin and TM5a-b loop. The Na^+-binding site was kept apart from the cytosolic space by the citrate bound in the protein. The implicated amino acids were determined accurately within the 2.8 Å structure where sodium interactions within the protein were described to be penta-coordinated (Mancusso *et al.*, 2012) (Nie *et al.*, 2017).

Each sodium cation interacts with two amino acid side-chain from the protein structure and three backbone carbonyl oxygen of the residues. The sodium ion at

Na1 is coordinated between the three backbone carbonyl oxygen atoms of S146, S150 and G199, the side-chain hydroxyl of S146 and the side-chain carbonyl of N151. All these residues are from the HPin, except G199, which belongs to the 5a-b loop (*Figure 1.7-A*)(Nie *et al.*, 2017).

Similarly, at the other half of the protein (C-terminal), VcINDY holds the Na2 distanced > 13 Å from the Na1 (Nie *et al.*, 2017). In this site, sodium binding is coordinated between the backbone carbonyls T373, A376 and A420 and the side-chain hydroxyl of T373 as well as the side-chain carbonyl of N378. According to the protein symmetry, Na2-binding site is framed by HPout and the 10a-b loop. Mutations of T373 and S146 to alanine shown that Na2 could be more relevant than Na1 for its promoting role. The binding of a sodium cation in Na2 at the outward-facing state could coordinate the binding of another sodium in Na1 (*Figure 1.7-B*) (Nie *et al.*, 2017).
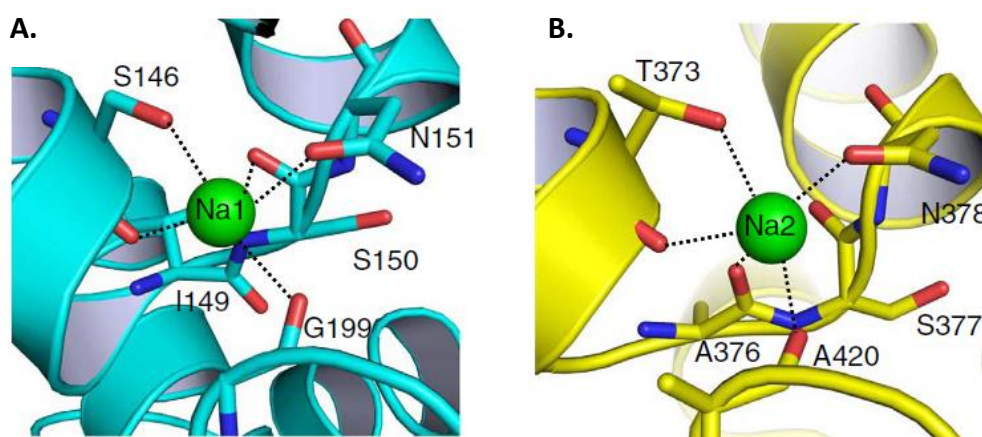
Figure 1.7: **View of the Na1 and Na2 binding sites of VcINDY.**

A) Na+- Binding site saw for the first time in Mancusso *et al.,* 2012. This sodium is bound to the N-terminal halve of the protein. **B)** Na⁺-binding site at the C-terminal half of the protein. First time accurately characterized. Na+ ions are green spheres and relevant amino acids are red and blue sticks. Important chemical interactions between the cations and the VcINDY structure are drawn as dashed lines. Taken from (Nie *et al.,* 2017)

Both sodium binding sites are coordinated with key amino acids, such as N151 and S150, which not only participate in the sodium binding site but also in the substrate-binding site (Nie *et al.*, 2017). Hence, it has been discussed that sodium binding coordinates several substrate-binding amino acids in an allosteric manner, given that substrate-binding takes place in the middle of Na1 and Na2-binding sites. Such an effect would aid the stabilization of the protein conformation via an induced-fit mechanism to help its union with the substrate (Nie *et al.*, 2017).

The fact that some amino acids are shared between the substrate and Na^+-binding sites would explain why their transport is very likely to be highly coupled (Mancusso *et al.*, 2012). It would also explain the absence of positive amino acids near the substrate-binding site, since non-positive amino acids would target the attraction of sodium cations and, any positive charge would repel them (Nie *et al.*, 2017).

1.4.2.4.   Substrate-binding site

The substrate-binding site was first characterized by Mancusso et al., with a citrate molecule. The citrate was found bound followed protein symmetry involving residues from HPin, TM5, HPout and TM10. Specifically, the residues S150, N151 and T152 from HPin and S377, N378 and T379 from HPout participate in its binding (*Figure 1.8-B*). In the same paper, citrate binding site was agreed to be the same for dicarboxylic substrates.

Nie et al., showed succeeding that succinate establishes interaction with its carboxylate group with the protein through H-bonds between the side-chain amide of N151 and the side-chain hydroxyl of T152 (*Figure 1.8-A*). Succinate also

interacts with the side-chain hydroxyl S377, the side-chain amide of N378 with the other carboxylate group. The aliphatic portion of T379 of the side-chain interacts with succinate by Van der Walls forces. Besides, N151 and N378 residues also interact with succinate generating H-bounds with S200 and T421. These extra bonds result in a higher stabilization of the substrate-bound (Nie *et al.*, 2017).
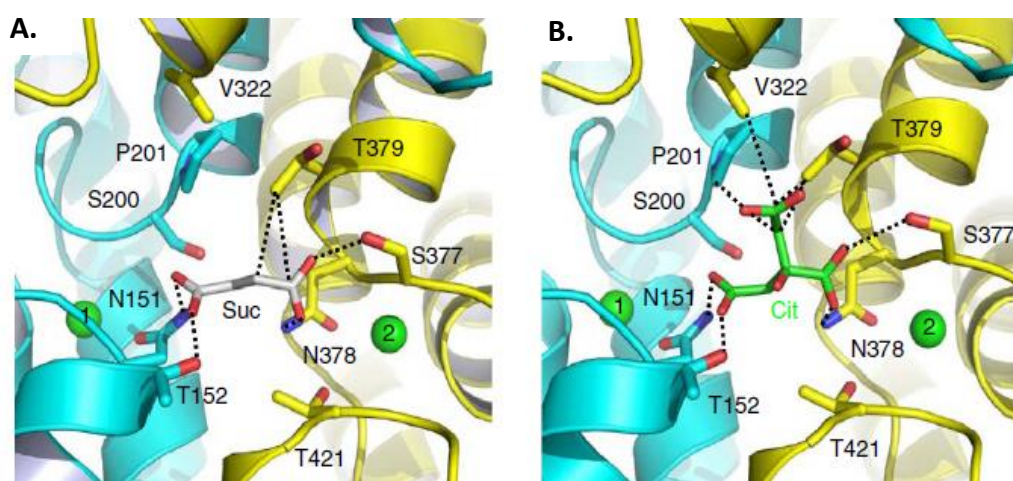
***Figure 1.8:* View of the substrate-binding site of VcINDY.**

A) Detailed map of succinate molecule (grey) bound at the binding site. **B)** Detailed map of citrate molecule (green) bound at the binding site. Na^+ ions are green spheres and relevant amino acids are red and blue sticks. Important chemical interactions between the succinate or citrate with VcINDY structure are drawn as dashed lines. Taken from (Nie *et al.,* 2017)

Mutations in those amino acids have been constructed to verify and assess all residues' potential importance in such crucial site (Nie *et al.*, 2017). Transport function was seen affected in SLC13 family members by individual mutations to alanine in VcINDY equivalent positions of N151, T152, S200, S377, N378, T379 and T421 (Nie *et al.*, 2017). It has been particularly suggested that threonine 379 may define substrate recognition. When this threonine was mutated to Proline (VcINDY T379P), transport interaction for succinate and sulfate was disrupted. Although, alanine mutation of T379 caused a mild impact on the transport capacity. The same outcome was detected for N151A mutants (Nie *et al.*, 2017).

1.5. THE NOVEL ELEVATOR TYPE-MECHANISM

VcINDY transport is electrogenic, pH-independent, sodium gradient dependent (but not coupled to any proton gradient), and a high-affinity transporter for C_4-dicarboxylates (Mulligan *et al.*, 2014). Interaction with three sodium ions aid recognition and transport of negatively charged substrates such as succinate (Mancusso *et al.*, 2012)(Fitzgerald, Mulligan and Mindell, 2017). In each cycle, the binding of one single substrate molecule per protomer is required for transport to happen. Interestingly, the dimer's two protomers are presumably independent since the succinate-binding sites are not cooperative with each other (Mulligan *et al.*, 2014).

The transport mechanism described for VcINDY is an elevator-type mechanism where proteins take large conformational changes to expose the substrate to one side or the other of the membrane (*Figure 1.9*) (Mulligan *et al.*, 2016). The movement involves shifts on the order of ~15 Å and it has been described to be shared between DASS members (Mulligan *et al.*, 2016).
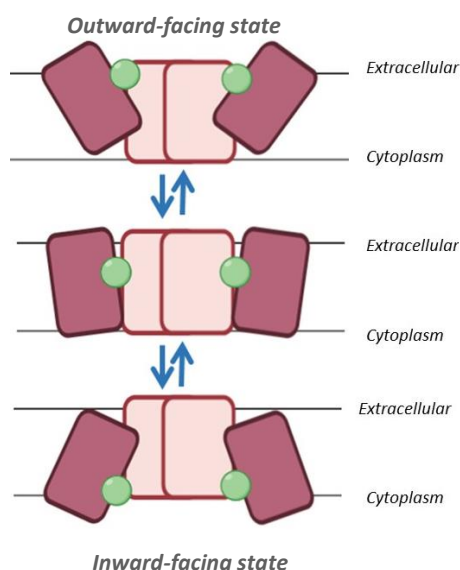
Figure 1.9: **Representation of VcINDY's binding site positions during transport from the inward-facing state to the outward-facing state.**

The substrate and sodium binding site (represented as a common green sphere) are shared between the transport domain (dark pink) and the scaffold domain (light pink). Throughout the elevator-type transport mechanism, the binding site moves along with the transport domain. To reach the inward-facing structure from the predicted outward-facing model structure, the protein is exposed to a ~43° rotation and a ~15 Å translocation (Mulligan *et al.,* 2016).

This elevator-type mechanism implies that cation and substrate-binding sites are presented in both domains of the protein; the scaffold domain and the transport domain. The transport domain movement results in two protein conformations: an inward-facing state and an outward-facing state. The two conformations alternate between them changing substrate accessibility to the cytoplastic site or extracellular site (respectively), probably via an occluded state (Mulligan *et al.*, 2016). The theoretical cycle movement is as described below (*Figure 1.10)*.
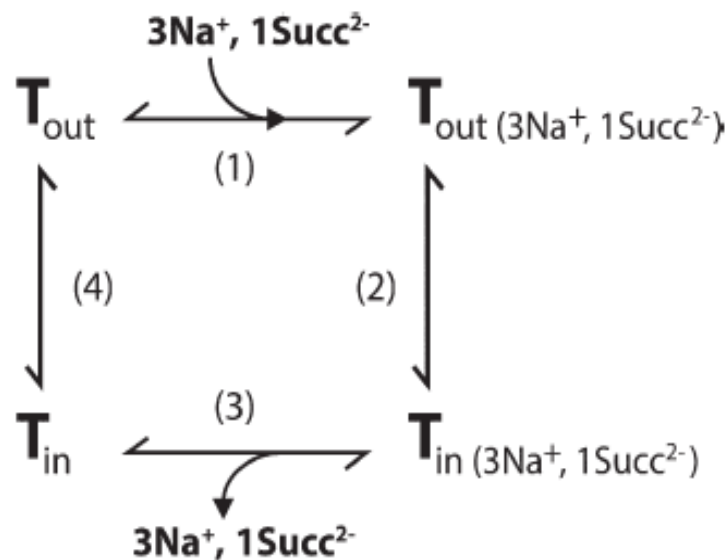
Figure 1.10: **VcINDY transport cycle from the outward-facing state to the inward-facing state.**

(1) VcINDY is in the outward-facing state conformation (Tout). Three sodium cations and one succinate get bound into the protein's respective binding sites**.** VcINDY binds first sodium, helping succinate binding to happen. Then, any remaining necessary Na$^+$ ions will then bind to the protein. **(2)** The full loaded transporter undergoes several conformational changes involving helix reorientations until the inward-facing state is adopted (Tin). **(3)** Succinate and sodium are released. **(4)** Once Na ions and succinate are dissociated from the protein in an unclear order, the empty transporter goes back to the outward-facing state.

Only the empty or fully loaded transporter will switch to the other conformation. In this case, from the inward-facing conformation, VcINDY shifts towards the outward-facing state to start the cycle again. Taken from (Mulligan *et al.*, 2014)

1.6. INSIGHTS INTO THE BINDING SELECTIVITY PUZZLE

1.6.1. VcINDY ION SELECTIVITY

VcINDY uses a sodium gradient to uptake substrates. The role of sodium in VcINDY transport has been described on many occasions and among other relative transporters (Mulligan *et al.*, 2014)(Strickler *et al.*, 2009)(Hall and Pajor, 2007)(Inoue et al., 2002)(Pajor, 1995). In some studies, the effects on transport in the presence of different positive charged ions have been approached. As expected, *E. coli* cells expressing VcINDY proved to transport succinate when a Na^+ gradient was present (Mulligan *et al.*, 2014).

VcINDY transport was also tested with other cations such as potassium and lithium. Lithium proved to drive transport with a much lower relative efficacy than sodium. However, driven transport was not observed with a potassium gradient as it owns a bigger ratio than sodium (Mancusso *et al.,* 2012).

1.6.2. VcINDY SUBSTRATE SELECTIVITY

Previous characterization suggested that VcINDY can transport succinate and interact with malate and fumarate, and other succinate derivatives and C5-carboxylates such as α-ketoglutarate. (Mancusso *et al.,* 2012)(Mulligan *et al.*, 2014).

Counterflow transport assays proved that at least malate, fumarate and oxaloacetate and other related dicarboxylate-containing compounds inhibited succinate transport (*Figure 1.11*). In the same paper, citrate's inhibitory effect resulted in being very low and it was declared not to be a transported substrate by VcINDY (Mulligan *et al.*, 2014).
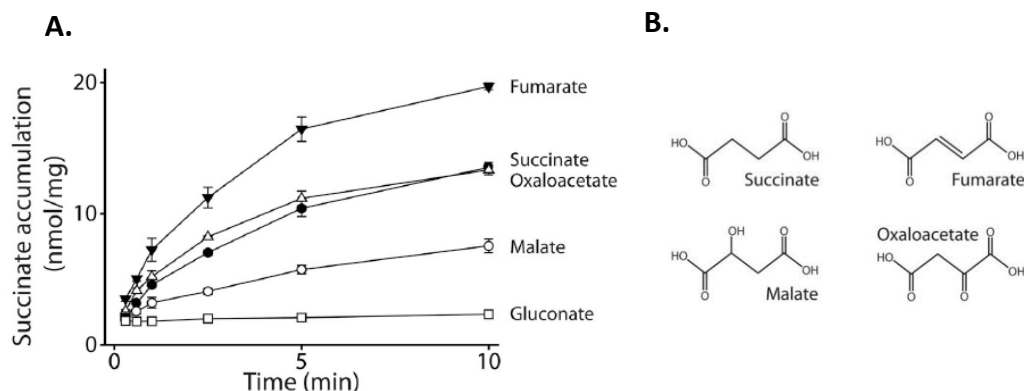
***Figure 1.11:* Substrates of VcINDY.**

A) Counterflow assay to validate substrate candidates of VcINDY. Liposomes with 1 mM inside the vesicles of succinate (closed circles), malate (open circles), fumarate (closed triangles), oxaloacetate (open triangles) and gluconate (open squares acting as negative control) were tested to determine the accumulation of radiolabelled succinate. **B)** Chemical structures of the possible substrate candidates of the study. Taken from (Mulligan *et al.*, 2014)

Considering that some of the amino acids enhancing substrate interactions are vastly conserved among this family, it is not surprising that interaction with similar dicarboxylates is observed in other VcINDY DASS homologs (Nie *et al.*, 2017). In fact, in DASS proteins a 'trans-dicarboxylate recognition' module shaped with HPin, HPout and TM10 is suggested to possibly bring ligand selectivity (*Figure 1.12*) (Nie *et al.*, 2017). Two critical amino acids located in the trans-dicarboxylate recognition module of VcINDY are P201 and T379, whereas, in other NaCT transporters, Glycine and Valine are found in those positions (Nie *et al.*, 2017). Proline and Threonine exclude the Pro-S carboxylate of citrate outside the protein, unable to neutralise its charges. Glycine and Valine, on the contrary, allow identification of citrate's Pro-S carboxylate stabilizing its negative charge.

These amino acids hint an explanation for positive charge ligands' rejection as substrates for mammalian DASS (Nie *et al.*, 2017) Besides, at the helix's tips of

HPin, HPout, TM10 and TM5 alfa-helical transmembrane positive dipoles are found facing the substrate-binding site offering more stabilization of substrate's two negative charges, such as succinate.
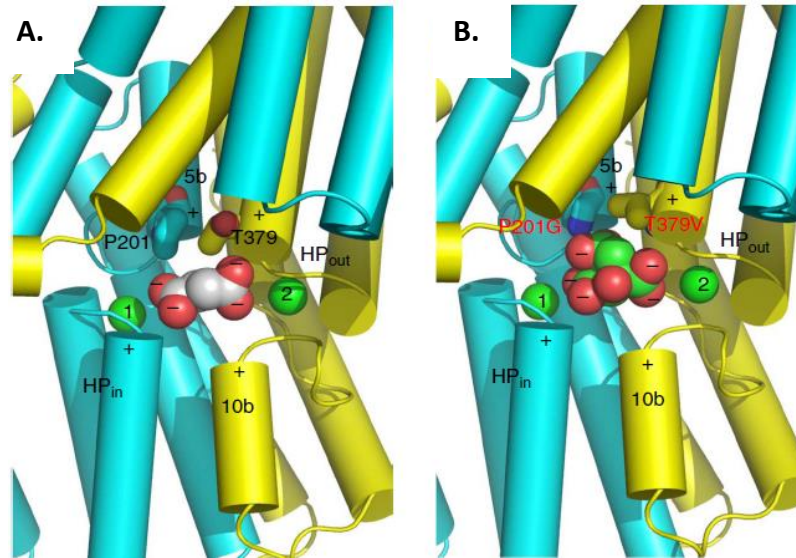
Figure 1.12: **DASS trans-dicarboxylate recognition' module**

A) Succinate (grey) sitting on the module of recognition of VcINDY protein**. B)** Citrate (green) sitting on the module of recognition of MT5. MT5 is an octuple mutant of VcINDY that resembles to a NaCT transporter of C6-tricarboxylate. MT5 has Glycine and Valine instead of Proline and Threonine. These mutations help stabilize the Pro-S of citrate. The charges on both substrates are predicted according to a pH7. The N and C halves of the protein are coloured in cyan and yellow, respectively. Transmembrane helices are represented as cylinders and their positives dipoles are marked with plus signs. The positive dipoles help to stabilise the negatively charged carboxylates (minus signs) of succinate and citrate. Sodium cations are numbered and coloured in green spheres. Taken from (Nie *et al.,* 2017).

1.7. STUDY MOTIVATION

Even though the 2.8 Å resolution X-ray structure has brought some insights into the structure of VcINDY, there are still questions about substrate and ion selectivity to be solved in the DASS family. Only the suggestion of a 'trans-dicarboxylate recognition´ module helped to explain substrate preference between carboxylate or sulfate transporters of SLC13 members (Mancusso *et al.*, 2012). However, there is not enough structural insight of these proteins to establish the backbone conditions of DASS transporters' ligand selectivity. Besides,

the sodium-binding effect over substrate-binding, as well as possible lithium's, in some DASS proteins has never been further explained. Therefore, there is a need to procure detailed knowledge of the individual structural components involved in substrate requirements among DASS proteins.

Until recently, the only detailed substrate interactions within a DASS protein described are with VcINDY in the presence of citrate and succinate.

Thermofluor assays techniques have been used in different studies to screen possible ligand candidates and ions coupling of membrane proteins. This assay is also named Fluorescence-based thermal shift assay since it measures the rate of fluorescence change which allows determining the melting point of the proteins (Pantoliano *et al.,* 2001). The melting point of membrane proteins measures its stability, which allows predicting substrate selectivity by observing changes in the melting point since substrate binding increases thermostability. Interestingly, this melting point is very reliably in VcINDY. It differs when the protein does not have anything bound compared to when it has a ligand bound.

1.8. AIMS AND OBJECTIVES

1.8.1. AIMS

This thesis aims to investigate the VcINDY residues involved in substrate binding to ascertain what yields substrate specificity. The project's main idea is to target relevant amino acids in the binding site, related to it, or in the action mechanism process, by which variation in substrate specificity occurs. Besides, the lithium and potassium effect using VcINDY wild-type will be a target in this project to assess substrate recognition depending on the anion bound into the protein.

Hopefully, these findings will help to address essential questions of DASS transporters while enhancing a better understanding of VcINDY's substrate selectivity and transport mechanism to design inhibitors for INDY proteins.

1.8.2. OBJECTIVES

For this reason, the mechanism of the bacterial representative of the DASS family, VcINDY, will be tested probing interactions between VcINDY and interactors such as putative substrates and three different cations.

To this goal, the objectives of this project are:

- Express and purify wild-type VcINDY and its alanine mutants for the study.

- Create SDS-PAGE gels to verify the correct purification of VcINDY.

- Describe substrate interactions of VcINDY alanine mutants with ten different anionic compounds compared to wild-type using a high-throughput thermostability-based approach.

- Identify important VcINDY residues involved in substrate selectivity accordingly to the ten compounds-screen analysis.

- Establish possible VcINDY's ligands' requirements for binding to the transporter.

- Study the effect of potassium and lithium cations in succinate binding in wild-type VcINDY.

- Study the effect of potassium and lithium cations in other ligands binding events in wild-type VcINDY

CHAPTER 2: MATERIALS AND METHODS

N.B. all materials, except chemicals, are obtained from Sigma-Aldrich unless stated otherwise. Chemicals are mainly obtained from Thermo-Fisher.

2.1. STRAINS AND PLASMID USED IN THIS STUDY

2.1.1. Escherichia coli STRAINS

Competent *E. Coli* TOP10 were used in this study to hold the plasmid of interest, which is described below (*Section 2.3.4*). The genotype of these cells is as follows: F– mcrA Δ(mrr-hsdRMS-mcrBC) φ80lacZΔM15 ΔlacX74 recA1 araD139 Δ(ara-leu)7697 galU galK λ– rpsL(StrR) endA1 nupG

BL21 strain Lemo21 *(New England Biolabs)* of *E.coli* were used for autoinduction and expression of the desired protein, as indicated by *Drew et al., 2017.* The genotype of these cells is as follows: F– ompT hsdSB (rB–, mB–) gal dcm (DE3).

2.1.2. PLASMID USED IN THE STUDY

A modified pET plasmid (pEThisVcINDY), encoding VcINDY expressed in-frame with an N-terminal deca-histidine tag (Love *et al.,* 2010), was used to transform *E. Coli* cells (*Table 2.0*)

PLASMIDS OF THE STUDY	
pEThisVcINDY wt	*pETHisVcINDYN151A*
pEThisINDYSNT1AAA	*pETHisVcINDYT152A*
pETHisVcINDYV66A	*pETHisVcINDYS200A*
pETHisVcINDYT67A	*pETHisVcINDYS290A*
pETHisVcINDYI96A	*pETHisVcINDYD319A*
pETHisVcINDYF100A	*pETHisVcINDYV322A*
pETHisVcINDYI149A	*pETHisVcINDYF326A*
pETHisVcINDYN151A	*pETHisVcINDYT421A*

Table 2.0: *pEThis* **plasmids used in the study.**

All plasmids contain a single alanine mutation except for wildtype and SNTAAA. The *petHisVcINDYSNTAAA* carries a triple alanine substitution.

2.2. MEDIA AND BUFFERS

Before each experiment, all media used in growing methodologies was autoclaved at 121 °C for 3 h. Storage conditions are specified in each case as it varies depending on chemical requests. If conditions are not specified, chemicals were stored at room temperature. All water used in the media and buffers was sterilised MilliQ water.

E.coli cultures were incubated at 37 °C overnight (unless otherwise stated). Liquid cultures were incubating rotating at 190 rpm to improve aeration. In the case of the continued growth, all liquid cultures were diluted back to a specific optical density the following day with the desirable fresh media to replenish the cells. In the following figures, the different components contained in media and buffers are depicted. By order, media for transformations (*Table 2.1*), protein expression induction (*Table 2.2*), buffer for protein extraction (*Table 2.3*) and, buffers for purification (*Table 2.4*) are depicted. Table 2.5 describes the components for the SDS-Page gels.

COMPONENTS OF THE GROWTH MEDIA USED IN THE STUDY

GROWTH MEDIA	Components (% w/v)
LB **(+Chloramphenicol)**	1 % NaCl 1 % Tryptophan 0.5 % Yeast Extract (25 µg/ml + Chloramphenicol in EtOH) Store at 4 °C
Agar Media *(+ Chloramphenicol and Kanamycin)*	1 % NaCl 1 % Tryptophan 0.5 % Yeast Extract 1 % Agar (25 µg/ml Chloramphenicol in EtOH) + (100 µg/ml + Kanamycin in dH$_2$O) Store at 4 °C

Table 2.1: **Media composition**

The LB media contained chloramphenicol as a selectable marker for *E.Coli* within the constructs. In agar plates, Kanamycin was added as an additional selectable marker for E. *Coli* transformed cells.

COMPONENTS OF PASM-5052 PROTEIN EXPRESSION AND INDUCTION MEDIA

PASM-5052 MEDIA (1 L)
• 2 mM MgSO$_4$. Store at 4 °C
• 5052 (0.5 % glycerol, 0.05 % glucose, 0.2 % α-lactose). Store at 4 °C
• NSP (50 mM Na$_2$HPO$_4$, 50 mM KH$_2$PO$_4$), 25 mM (NH$_4$)$_2$SO$_4$.
• 1000x metals (20 µM FeCl$_3$, 200 µM CaCl$_2$, 200 µM MnCl$_2$, 200 µM ZnSO$_4$, 40 µM CoCl$_2$, 20 µM CuCl$_2$, 20 µM NiCl$_2$, 20 µM Na$_2$MoO$_4$, 20 µM Na$_2$SeO$_3$, 20 µM H$_3$BO$_3$)
• 200 µg/ml 17aa. Store at 4 °C
• 500 µg/ml Methionine. Store at 4 °C
• 0.25 mM L-Rhamnose. Store at 4 °C
• 900 ml of dH$_2$O

Table 2.2: media composition for protein expression induction

COMPOSITION OF THE PROTEIN EXTRACTION BUFFERS

Lysis Buffer (Store at 4 °C)	
1 M Tris pH7	50 mM Tris pH 8
50 % glycerol	5 % (vol/vol) glycerol.
4 M NaCl	100 mM NaCl
Buffer A (Store at 4°C)	
1 M Tris pH8	50 mM Tris pH 8
50 % glycerol	5 % (vol/vol) glycerol.
4 M NaCl	100 mM NaCl

Table 2.3: Protein extraction buffers composition.

COMPOSITION OF THE PROTEIN PURIFICATION BUFFERS

Wash Buffer 1 (5 CV-5 ml)	Elution Buffer 1 (2 CV-2 ml)
50 mM Tris pH8	20 mM HEPES pH7.5
5 % (vol/vol) glycerol.	50 mM NaCl
100 mM NaCl	0.05 % DDM
10 mM 4 M imidazole pH8	10 µg/ml Trypsin
0.05 % DDM	-
Wash Buffer 2 (5CV- 5 ml)	Elution Buffer 2(2 CV-2 ml)
20 mM HEPES pH7.5	20 mM HEPES pH7.5
50 mM NaCl	50 mM NaCl
20 mM 4 M imidazole pH8	0.05 % DDM
0.05 % DDM	-

Table 2.4: Protein purification buffers

Resolving Gel (for 2 x 1 mm 12% gels)	Stacking Gel (for 4 x 1mm 4 % stacking gels)	4x sample buffer (Store at -20°C)
4 ml 30% (w/v) acrylamide/0.8% (w/v) bisacrylamide	1.3 ml 30 % (w/v) acrylamide/0.8 % (w/v) bisacrylamide	12 g glycerol
2.5 ml 1.5 M Tris pH 8.8	2.5 ml 0.5 M Tris pH 6.8	3 g H2O
3.4 ml H2O	6.1 ml H2O	10 ml 10 % SDS
100 μl 10% SDS	100 μl 10 % SDS	1 ml 1 M Tris pH 7.2
100 μl 10 % APS	100 μl 10 % APS	0.06 g Bromophenol Blue
10 μl TEMED	10 μl TEMED	Add 3 μl β-mercaptoethanol per 100 μl
Coomassie Brilliant Blue Dye	**Destain**	**10x Running buffer**
50 % Methanol	10 % Ethanol	30 g/L Tris
50 % Acetic Acid	10 % Acetic Acid	140 g/L glycine
0.2 % Coomassie Blue	80 % H2O	10 g/L SDS

Table 2.5: SDS-PAGE gels components composition.

2.3.   MOLECULAR BIOLOGIC APPROACHES

2.3.1. ALANINE MUTANTS

All alanine mutants were designed and generated by other laboratory members using a QuikChange II Site-Directed Mutagenesis Kit (Agilent Technologies). Residues selected for mutational analysis were chosen based on their localization according to the succinate-bound crystal structure (*Nie et al. 2017*). Residues mutated and their relevance within their position is detailed in *Table 2.6*.

MUTANTS LOCATION CREATED FOR THE STUDY

Position within the crystal structure	Residues mutated
Scaffold/oligomerization domain	V66, T67, I96, F100, S290, D319, V322 and F326.
Sodium proximity	I149 and N151.
Succinate-binding site	N151, T152, S200 and T421.

table 2.6: **Mutants location within VcINDY structure.**

2.3.2. DNA MINIPREP OF *E.coli* TRANSFORMANTS

Following successful site-directed mutagenesis and transformation into competent cells, the mutant plasmid was mini-prepped and sequenced. Miniprep was performed using QIAprep Spin Miniprep Kit, QIAGEN , to extract DNA. Stocks of each mutant plasmid were preserved at -20 $^{\circ}$C. The mutant plasmid was then transformed into the desired expression strain, as explained in *Section 2.3.4.*

2.3.3. COMPETENT CELLS

LEMO21 cells were streaked on an LB plate selective for Chloramphenicol and incubated overnight at 37 $^{\circ}$C for growth. On the following day, 1 colony was added to 10ml of fresh LB and incubated overnight. Following overnight growth, 4 ml of LEMO21 culture was used to inoculate 400 ml LB under sterile conditions. Cells were transferred into 250 ml centrifuge bottle once OD$_{600}$ reached 0.4, after 2 to 3 hours approximately. Then, cells were incubated for 20 min on ice before centrifuging them at 3000 xg for 10 min in a lab rotor (Heradeus magefuge 16R: Thermoscientific). The pellet of cells was kept on ice until resuspended in 30 ml of cold 0.1 M CaCl$_2$. Another incubation on ice took place for 30 minutes before the centrifugation step was repeated as described above for 10 minutes. The

supernatant was removed, and the pellet was resuspended in 16-20 ml 0.1 M CaCl$_2$

and 15 % glycerol. 200 µl aliquots were made into 1.5 ml Eppendorf, which were

snap-frozen into dry ice before storing them in a -80 °C freezer.

2.3.4. TRANSFORMATION OF LEMO21

E. *coli* was transformed as done previously by Mulligan *et al.,* 2016.

Two methodologies were followed depending on the availability of competent

cells.

2.3.4.1.   Transformation using the freeze-thaw method

First, a scrape of LEMO21 cells from the desirable glycerol stock was used

to inoculate 2 ml of fresh LB with 25 µg/ml Chloramphenicol (Chl) and incubated

overnight at 37 °C. The following morning, 500 µl of the overnight culture was used

to inoculate 4.5 ml fresh LB with Chl antibiotic resistance and incubated for 1 hour.

After incubation, 833 µl of culture was distributed into sterile 1.5 mL Eppendorf's

for one shot of competent cells. Cells were harvested by centrifugation at 13000

xg for 1 minute in a table microcentrifuge (SLS Lab basics). The resulting pellet was

resuspended in 50 µg ice-cold 100 mM NaCl$_2$ and left on ice until DNA addition.

For each transformation 100 ng of DNA was added into prepared cells aliquot and

vortexed to mix. The sample mixture was snap-frozen in dry-ice-ethanol for 1.5

minutes and immediately after the sample was thawed at 37 °C in a dry heating

block for 2 minutes. Finally, 200 µl of SOC or LB (25 µg/ml Chloramphenicol and

100 µg/ml Kanamycin) were added into the cell suspension and incubated for an

hour in a shaking incubator. 10 µl cell suspensions were spread onto a selective LB

plate (25 µg/ml Chloramphenicol and 100 µg/ml Kanamycin) following incubation.

The remaining ~190 µl of cell suspension was spread on a second selective LB plate. Plates were incubated overnight at 37 °C for the growth of colonies.

2.3.4.2. Transformation using the heat-shock method

An aliquot of ready-made chemically competent cells was thawed on ice for ~30 minutes. Forthwith 100 ng of plasmid DNA was added to 50 µl aliquot of competent cells and incubated on ice for 30 minutes. After 30 minutes of incubation, the mixture was incubated for 1.5 minutes at 42 °C. This was followed by a 1-hour incubation with cells into fresh 200 µl of SOC without shaking for expression of the antibiotic resistance (25 µg/ml Chloramphenicol and 100 µg/ml Kanamycin). After 1 hour, 10 µl of the cell suspension was laid on a selective LB plate. The remaining ~190 µl of cell suspension was spread on a second selective LB plate. Plates were incubated overnight at 37 °C for colonies to grow.

2.4. PROTEIN PREPARATION

2.4.1. EXPRESSION OF VcINDY

To gain expression of membrane proteins to a high level, the expression of pEThisVcINDY was tightly regulated using the MemStar system (AzizQureshi *et al.,* 2017).

After a successful transformation, one colony from an agar plate with 25 µg/ml Chloramphenicol and 100 µg/ml + Kanamycin was added into 150 ml of fresh LB and incubated overnight at 30 °C, 190 rpm. The next morning, 20 ml of the O/N culture was introduced in PASM-5052 autoinduction media in the presence of 100 µg/ml kanamycin, 25 µg/ml chloramphenicol, and 0.25 mM L-rhamnose added before the cultured cells. The culture was then incubated at 37 °C for the duration

of 2.5 h until OD 600 of 0.5 was achieved. Protein expression was at that point induced by the addition of 0.4 mM isopropyl β-d-1-thiogalactopyranoside (IPTG). Finally, the culture is left incubating at 25 °C overnight.

2.4.2. PURIFICATION OF VcINDY

Protein was purified as done previously by Mulligan *et al.,* 2016. To express and purify VcINDY, the pEThisVcINDY plasmid must be expressed in culture the previous day. After overnight induction, the absorbance of 0.04-0.06 at OD 600 would be expected to continue into purification. Once OD of the culture was checked, cells were harvested by centrifugation at 4000 xg for 20 minutes at 4 °C. The resulting pellets were harvested and lysed using a homogenizer (EmulsiFlex-C3; Avestin) in Lysis Buffer (*Table 2.3*) before being subjected to sonication to disrupt bacterial membranes. Protease inhibitor cocktail and DNase (Invitrogen) were added prior to sonication. Sonication was performed with 3s on-7s off for 5 minutes, with a pause of 2.5 minutes before 5 more minutes sequence repetition. A further centrifugation step at 21000 xg for 20 minutes at 4 °C was used to remove large cell debris before ultracentrifugation. Ultracentrifugation at 41000 rpm for 2 h at 4 °C allowed to obtain membrane particles. These membrane particles were resuspended in Buffer A, detailed previously in *Table 2.3*. VcINDY protein was extracted from the membrane pellet suspensions by solubilisation using 1 % n-dodecyl-β-D-maltoside (DDM:Anatrace). Another ultracentrifugation step for 30 min at 4 °C and 41000 rpm was required to remove any insoluble material. The soluble fraction was then incubated with TALON metal affinity resin

(Takara Bio Inc.) containing Cobalt ions that bind with high affinity to the decahis-tagged protein (binding capacity of 5-18 mg protein/ml resin). DDM-solubilised protein with 1 ml of Talon Resin was incubated overnight at 4 °C rotating. The next morning, the sample was poured into an Econopac Column (20ml capacity: Biorad). At that point, the resin was washed with 5 column volumes (CV) of PB1 using low concentrations of imidazole to remove any contaminant proteins and after 5 CV PB2 (*Table 2.4*). Bound protein was eluted while the affinity tag is simultaneously cleaved using trypsin by addition of 2.5 CV of EB1 containing 10 µg/ml trypsin after one-hour incubation at 4 °C. An extra 2.5 CV of elution buffer, EB2, was used to collect all remaining proteins directly in the column. Protein concentration was calculated using the absorbance at 280 nm and the theoretical extinction coefficient. Finally, purified proteins were checked on SDS-PAGE gels (BIO-RAD protean mini-gels). Components for the gels were calculated and are described above in *Table 2.5*. The protein was either used immediately or snap-frozen and stored at - 80 °C until required.

2.5. CPM-BASED THERMOSTABILITY ASSAY

CPM assay methodology was adapted from (Crichton *et al.*, 2015).

Purified VcINDY proteins were thawed on ice before use. Substrate stocks were made at 60 mM in dH_2O, and pH adjusted to pH 7.5 using either concentrated KOH or HCl before being aliquoted and stored. 5 mg/ml of N-[4-(7-diethylamino-4-methyl-3coumarinyl) phenyl] maleimide (CPM) in aliquots prepared in DMSO were made and thawed at room temperature quickly before being used. All the stocks were stored at -80 °C until future use. CPM assay buffer (20 mM HEPES, pH

7.5, 50 mM NaCl, 2 mM DDM, unless stated otherwise) was made fresh on the assay day.

On the day of the assay, 2 μg of protein was diluted into 45 μl of CPM Assay Buffer containing substrates of interest in thin-walled optical cap PCR tubes *(Bio-Rad)* on a 96 well plate. Everything was incubated for 10 minutes on ice. Then, 5 μl of CPM diluted previously 25-fold into the appropriate assay buffer, were added into the tubes and set 15 more minutes on ice with occasional mixing. Samples were finally transferred to a qPCR thermocycler (Thermo Fisher QuantStudio 3) for reading. The thermocycler programme was the same for all the experiments.

The program was designed by another member of the laboratory. As summarised graphically in *Figure 2.0*, before the initiation of readings, the programme was designed to cool down to 5 °C at a rate of 1.6 °C per second. Automatically after, the melt curve programme rises from 5 °C to 95 °C at a rate of 1.6 °C/s. It takes fluorescence readings, stepping and holding for 5 seconds, every 1 °C. Sybr Green fluorescence filters were used, with an excitation of 470 ± 15nm and emission of 520 ± 15 nm.
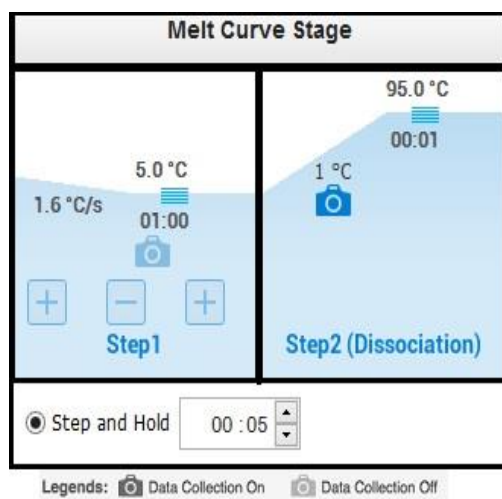

Figure 2.0: **CPM assay program software.**

Readings started at 5 °C and ended at 95 °C, taking a reading for each degree of difference.

2.6. DATA COLLECTION, ANALYSIS AND STATISTICAL TESTING

All experimental data from the qPCR machine was read on QuantStudios^{TM} Design & Analysis software v1.5.1 (Applied biosystems by ThermoFisher Scientific). From there data was exported for analysis in Microsoft Excel. On Excel, the derivative peak on the data set was taken as a melting temperature (Tm). Changes in Tm in different conditions were calculated by using no substrates as a baseline. Triplicates from the same condition were carried out. Hence, temperature changes are expressed as mean and deviation (SEM) values.

To investigate this statistically, a two-way ANOVA statistical analysis was carried out on Excel to assess if the differences between substrate and non-added substrate conditions were significant. P-values smaller than 0.05 were accepted as significant. Raw data were normalised on Excel to obtain melting curve graphs for each protein and substrate. Figures and charts from the CPM experiments were made with GraphPad Prism 6. Other VcINDY 3D images were taken from PyMOL.

CHAPTER 3: RESULTS

3.1. VcINDY PURIFICATION

3.1.1. THEORETICAL FRAME OF THE PROTEIN PURIFICATION

Protein expression and purification are required prior to any further experimentation to have purified protein to perform the necessary experiments. Only purified protein can be used for Thermofluor assays. Therefore, VcINDY proteins are expressed and purified as described in the Materials and Methods section (*Section 2.4*) and illustrated here in *Figure 3.0.*
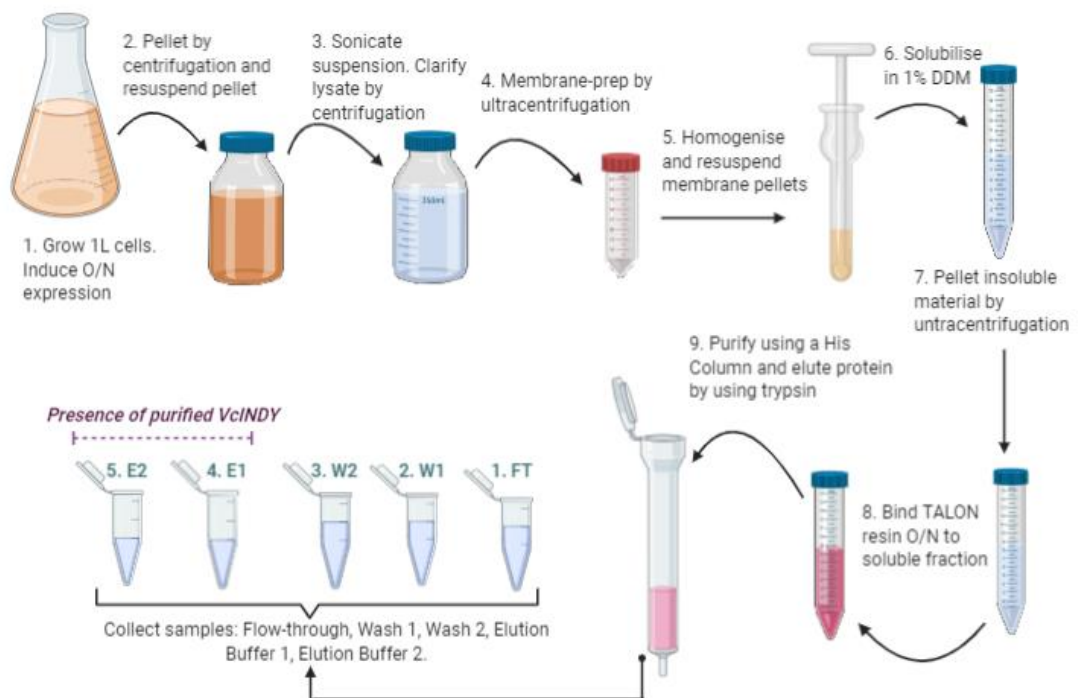
***Figure 3.0:* VcINDY expression and purification scheme.**

Overnight induced cells are harvested by centrifugation and then subjected to sonication to disrupt cellular membranes. A further centrifugation step is used to remove large cell debris and unbroken cells, before ultracentrifugation to obtain membrane vesicles. The membrane pellets are resuspended using a homogeniser. VcINDY protein is then extracted from the membrane pellet suspensions by solubilisation using 1% DDM (aqueous phase). This soluble fraction is then incubated with TALON resin containing Cobalt ions. The resin is then washed using low concentrations of imidazole. Bound protein is eluted whilst the affinity tag is simultaneously cleaved using trypsin. (Created with BioRender.com)

The his-tag of expressed proteins contains imidazole groups that have a great affinity for Nickel and Cobalt ions. Here, were purified VcINDY proteins containing a His-tag using immobilised metal affinity chromatography (IMAC) using Cobalt ions. Cobalt ions bind to the his-tagged protein with high affinity. Wash buffers contain imidazole which washes away the protein bound to the resin. Only proteins with his-tag, the primary one being VcINDY, remain attached to the resin.

3.1.2. CLEAVAGE OF THE His-TAG

The his-tag of VcINDY is formed by 10 Histidines followed by a TEV-protease (*Tobacco Etch Virus Protease*) section linked to the protein sequence. The TEV-protease contains an arginine, as the last amino acids before the protein, but in a later modification Mancusso *et al.*, added a Lysine just before the start of the protein sequence (*Figure 3.1*). Trypsin is a serine protease that recognizes arginine (R) and Lysine (K) and generally cleaves peptide chains at the carboxyl side of those amino acids. Therefore, purified VcINDY proteins are obtained by incubating the protein-bound resin with trypsin and collecting the protein that is eluted.
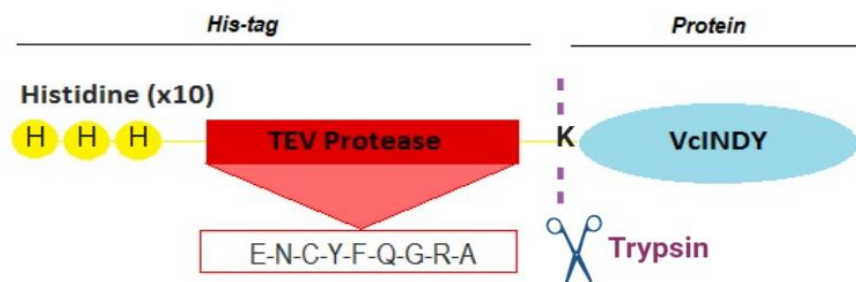

Figure 3.1: **Representation of his-tagged VcINDY and trypsin mechanism.**

VcINDY his tag is formed of 10 histidine (yellow), followed by a TEV protease(red) and finally, the VcINDY protein (blue). The amino acids of the end section of TEV protease are described. Trypsin recognises the Lysine located next to the start of the protein sequence and separates the His-tag from VcINDY.

3.1.3. QUANTITY AND PURITY PURIFICATION

The eluted protein is analysed using SDS electrophoresis gel to assess the purity and quantity obtention of VcINDY by using absorbance A280. The dimer size of VcINDY is approximately 112 kDa but only a band at 35KDa is visible in all the gels containing VcINDY. VcINDY proteins are split out into two monomers of ~50 kDa each due to the presence of SDS detergent in the gel. As VcINDY is a membrane protein, it is thought to not be fully unfolded in SDS detergent and as with most membrane proteins, VcINDY does not run true to its MW (molecular weight) on an SDS-PAGE. Therefore, the proteins monomers are more compact, run faster and, the band for VcINDY comes at 35 kDa when elution buffers are analysed.

For this study, thirteen single-mutant proteins and a single triple alanine mutant for the best-conserved amino acids (SNT) were created (*Figure 2.0*). VcINDY wild-type and alanine mutant I149A gels were run (*Figure 3.2*). Wild-type VcINDY appears at the mentioned 35 kDa band (*Figure 3.2-A*), whereas, I149A does not show the expected band (*Figure 3.2-B)*. Thus, I149A mutant could not be expressed and purified probably because the mutation compromises protein stability. The presented band for I149A could be due to contamination. Thus, I149A mutant does not express. The other mutants of the study were produced following the same guides as VcINDY wild-type. Further gels of each mutant are shown in Appendix B (*Supplementary figures 6.2.1*). The wild-type gel shown here is representative of the other mutants.
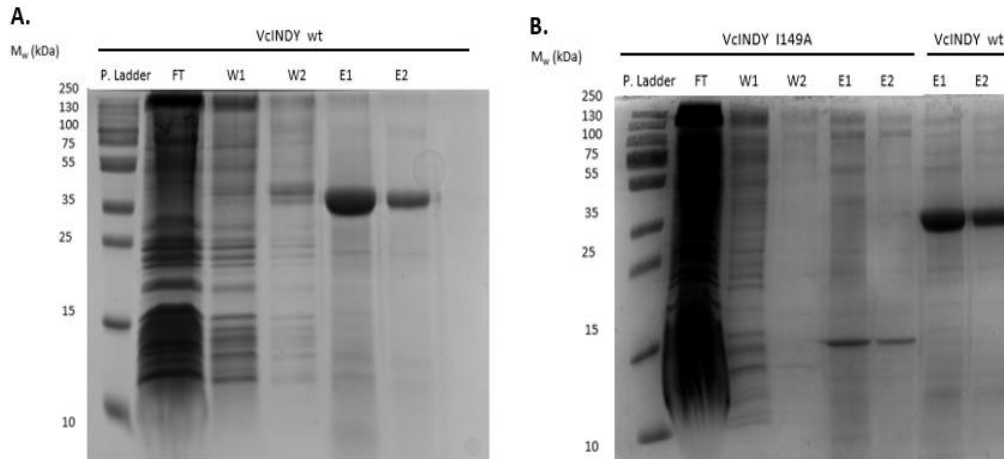
Figure 3.2: **SDS-PAGE analysis of VcINDY purification and I149A.**

A) Purification gel of wild type VcINDY. Isolated VcINDY proteins appear in E1 and E2 **B)** Purification gel of I149A, an alanine mutant that could not be expressed and purified. E1 and E2 of wild type are present as controls. In order. the first column is the protein ladder (P. Ladder), Flow-through (FT), Wash buffer one (W1), Wash buffer two (W2), Elution buffer one (E1) and, Elution buffer two (E2). Columns of E1 and E2 with a band at 35 kDa indicate the presence of VcINDY protein.

3.2. FOUNDATIONS OF THE THERMOFLUOR ASSAY

3.2.1. THEORETICAL FRAME OF CPM ASSAY

It is well known that the melting point (Tm) of proteins is higher when a ligand is bound due to an increase of chemical interactions, requiring more thermal energy to break bonds and denature the protein. One way of measuring membrane proteins' stability is by observing the melting point of the protein when exposed to increasing temperatures.

The melting temperature is a good way of determining protein:ligand interactions. Thermofluor assay or CPM assay is a quick technique based precisely on membrane protein stability by melting temperature (Tm) observation. In this study, the CPM assay is used to observe plausible interactions between VcINDY and anionic ligands. But first, foundations of the Thermofluor assay with CPM were

established to corroborate its fitting approach for the eventual goal of the project; have a better understanding of VcINDY binding selectivity.

Here, proteins are detergent-solubilized in a buffer containing CPM dye which binds to the thiol group of cysteines (Alexandrov et al., 2008). Wild-type VcINDY possesses three endogenous cysteine residues: 331 from TM9a, 413 from TM10a, and 449 from TM11a. Based on the crystal structure, C413 and C449 are located in the HP2 of the transport domain whereas C331 is located in the oligomerization domain. Upon protein temperature-induced unfolding, the cysteines of the VcINDY get unburied (Alexandrov *et al.,* 2008). When the CPM can bind to the cysteines, it emits a higher level of fluorescence (Wang *et al.,* 2015) (*Figure 3.3*). An increase of fluorescence should be seen with temperature due to the exposition of the cysteines (*Figure 3.3-A*). By taking the derivative (dF/dT) of such reading, which is the rate of change of fluorescence with time, the melting point of the protein should be found (*Figure 3.3-B).* Protein's stability can increase when a substrate or inhibitor is bound. The melting point would differ whether a ligand of VcINDY is present (*Figure 3.3-C, D*).

Calibration controls were carried out to demonstrate that only a single melting point of VcINDY wild-type appears when the dye and the protein are present (*Supplementary Figure 6.2.2*). As expected, a single melting curve in the calibration controls was exclusively seen when CPM dye and protein were presented (*Supplementary Figure 6.2.2-C).* Tests were carried out so there were controls of no buffer only, CPM dye only and protein only CPM-experiments. Pairs of buffer, dye and protein were also checked to demonstrate the veracity of the study assay.
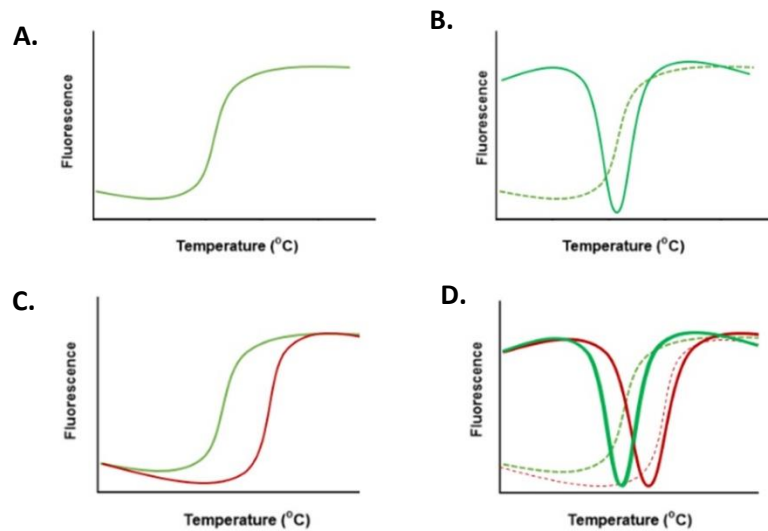
Figure 3.3: **Thermofluor assay foundations' representation in ligand presence or absence.**

A) Cartoon of the increase in fluorescence as the proteins gets unfolded and CPM can bind to the now uncovered cysteines. **B)** Cartoon of the derivative dF/dT of the fluorescence in A. **C)** Cartoon showing the differences in fluorescence reading between protein without a ligand (green) and a ligand-bound protein (red). **D)** Derivative curves of the situation C. Melting curves appear in higher temperatures according to a higher number of interactions with the ligand that give more protein stabilization.

3.2.2. TESTING BINDING-SITE SPECIFIC INTERACTIONS BETWEEN TRANSPORTER AND LIGAND

To confirm specific binding interaction happening on the CPM assay, VcINDY thermostability was tested in the presence of succinate. The melting point of wild-type VcINDY without the presence of any compound was established. The melting temperature of VcINDY is reliable and it normally comes around 53 °C when the protein is in its apo state (*Figure 3.4)*. In the presence of 5 mM substrate, the melting point increases by 8 °C. When VcINDY does not have anything bound, it is less stable and it melts at lower temperatures, whereas, in the presence of succinate, more bonds are generated between protein and substrate and it has a melting point at 61 °C (*Figure 3.4*-A).

This methodology demonstrates interactions between protein and ligand. It could be used to witness substrate selectivity by observing changes on the melting point. Yet, a triple alanine mutant was tested to further validate those ligand interactions observed in wild-type were specific with the protein and responsible for its stabilization, instead of some non-specific interactions (*Figure 3.4*).

SNTAAA is a VcINDY mutant that has three critical binding-site amino acids changed for a neutral alanine. Those amino acids are S150, N151 and T152 of the functionally important and conserved SNT motif accordingly to the crystal structure (Nie *et al.*, 2017). As a result, SNTAAA should not be capable of transporting nor binding succinate (*Figure 3.5)*.
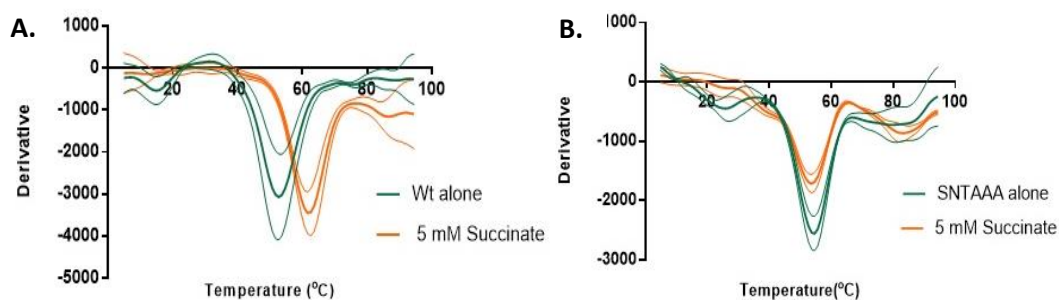

***Figure 3.4:* Validation of specific substrate-protein induced interactions with VcINDY wt and triple mutant.**

A) Derivative curve of VcINDY wild type in the presence of 5 mM succinate (orange) or alone (green) **B)** Derivative curve of SNTAAA VcINDY in the presence of 5 mM succinate (orange) or alone (green). Measures were taken as triplicates with each protein and condition. Mean is represented as the ticker line.

From the data plotted, in the absence of succinate the Tm of SNTAAA protein is similar to wildtype Tm, suggesting that the introduction of these mutations into the substrate-binding site did not compromise VcINDY's stability (*Figure 3.4*). On the contrary of wild-type VcINDY, SNTAAA mutant did not exhibit any increase in melting temperature when 5 mM of succinate was present (*Figure 3.4-B)*. These

data confirm that the previous shifts in the melting temperature of wild-type VcINDY were caused thanks to specific interactions between amino acids in the binding site and succinate.

3.3. OPTIMIZATIONS OF THE THERMOFLUOR ASSAY

Once VcINDY ligand's interaction was proven to be observable, a sequence of optimizations was performed before proceeding to study the interaction between a diverse range of ligands and alanine protein mutants. The determination of optimal protein, substrate and DDM detergent concentration was achieved by using wild-type VcINDY. The set of conditions that conferred a better melting temperature curve for the study were selected. The best sodium concentration was 50 mM as estimated previously in other studies (C.D.D. Sampson and C. Mulligan, Unpublished data).

3.3.1. EFFECT OF DIFFERENT PROTEIN CONCENTRATIONS ON THE MELTING TEMPERATURE OF VcINDY

To test the effects of protein concentrations variations, CPM assays with wild-type VcINDY in the following concentrations were tested: 0 mg/ml, 0.05 mg/ml, 0.1 mg/ml and 0.2 mg/ml (*Figure 3.5*).

As expected, without protein there was no melting point (*Figure 3.*5-A). The 0.05 mg/ml concentration seemed insufficient to obtain melting curves with high amplitude, but enough to peek at a minimal curve due to the presence of protein (*Figure 3.5-B*). Between 0.1 mg/ml and 0.2 mg/ml (*Figure 3.5-C, D, respectively*), the best melting curve with the highest amplitude happen with protein

concentration of 0.2 mg/ml. The melting curves for 0.1 mg/ml and 0.2 mg/ml

concentrations were observed with 5 mM of succinate and alone (*Figure 3.5-E, F,*

respectively). In the 0.2 mg/ml the amplitude of the curve had a better signal-to-

noise ratio than 0.1 mg/ml concentration. It showed as well to be more suitable

for observing differences between the presence and absence of substrate (*Figure*

3.5- F). Consequently, the protein concentration of 0.2 mg/ml was selected for all

the studies.
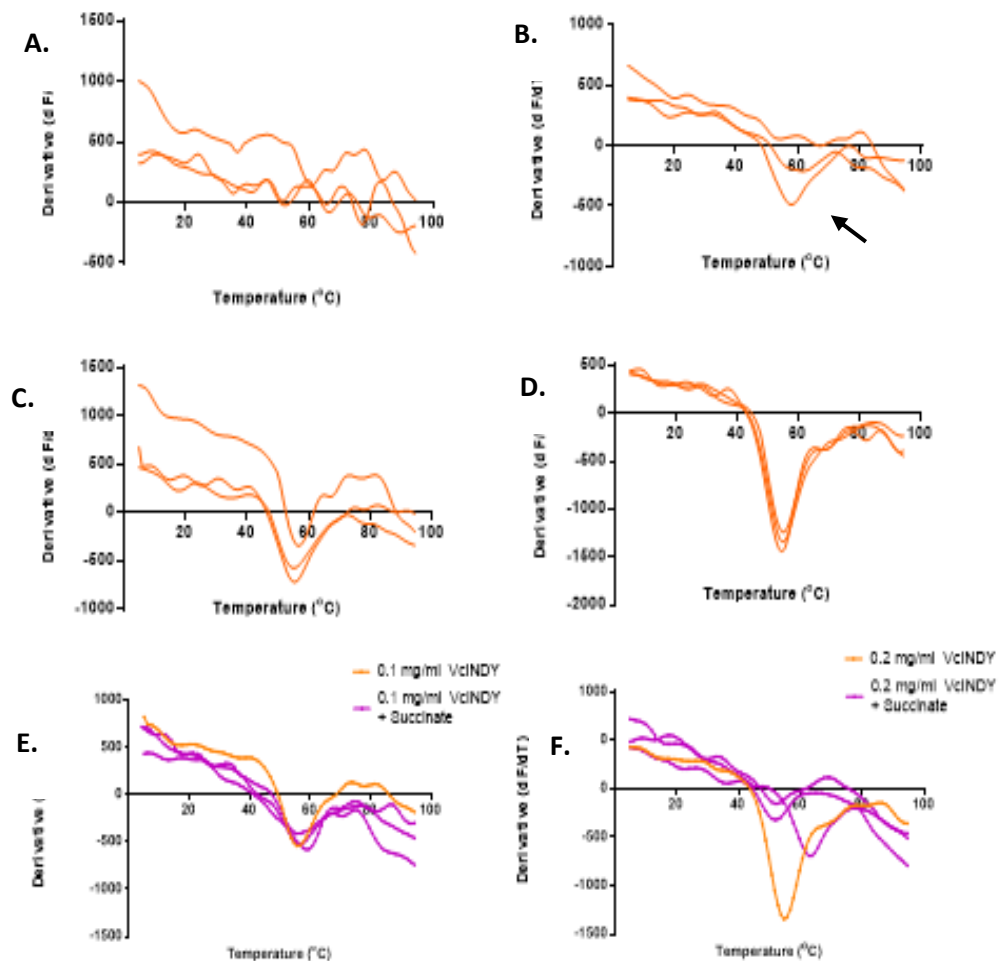
Figure 3.5: **Effect of different protein concentrations on the Tm of VcINDY.**

Graphs represent the derivative curve in the presence of different protein concentrations: **A)** without VcINDY protein **B)** 0.05 mg/ml of VcINDY **C)** 0.1 mg/ml of VcINDY **D)** 0.2mg/ml of VcINDY. The concentrations of 0.1 and 0.2 were further tested in the presence of 5 mM succinate (purple) or alone (orange). Graphs **E** and **F** represent the derivative curve of 0.1 mg/ml and 0.2 mg/ml of VcINDY, respectively. Measures were taken as triplicates for each protein concentration and condition. Mean is represented as the ticker line.

3.3.2. EFFECT OF DIFFERENT DETERGENT CONCENTRATIONS ON THE MELTING TEMPERATURE OF VcINDY

DDM is a common non-ionic membrane detergent that prevents protein aggregations once they are removed from the lipid environment. The critical micelle concentration (CMC) of DDM is 1.7 x10^{-4} mM. Above this concentration, micelles are spontaneously formed, but if it is too high detergent-protein complexes are generated free from lipids (Hutchison *et al.*, 2017). Below the CMC, detergent resides at the aqueous interface without resulting in micelles.

As VcINDY is a hydrophobic membrane protein, the assembly of micelles is necessary to maintain protein structure. Therefore, to test the effect of the solution detergent a set of CPM assays with wild-type VcINDY in the following concentrations were tested: 0.001 %, 0.1 %, 0.5 %, and 1 % (*Figure 3.6*). The melting curves for each concentration were observed with 5 mM of succinate and absence of it.

It was not surprising that cleaner melting curves become visible when buffer contains higher percentages of detergent DDM (*Figure 3.6-C, D*). Although 0.1 % DDM showed a bigger difference between conditions, repetitions were needed to accomplish well-defined curves. Based on this data, 1 % of DDM was decided to be used throughout this study since it gives better a signal-to-noise curves.
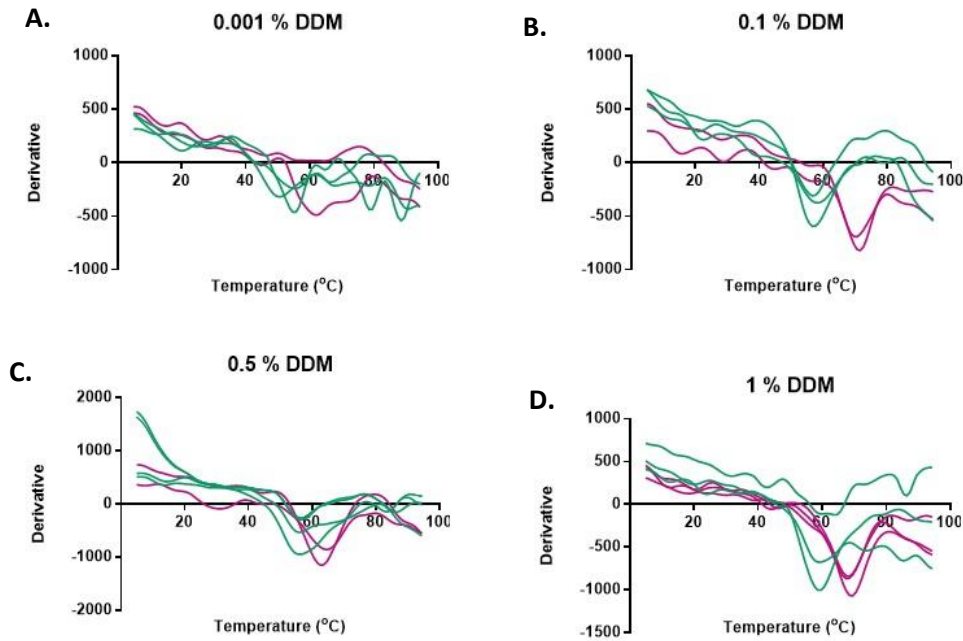
Figure 3.6: **Effect of the detergent concentration on the Tm of VcINDY.**

Graphs represent the derivative curve of VcINDY in the presence of 5 mM succinate (purple) or alone (green**)** and **A)** 0.001 % DDM. **B)** 0.1 % DDM. **C)** 0.5 % DDM. **D)** 1 % DDM. Measures were taken as triplicates for each protein concentration and condition. Mean is represented as the ticker line.

3.3.3. EFFECT OF DIFFERENT SUBSTRATE CONCENTRATIONS ON THE MELTING TEMPERATURE OF VcINDY

The binding of substrates provides VcINDY with higher thermostability in CPM assays. To test the optimal substrate concentration, the melting temperature (Tm) of VcINDY in the presence of different concentrations of two known substrates, succinate and fumarate, was determined. The Km for succinate is 1.0 ± 0.2 µM (Mulligan *et al.*, 2014). To observe the thermostability of VcINDY, the protein was tested with higher amounts of succinate than the Km, which were: 1 mM, 5 mM and, 10 mM. The same concentrations were applied for the fumarate test, which is the second most efficient transported substrate after succinate (Mulligan *et al.*, 2014).

Within all these concentrations, a clear melting curve resulted from the binding between wild-type VcINDY and the substrate *(Figure 3.7)*. Therefore, an increase in VcINDY thermostability was visible in succinate and fumarate presence (*Figure 3.7- A, B, respectively*). The amplitude of the derivative curves is higher with a maximum concentration of 10 mM, probably due to a saturation of the transporters. As a result, 10 mM was the substrate concentration decided to test any further ligands of the study.
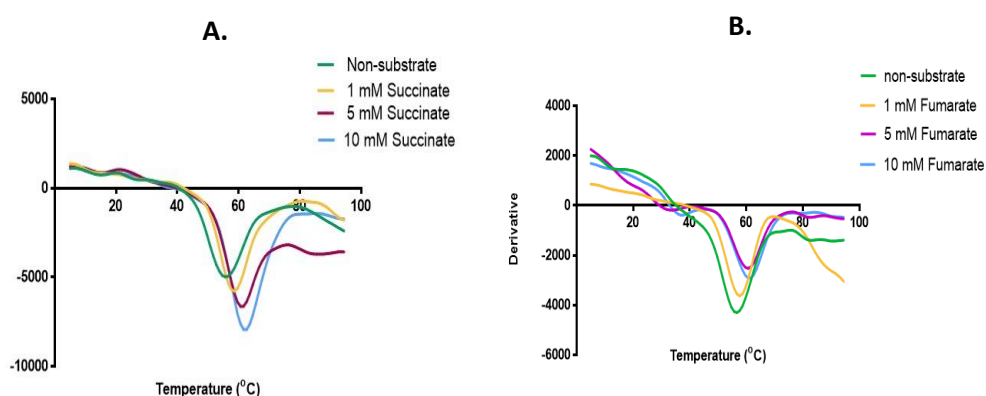

Figure 3.7: **Effect of different substrate concentrations on the Tm of VcINDY.**

A) VcINDY Tm derivative curves of succinate in increasing concentrations**. B)** VcINDY Tm derivative curves of fumarate in augmenting concentrations. Single measures were taken for each protein concentration and condition.

3.4. SCREEN OF SUBSTANTIAL SUBSTRATES FOR VcINDY

3.4.1. SELECTION OF COMPOUNDS FOR THE THERMOFLUOR ASSAY APPROACH

To test the hypothesis that some amino acids on VcINDY may play critical roles for substrate recognition, a sequence of different compounds were used to assess changes in VcINDY's selectivity.

The library of anionic compounds selected was: succinate (4C), oxalate (2C), oxalacetate (4C), fumarate (4C), malate (4C), citrate (5C), tricarballyate (5C),

icatonic acid (4C), 5'-sulfosalisilic (C7) and adipate (6C). The molecule's structure of these compounds is displayed on Appendix B (Supplementary *Figure 6.2.3*)

Succinate and oxalate were included as positive and negative substrate controls, respectively. Succinate is the transporter's best-known substrate while oxalate has not been described to get bound the VcINDY, neither being transported. Fumarate, oxalacetate and malate were selected as they could be transported by VcINDY (Mulligan *et al.*, 2014). Citrate was added to the library as it interacts within a known way at the protein's binding-site, offering VcINDY thermostability (Mancusso *et al.*, 2012). Finally, tricarballyate, icatonic acid, 5'-sulfosalisilic and adipate, were selected accordingly to their positive stabilization effect in previous Thermofluor assay studies (C.D.D. Sampson and C.Mulligan, Unpublished data).

3.4.2. SUCCINATE THERMOSTABILITY EFFECT CONTRAST IN DIFFERENT ALANINE MUTANTS

If substrate selectivity variation can be induced by mutations in specific locations, it is sought to observe differences between VcINDY mutants in the presence of the same ligand. To test this, the thermostability of VcINDY wild-type and mutants in the presence of succinate was analysed following a CPM assay. The melting point of the VcINDY proteins with or without succinate was ascertained (*Figure 3.8*).

In line with previous findings, the melting temperature shift (ΔTm) of wild-type was of 8 $^{\circ}$C. Single-alanine mutants tested in the presence of succinate showed a

ΔTm higher (D319A, V322A, F100A, V66A), lower (SNTAAA, I96A, T152) or similar (T67A, N151A, S290A, F326A) than wild-type. The results also revealed variation on the baseline of each mutant (*Figure 3.8*). Hence, changes in the amino acid sequence can provoke changes in the number of bonds inside the protein, which ultimately affects protein's stability.
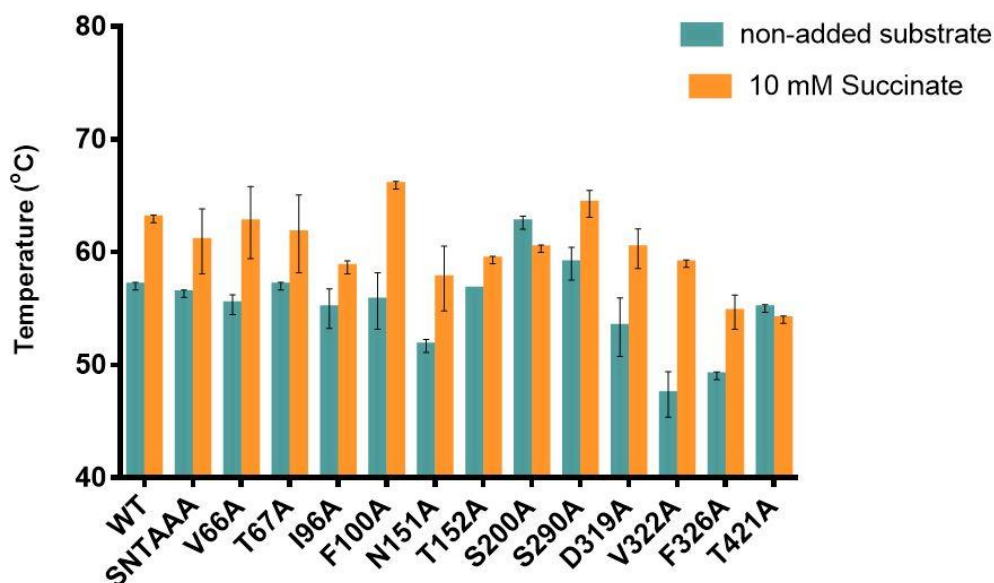

Figure 3.8: **Melting temperature variation of VcINDY wild-type and alanine-mutants**

Bars represent the melting temperature of VcINDY accomplished in the presence of 10 mM succinate (orange) and without added substrate (blue). Baselines differ between proteins due to differences in their thermostability. Measures were taken as triplicates for each protein type and condition. Mean and SEM are both represented.

However, despite discrepancies at their thermostability baseline, mostly all had an increase in thermostability in the presence of 10 mM succinate (*Figure 3.8*). Only in two cases, S200A and T421A, the protein in the absence of substrate were equally or more stable when succinate was not added. This could be due to increased hydrophobic interactions within the protein when an alanine substitutes a serine or a threonine in such positions. However, it remains unclear to which degree these baseline differences are attributed to changes in the protein structure caused for alanine mutations or undesired experimental variations.

Therefore, any ligand effect has been compared to the baseline of the same experimental set to avoid experimental disparity between days when analysing the data.

3.4.3. SUMMARIZED OUTCOMES OF THE THERMOFLUOR ASSAY APPROACH

All the experiments were performed within the constant presence of 1% DDM, 50 mM sodium and 2 mg/ml of protein, and either with 10 mM of a testing compound or not (unless indicated otherwise).

This section has the aim to summarise the findings and contributions made in this study regarding alanine mutant's changes in compound selectivity. Hence, two summarized tables of the ΔTm and statistical values of wild-type and alanine mutants are presented subsequently *(Table 3.1* and *Table 3.2)*.

The melting temperature shift (ΔTm) of VcINDY were calculated from the difference between the Tm in the presence of the compound and the Tm in the absence of it. All data analysis was conducted in the same way for any subsequent CPM assays. Importantly, as shown on the tables, statistical values were significant in most of the alanine mutants tested. Variation in individual thermostability among mutants is visible, as well as, melting temperature shifts depending on the ligand added. Ligands offering a better thermostability to the mutants are presented on top while ligands with lower thermostability effect are at the bottom of the tables. Hence, by observation of the gathered results, we could agree that the best recognised substrates are succinate, followed by malate, fumarate and 5'-sulfosalisilic acid.

In addition, these results broadly confirm that CPM assay is a high-quality choice for determining substrate selectivity allowing screening of different candidates for VcINDY transporters.

Melting temperature shift in the presence of substantial substrates for VcINDY wild-type, SNTAAA, V66A, T67A, I96A, F100A and N151A

Mutant/ Substrate	Wildtype	SNTAAA	V66A	T67A	I96A	F100A	N151A
Alone	54,76 ± 2,19	53,60 ±1,60	53,60 ± 1,31	57,04 ± 0,89	53,57 ± 1,58	54,76 ± 1,59	51,78 ± 0,59
Succinate	8± 0,00	1,3± 0,81	8± 0,47	8± 0,47	1,3± 0,81	4± 0,47	-0,3± 0,00
	P. Value: 0,000	P. Value: 0,275	P. Value: 0,000	P. Value: 7,1E-05	P. Value: 0,275	P. Value: 0,001	P. Value: 0,374
Malate	4± 0,00	1± 1,40	4± 0,47	4,3± 0,81	3±1,24	8,6± 0,00	0,6± 0,94
	P. Value: 0,002	P. Value: 0,551	P. Value: 0,001	P. Value: 2,9E-03	P. Value: 0,033	P. Value: 0,000	P. Value: 0,374
Fumarate	4± 0,81	1,6± 0,47	4,6±1,24	4± 0,94	-0,6± 0,81	1± 0,47	0,3± 0,47
	P. Value: 0,008	P. Value: 0,148	P. Value: 0,008	P. Value: 5,8E-03	P. Value: 0,561	P. Value: 0,101	P. Value: 0,374
5'-Sulfosalisilic Acid	4± 0,81	-0,2± 0,50	2± 0,00	-0,6± 0,81	1,6± 0,47	1± 0,47	1,3± 0,47
	P. Value: 0,013	P. Value: 0,698	P. Value: 0,000	P. Value: 3,7E-01	P. Value: 0,024	P. Value: 0,348	P. Value: 0,016
Adipate	2,3± 0,47	1,3± 0,00	3± 0,47	1,7± 0,90	-1,3± 0,47	-2,3± 0,47	-0,6± 0,47
	P. Value: 0,025	P. Value: 0,204	P. Value: 0,003	P. Value: 3,5E-01	P. Value: 0,230	P. Value: 0,008	P. Value: 0,116
Tricarballylate	2,6± 0,47	2,6± 0,47	3± 0,81	3± 0,68	1,6±0,47	1± 0,47	0± 0,81
	P. Value: 0,016	P. Value: 0,047	P. Value: 0,007	P. Value: 3,9E-04	P. Value: 0,024	P. Value: 0,101	P. Value: 1,000
Icatonic Acid	1,3± 0,47	0,6± 1,24	1,3± 0,00	0,3± 0,00	1,3± 0,00	3,3± 0,47	0,3± 0,47
	P. Value: 0,116	P. Value: 0,467	P. Value: 0,016	P. Value: 3,8E-01	P. Value: 0,016	P. Value: 0,230	P. Value: 0,374
Oxalacetate	1± 0,00	2± 0,47	2± 0,00	2± 0,81	0,6± 0,47	0± 0,47	-0,3± 0,00
	P. Value: 0,000	P. Value: 0,101	P. Value: 0,000	P. Value: 2,6E-02	P. Value: 0,230	P. Value: 0,999	P. Value: 0,374
Citrate	-0,6± 0,47	0,3± 0,47	0,3± 0,00	-1,3± 0,47	-2± 0,94	-0,6± 0,47	1,3± 0,94
	P. Value: 0,373	P. Value: 0,519	P. Value: 0,000	P. Value: 4,7E-02	P. Value: 0,251	P. Value: 0,519	P. Value: 0,148
Oxalate	-1,3± 0,47	1,3± 0,81	-0,6± 0,00	-5,3± 0,47	-0,3± 1,24	-2,6± 0,47	0± 0,81
	P. Value: 0,116	P. Value: 0,274	P. Value: 0,116	P. Value: 3,5E-04	P. Value: 0,741	P. Value: 0,005	P. Value: 0,999

Table 3.1: **Melting temperature shift effect of VcINDY wild-type and mutants in the presence of the compounds of the study.**

Table representing the melting temperature shift (ΔTm) of VcINDY wild-type, SNT1AAA and single alanine-mutants V66A, T67A, F100A and N151A. ΔTm is represented as a mean together with its standard deviation (blue squares). Below each condition and ΔTm, the p-values are noted. This statistical value was subtracted by comparing the triplicated results of VcINDY protein without substrate as a baseline and the protein with the corresponding ligand. Ligands are ordered by thermostability increase produced on the proteins tested, being succinate the best recognised and oxalate the worse.

Melting temperature shift in the presence of substantial substrates for VcINDY T152A, S200A, D319A, V322A, F326A and T421A

Mutant/ Substrate	T152A	S200A	S290A	D319A	V322A	F326A	T421A
Alone	56,67± 0,54	62,31± 1,64	55,84 ± 2,15	51,26 ± 1,49	50,37± 2,21	49,32± 1,43	55,84± 0,83
Succinate	4± 0,47	0 ± 0	6,3± 0,47	8,6± 0,81	7± 0,94	8,9± 0,50	-1± 0,47
	P. Value: 0,013	P. Value: 1	P. Value: 4,5E-05	P. Value: 0,000	P. Value: 0,001	P. Value: 0,006	P. Value: 0,101
Malate	-1± 0,47	-3,3± 0,47	3,6± 1,24	8,6± 0,81	3,3± 0,47	2 ± 2,48	-1± 0,47
	P. Value: 0,349	P. Value: 0,008	P. Value: 1,4E-02	P. Value: 0,000	P. Value: 0,002	P. Value: 0,485	P. Value: 0,101
Fumarate	0,6± 0,47	-0,3± 0,47	4,6± 0,47	8± 3,38	2,3± 0,47	5± 1,24	-1,6± 0,47
	P. Value: 0,518	P. Value: 0,644	P. Value: 1,5E-04	P. Value: 0,030	P. Value: 0,091	P. Value: 0,027	P. Value: 0,067
5'-Sulfosalisilic Acid	1,6± 0,00	-1,3± 0,00	2,3± 0,47	8,3± 0	-0,3± 0,94	3± 1,69	0,6± 0,00
	P. Value: 0,007	P. Value: 0,016	P. Value: 2,2E-03	P. Value: 0,000	P. Value: 0,795	P. Value: 0,174	P. Value: 0,116
Adipate	0,6± 0,47	-1,7± 1,24	3,6± 0,47	6,3± 0,47	0,6± 0,00	3,3± 1,24	-1± 0,47
	P. Value 0,519	P. Value: 0,152	P. Value: 3,9E-04	P. Value: 0,000	P. Value: 0,116	P. Value: 0,067	P. Value: 0,101
Tricarballyate	0,6± 0,47	-2.6± 0,47	3,6± 0,00	6± 0,47	2± 0,47	0,8± 2,04	-0,6± 0,47
	P. Value: 0,519	P. Value: 0,001	P. Value: 3,9E-04	P. Value: 0,000	P. Value: 0,101	P. Value: 0,692	P. Value: 0,230
Icatonic Acid	0,6± 0,94	-2,7± 0,47	1,3± 0,47	5 ± 0,94	1± 0,47	1,1± 0,94	-1± 0,47
	P. Value: 0,580	P. Value: 0,005	P. Value: 4,7E-02	P. Value: 0,003	P. Value: 0,101	P. Value: 0,302	P. Value: 0,101
Oxalacetate	0± 0,47	-1± 0,00	1± 0,81	2,6± 1,24	0± 0,94	0,3± 1,69	-1± 0,47
	P. Value: 0,999	P. Value: 0,000	P. Value: 1,6E-01	P. Value: 0,047	P. Value: 1,000	P. Value: 0,842	P. Value: 0,101
Citrate	1± 0,47	-5,2± 0,47	5,4± 0,50	0± 0,47	-1,7± 1,72	0,2± 1,69	-1,3± 0
	P. Value: 0,349	P. Value: 0,001	P. Value: 6,7E-04	P. Value: 1,000	P. Value: 0,124	P. Value: 0,923	P. Value: 0,016
Oxalate	-1,3± 0,94	-2,65± 0,47	-0,3± 0,47	1 ± 0.81	-1± 0,94	8± 1,87	-1,3± 0,00
	P. Value: 0,294	P. Value: 0,001	P. Value: 3,7E-01	P. Value: 0,643	P. Value: 0,251	P. Value: 0,019	P. Value: 0,053

Table 3.2: **Melting temperature shift effect of VcINDY mutants in the presence of the compounds of the study.**

Table representing the melting temperature shift (ΔTm) of VcINDY single alanine-mutants of T152A, S200A, S290A, D319A, V332A, F326A and T421A. ΔTm is represented as a mean together with its standard deviation (blue squares). Below each condition and ΔTm, the p-values are noted. This statistical value was subtracted by comparing the triplicated results of VcINDY protein without substrate as a baseline and the protein with the corresponding ligand. Ligands are ordered by thermostability increase produced on the proteins tested, being succinate the best recognised and oxalate the worse.

3.5. COMPOUND SCREEN WITH ALANINE VcINDY MUTANTS REVEAL DIFFERENCES IN LIGAND'S SELECTIVITY

In this section, all the experimental results from the data collection outlined on the previous (*Section 3.4.3),* are presented and examined in detail for all individual VcINDY transporters tested.

A bar chart representing the mean of the melting temperature shift from all 10 compounds of the library of this study is presented for each protein analysed. For clarity, the results will be presented according to the location of the mutations in the protein's structure.

In addition, the raw data of the readings are shown for better comprehensibility. This untouched data may be found in Appendix B (*Supplementary Figures 6.2.4-6.2.16)*

3.5.1. ASSESSING BINDING SELECTIVITY OF VcINDY WILD-TYPE

The 10-compound screen was first accomplished with the VcINDY wild-type to establish the protein's natural binding selectivity. VcINDY wild-type CPM assay was carried out in the presence of 1 % DDM, 50 mM Na$^+$ and 2 mg/ml of protein, in addition to the absence or presence of 10 mM of a compound of the study. The results present the melting temperature shifts of wild-type for one and each library's ligands, together with the normalised melting curves graphs (*Figure 3.9*).

Remarkably, succinate, fumarate, 5'-sulfosalisilic acid and malate create the higher stabilization among all ligands (*Figure 3.9*). Out of the four of them, succinate is providing the highest stabilisation, with 8 °C of melting temperature shift between conditions. Succinate stabilisation is followed by fumarate, malate and 5'-sulfosalisilic acid with 4 °C melting temperature shift (*Table 3.1*).

In the case of oxalacetate, despite it has four carbons and it has been described as a substrate of VcINDY, its stabilisation effect was of 1 °C, similar to icatonic acid's. However, because of the lack of statistical significance positivity, icatonic acid thermostability effect on VcINDY will not be commented on further (*Table 3.1*).

Tricarballyate and adipate are larger ligands that have a great thermostability effect but less than four-carbon ligands (*Figure 3.9*). Interestingly, citrate, another five-carbon ligand of the study with a similar structure to tricarballyate, did not offer VcINDY stabilisation (*Figure 3.9*).
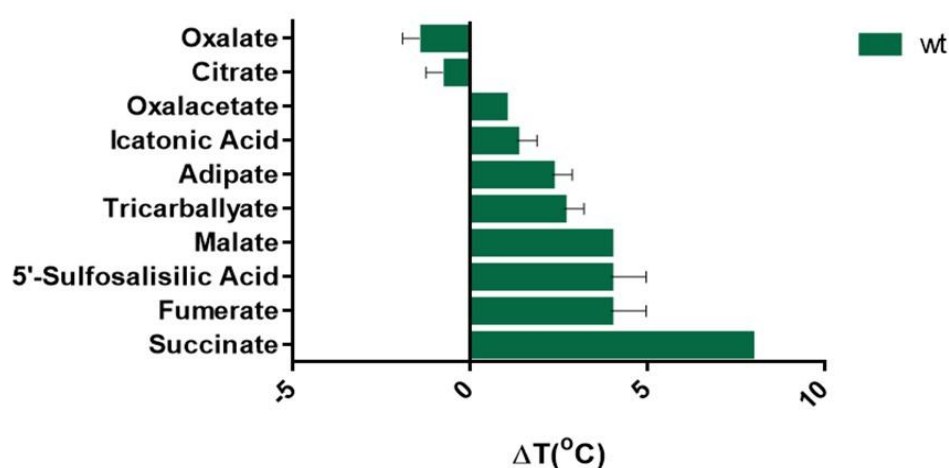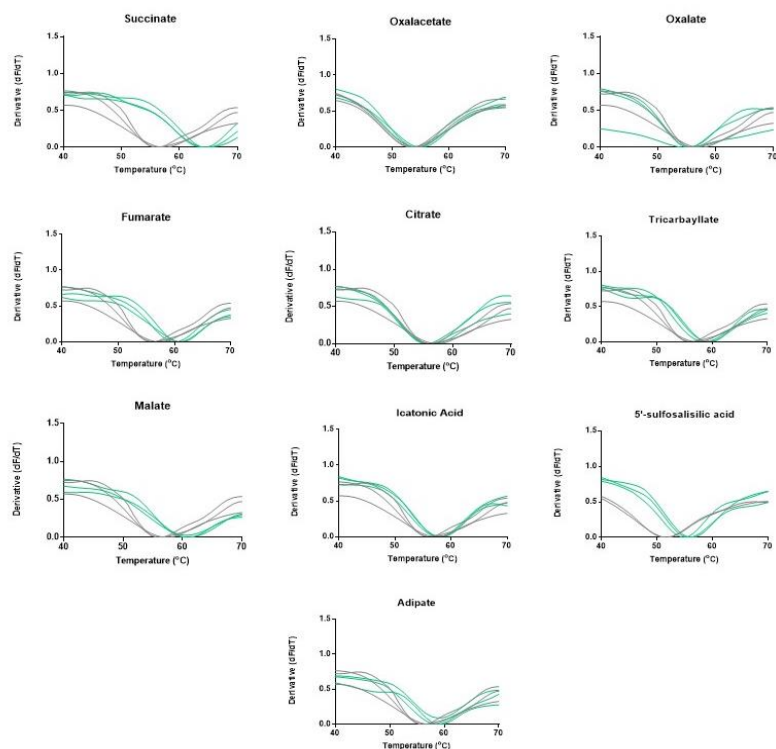

(Figure continues on next page)

Figure 3.9: **10 compounds thermostability screen using VcINDY wild-type.**

Average melting temperature shift (ΔTm) of VcINDY in the presence of each compound was determined by subtracting the VcINDY Tm in the absence of substrate from the Tm in the presence of the indicated compound. Observation of the transporter stabilisation was measured in the presence of 50 mM Na$^+$. Data are organised by the compounds that increased stability at the bottom and the compounds that induced destabilisation at the top. Results are shown in graphs representing normalised melting curves from the derivative of the untouched data of VcINDY wild-type, in 10 mM of the indicated compound above or in its absence (grey). Each line represents a single outcome of the triplicated data.

Overall, these results tie well with previous studies wherein competition transport assays demonstrate that VcINDY substrate selectivity is dependent on the chain length (Mulligan *et al.*, 2014). Therefore, the transporter has a preference for ligands of four carbons such as succinate (4C), malate (4C) and fumarate (4C) probably because they can be easily recognised by the protein. For the same reason, oxalate has a carbon chain too short to be recognised by critical elements on the protein's binding-site (Mulligan *et al.*, 2014).

Modest stabilisation was observable from ligands with six and five carbons, as adipate(6C) and tricarballyate (5C), which is in line with previous studies where these substrates were able to provide with some stabilisation (C.D.D. Sampson and C. Mulligan, Unpublished data). Larger compounds such as 5'-sulfosalisilic acid (7C) should not offer stabilisation. Here, the VcINDY's melting temperature shift of 5'-sulfosalisilic acid did not match with what could have been predicted accordingly to VcINDY carbon-length filter. Observation of the oxalacetate's and icatonic acid's stabilisation effect leads to more discrepancy. They are four-carbon chain compounds, but they provided VcINDY with less stabilisation than other 4C-ligands tested.

3.5.2. ASSESSING BINDING SELECTIVITY OF VcINDY MUTANTS OF THE SUBSTRATE-BINDING AND SODIUM-BINDING SITE

The binding-site where substrate gets bound involves residues from HPin, TM5, HPout and, TM10 (Nie *et al.*, 2017). Bound succinate seems to form bonds with N151 and T152, with one of its carboxylate groups, and S377 and N378, with another of succinate's carboxylate group. Succinate interacts as well with S200A and T421 through the formation of H-bounds. As mentioned before, both sodium binding sites are coordinated with key amino acids, such as the asparagine in position N151 (Mancusso *et al.*, 2012) (Nie *et al.*, 2017).

To cast some light on why this variance is present within different compounds and to keep with our goal to detect important amino acids, amino acids related to the binding site were mutated to alanine. Alanine has an aliphatic functional group, which means that it can be located inside or outside the protein structure.

Here, alanine mutants SNTAAA, N151A, T152A, S200A and T421A were tested for the examination of ligand's selectivity by determining ΔTm with CPM assays (*Figure 3.10*). Alanine mutants of S377, N378 and I149A were not possible to create, which suggests that these positions may be critical for protein's assembly and structure.
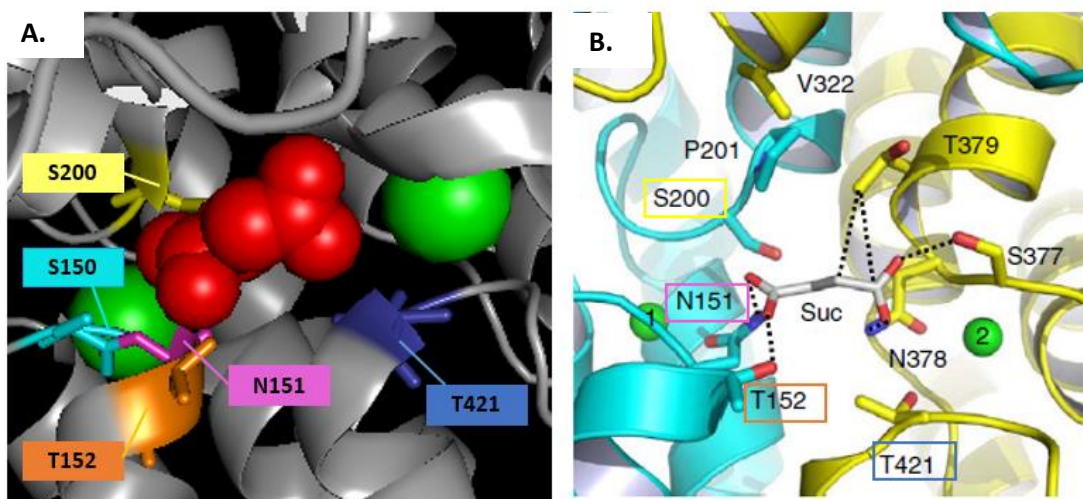

Figure 3.10: **Representation of tested amino acids located near the binding site in the VcINDY crystal structure at the inward-facing state.**

Representation of the amino acids locations N150 (light blue), N151(pink) and T152 (orange) from the SNT motif, and S200 (yellow) and T421 (dark blue), in (**A**) a 3D model taken from a PyMOL file of the VcINDY inward-facing state from Mancusso *et al.,* 2012 (**B**) a drawing representation taken from (Nie *et al.,* 2017). In both images, sodium cations are represented as green spheres, while succinate is shown as red spheres in A and as sticks in B.

3.5.2.1. SNTAAA

The first mutant to be tested was SNTAAA from the SNT motif located in HPin and HPout of VcINDY amino acid structure. By mutating those three amino acids to alanine, VcINDY substrate recognition should be impaired, as it was previously proven with 5 mM succinate (*Figure 3.4*). The data gathered is shown in the same way as before.

SNTAAA outcomes lack statistical value since the difference with the substrate was not sufficient enough when compared to the condition with the absence of it. In most of the cases, shifts were not bigger than 1.6 ℃ (*Figure 3.11*). Only tricarballyate provoked an almost significant shift exactly equal to wild-type with 2.6 ±0.47 ℃, but not very significant (p-value 0.047) (*Table 3.1).*

These results go beyond the previous reports of succinate, showing that SNTAAA is not able to recognise any ligand since the melting point of this tested VcINDY is similar in every condition. On account of these results and as expected, the SNT motif seems key to recognise substrates.

To a better understanding and investigation of any critical amino acid's role, the arginine and threonine amino acids from the SNT motif were studied individually.
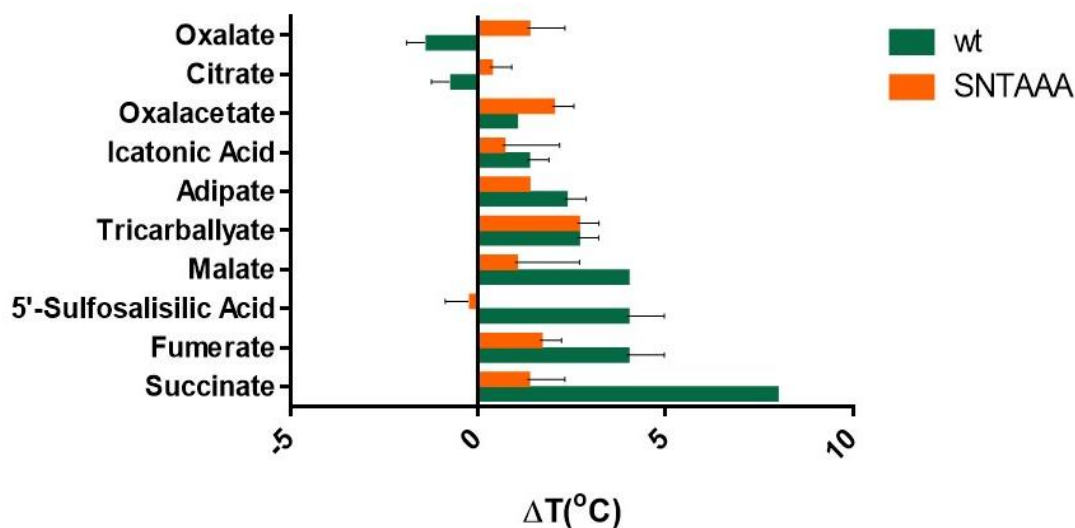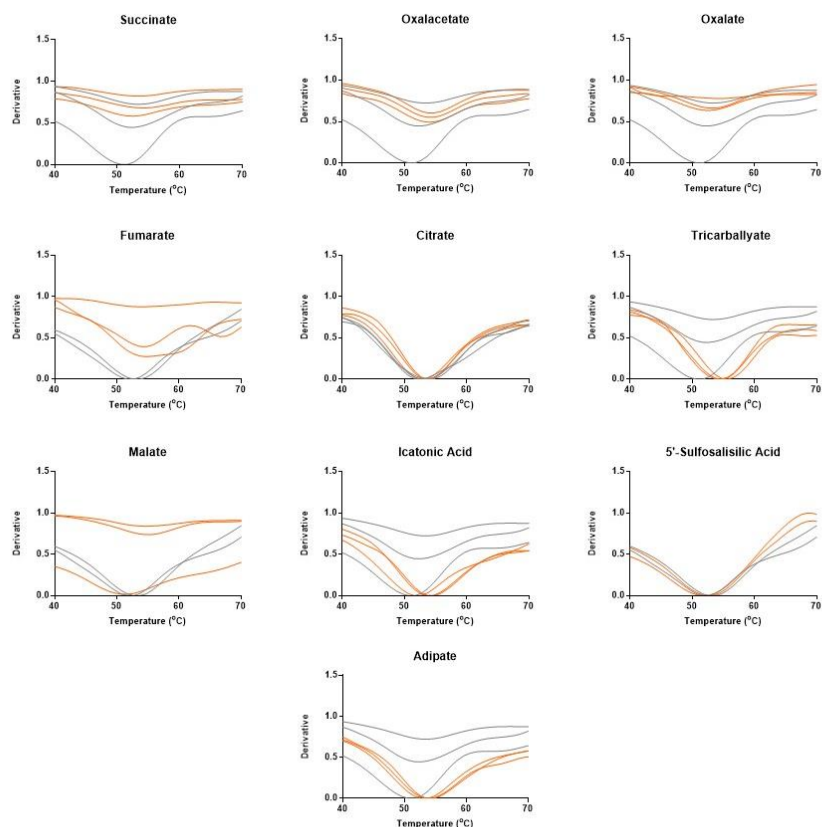

(Figure continues on next page)

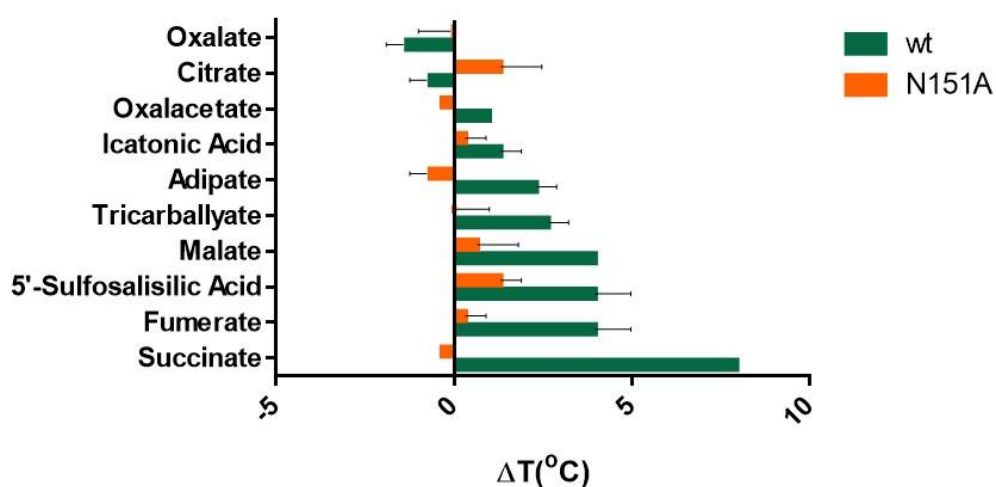***Figure 3.11:*** **10 compounds thermostability screen using VcINDY triple alanine mutant SNTAAA.**

Average melting temperature shift (ΔTm) of VcINDY in the presence of each compound was determined by subtracting the VcINDY Tm in the absence of substrate from the Tm in the presence of the indicated compound. The results of the mutant (orange) are shown next to wild-type VcINDY outcomes for the same compound (green) for comparison. The bars shown are the average of triplicated datasets with their error bars represented SEM. In addition, below normalised melting curves graphs from the derivative of the untouched data of VcINDY SNTAAA in 10 mM of the indicated compound present (orange) and in its absence (grey). Each line represents a single outcome of the triplicated data.

3.5.2.2. N151A

The asparagine of the SNT motif has a functional amidic group side-chain. This functional group has been described from the crystal structure to interact with one succinate's carboxylate group. In addition, the carboxyl side-chain from N151 also interacts with the sodium located in the Na1 (Nie *et al.*, 2017). Therefore, N151 could be a critical amino acid at the HPin of VcINDY's transport domain since it is shared with both substrate and sodium-binding sites.

By means of modification of the functional side-chain of the 151 amino acid, its contribution to substrate recognition was judged (*Figure 3.12*). The ΔTms were not bigger than approximately 0.6 °C. For this reason, no significant melting temperature shifts were observed with the different compounds, except from citrate and 5'-sulfosalisilic acid with a shift of 1.3± 0.94 and 1.3± 0.47 °C, respectively (*Table 3.1*). However, only 5'-sulfosalisilic acid shift was statistically significant, being lower than the respective value found for wild-type (*Table 3.1*).

In general, the data obtained from N151A suggests that N151 has a role in substrate selectivity and, perhaps the chain-length filter rule. The fact that only 5'-sulfosalisilic acid presented a positive stabilisation implies that the amidic group of the asparagine implements, to some extent, the chain-length filter. N151 recognises the carboxylic group at one end of the ligand's molecular structure, getting bound to HPin. 5'-sulfosalisilic acid is the only ligand from the library that does not follow a chain structure with a carboxylic group at the ends. Therefore, it can be conceivably bond to the binding site when an alanine is in position 151.
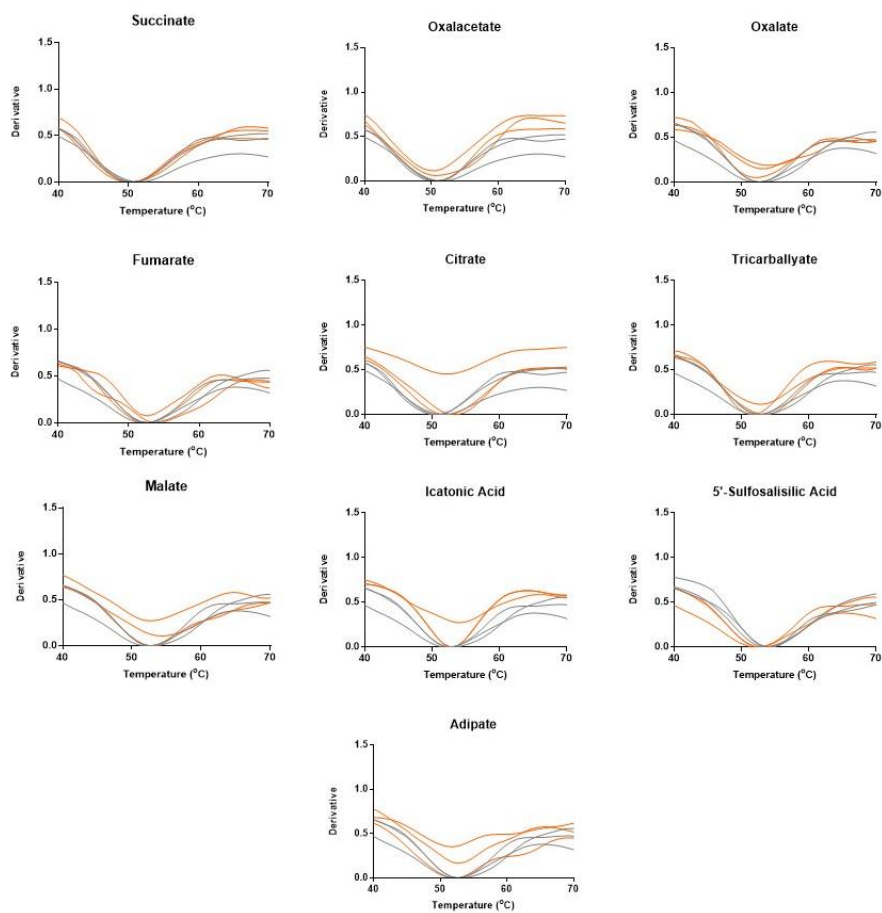

(Figure continues on next page)

Figure 3.12: **10 compounds thermostability screen using VcINDY alanine mutant N151A.**

Average melting temperature shift (ΔTm) of VcINDY in the presence of each compound was determined by subtracting the VcINDY Tm in the absence of substrate from the Tm in the presence of the indicated compound. The results of the mutant (orange) are shown next to wild-type VcINDY outcomes for the same compound (green) for comparison. The bars shown are the average of triplicated datasets with their error bars represented SEM. In addition, below normalised melting curves graphs from the derivative of the untouched data of VcINDY N151A in 10 mM of the indicated compound present (orange) and in its absence (grey). Each line represents a single outcome of the triplicated data.

3.5.2.3. T152A

This is the second amino acid individually tested from the SNT motif. The threonine in this position possesses a hydroxylic functional group as a side-chain. This amino acid functional group has been well described to interact with the same carboxylate group from succinate than the previous N151 amino acid. N151 and T152 are next to each in sequence and structure, interacting closely with the substrate. Studying the effect of alanine substitution on this position could help to

further understand the relevance of T152 in the game of VcINDY's substrates selectivity filters.

The same ten compounds were tested on a CPM assay with T152 (*Figure 3.13*). Surprisingly, changing the threonine for an alanine did not prevent succinate from binding to the protein. The ΔTm observed for succinate was 4 $^{\circ}$C, half from the one found for wild-type (*Table 3.2*). When observing the other compounds, there were slightly larger ΔTm values than the previous mutant (*Figure 3.12*). However, none of them were statistically significant. Again, 5'-sulfosalisilic acid with a ΔTm of 1.6± 0.0003 $^{\circ}$C and, succinate shown a true difference observable on the melting curves graphs (*Figure 3.13).*

In comparison with N151A, the threonine in position 152 seemed to be equally important to allow binding of ligands, since most of the library's compound could not offer thermostability when T152 was mutated to an alanine. T152A allowed binding of 5'-sulfosalisilic acid to a similar degree that N151A did. Therefore, it can be speculated that this might be due to the importance of a hydroxyl residue in position 152 to form a bond with the substrates' carboxylate group. However, based on the finding for these two amino acids, the role of the amino acid T152 to implement a side chain filter is lower than the one thought for N151, as T152A did not fully impair succinate binding.
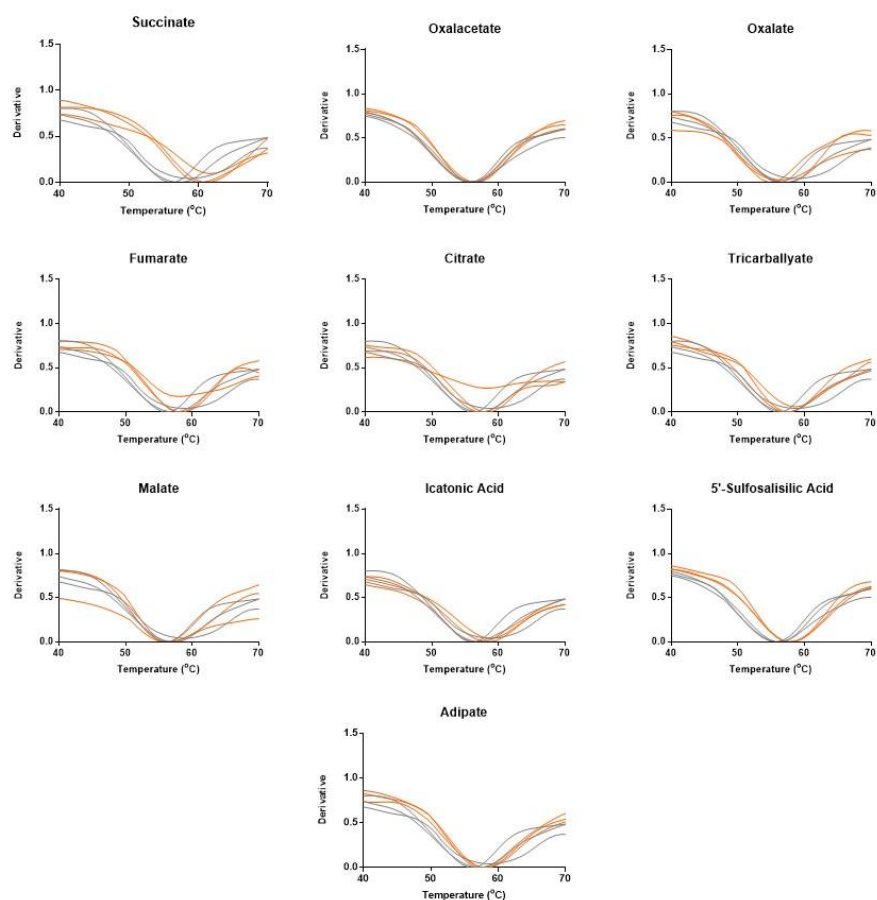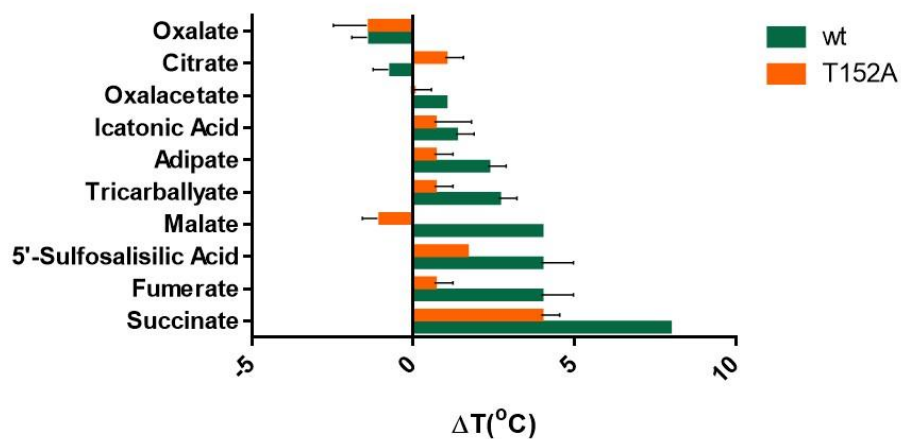
Figure 3.13: **10 compounds thermostability screen using VcINDY alanine mutant T152A.**

Average of melting temperature shift (ΔTm) of VcINDY in the presence of each compound was determined by subtracting the VcINDY Tm in the absence of substrate from the Tm in the presence of the indicated compound. The results of the mutant (orange) are shown next to wild-type VcINDY outcomes for the same compound (green) for comparison. The bars shown are the average of triplicated datasets with their error bars represented SEM. In addition, below normalised melting curves graphs from the derivative of the untouched data of VcINDY T152A in 10 mM of the indicated compound present (orange) and in its absence (grey). Each line represents a single outcome of the triplicated data.

3.5.2.4. S200A

This serine belongs to the binding site and it is located in the transport domain. Serine is a hydroxylic amino acid that forms H-bonds with the substrate, as seen in the succinate-VcINDY crystal structure (Nie *et al.*, 2017). Interestingly, S200A was one of the mutants that presented higher stabilisation without succinate than with it being present (*Figure 3.8*). CPM results established S200A basal thermostability around $62.3 \pm 1.64\ ^{o}C$, which is the same as VcINDY wild-type when succinate is bound to the transporter (*Table 3.2*). To investigate what gives S200A such stability a CPM assay was performed for this mutant.

In this experiment, succinate binding to the protein did not lead to any difference according to the basal baseline of S200A without any added ligand (*Figure 3.14*). By observation of the statistical values in *Table 3.2*, succinate and fumarate did not present a melting temperature shift between conditions. On the contrary, for all the other compounds, a significant p-value was achieved. However, in any case, a better stabilisation of the transporter occurred in the presence of ligands (*Figure 3.14*).

These results demonstrate two things. First, S200A mutant is less stable when ligands are present. One explanation for this could be because the alanine in position 200 forms stronger interactions by increasing hydrophobic interactions inside the protein than any possible substrate could form. Second, the presence of an aliphatic amino acid in position 200 could disturb the binding of succinate and fumarate. Succinate binds to the protein in an extended form comparable to

fumarate's structure (Mulligan *et al.*, 2014). Thus, it was not surprising that neither succinate nor fumarate offered VcINDY a thermal shift in its presence.
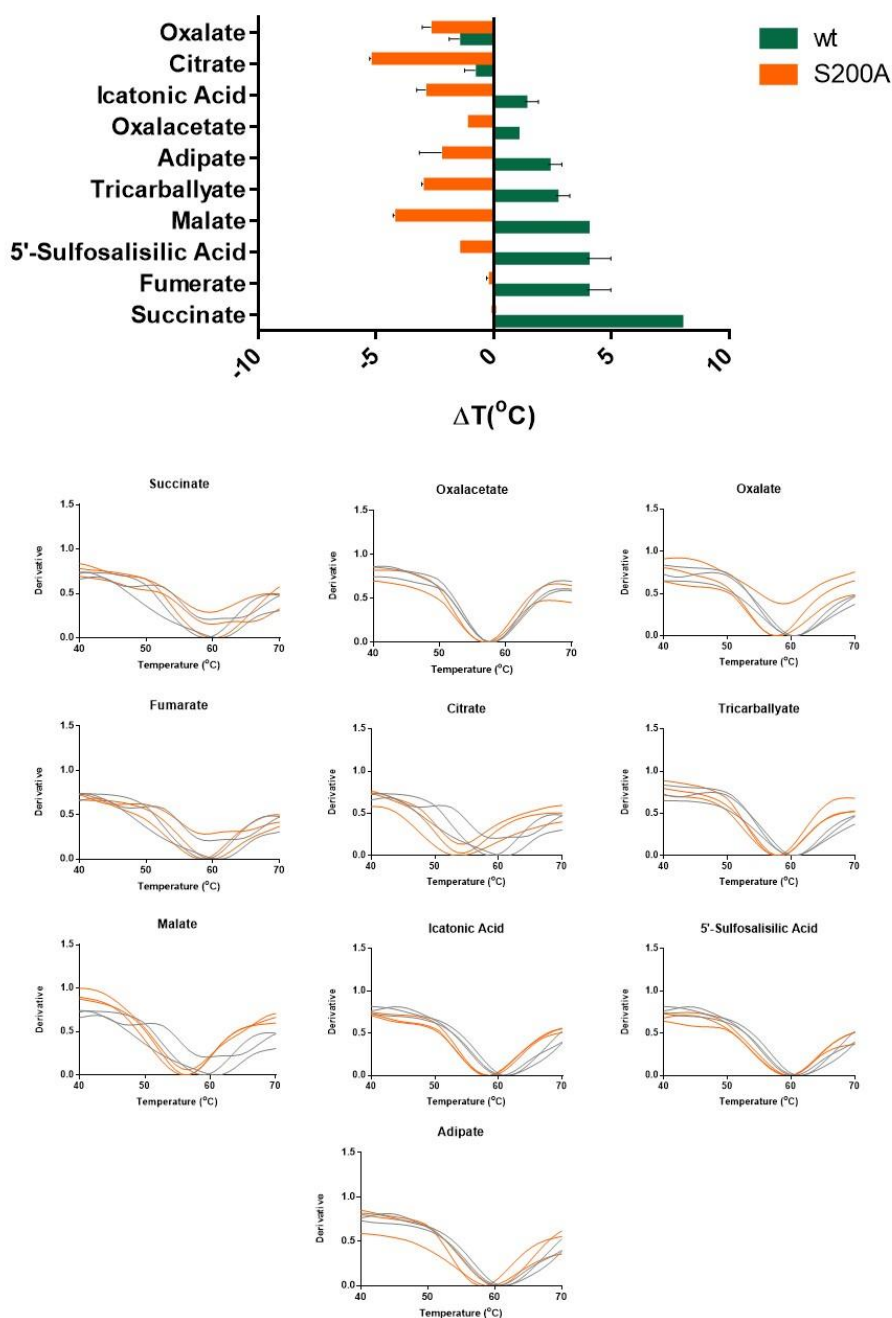

Figure 3.14: **10 compounds thermostability screen using VcINDY alanine mutant S200A.**

Average melting temperature shift (ΔTm) of VcINDY in the presence of each compound was determined by subtracting the VcINDY Tm in the absence of substrate from the Tm in the presence of the indicated compound. The results of the mutant (orange) are shown next to wild-type VcINDY outcomes for the same compound (green) for comparison. The bars shown are the average of triplicated datasets with their error bars represented SEM. In addition, below normalised melting curves graphs from the derivative of the untouched data of VcINDY S200A in 10 mM of the indicated compound present (orange) and in its absence (grey). Each line represents a single outcome of the triplicated data.

3.5.2.5. T421A

The threonine in position 421 is the only one from this set to be located near the HPout of VcINDY structure. This amino acid belongs to the TM10b which is thought to be critical for transport movement (Mancusso *et al.*, 2012)(Sauer *et al.*, 2020). The loop formed between TM10a and TM10b it is also involved in creating the space for the Na2 sodium-binding site. In particular, T421 acts in a similar way to S200, generating H-bonds with succinate to enhance binding stability. A CPM assay following the same steps was performed to investigate T421 role in protein stability and substrate binding.

In this case, the ten compounds tested did not stabilise VcINDYT421A positively (*Figure 3.15*). The ΔTm resulting from the different compounds' screen was not significant, excluding the effect of oxalate and citrate showing a significant ΔTm (*Table 3.2*). The effect of citrate and oxalate on protein's thermostability was negative compared to the protein stability without added compounds (*Figure 3.15*). The destabilisation caused by oxalate and citrate it is commonly shared with some VcINDY alanine mutants, as these two molecules are not substrates of VcINDY. However, the causes of such destabilisation effects remain unclear.

Within the results of T421A experiment, it can be concluded that T421 probably plays a particular role in substrate selectivity. Mutating the threonine with an alanine completely disturbs anionic compounds binding to the protein. T421A together with S200A were the only two mutants with more stability in the absence of succinate (*Figure 3.8*). Hence, it could be suggested that the H-bonds formed by these two positions with the substrate are not just to reinforce the binding, but

they are necessary for substrate recognition and general protein stabilisation. The destabilisation effect in the presence of ligands could be due to the inability of the mutated transporter to form H-bonds with the compounds. Also, it could be caused by the formation of hydrophobic interactions within the protein's structure because of compounds sitting at the binding site impairing it.
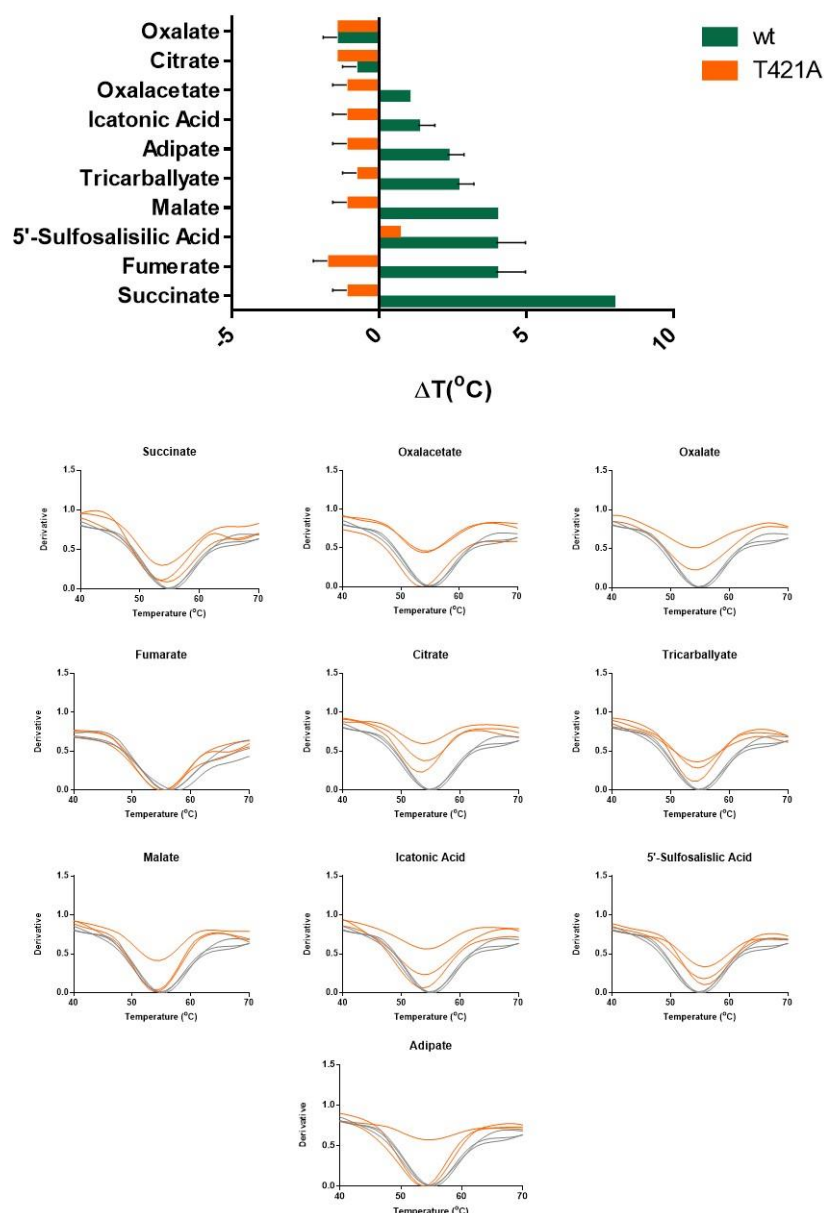

Figure 3.15: **10 compounds thermostability screen using VcINDY alanine mutant T421A.**

Average melting temperature shift (ΔTm) of VcINDY in the presence of each compound was determined by subtracting the VcINDY Tm in the absence of substrate from the Tm in the presence of the indicated compound. The results of the mutant (orange) are shown next to wild-type VcINDY outcomes for the same compound (green) for comparison. The bars shown are the average of triplicated datasets with their error bars represented SEM. In addition, below normalised melting curves graphs from the derivative of the untouched data of VcINDY T421A in 10 mM of the indicated compound present (orange) and in its absence (grey). Each line represents a single outcome of the triplicated data.

3.5.3. ASSESSING BINDING SELECTIVITY OF VcINDY MUTANTS OF THE SCAFFOLD DOMAIN

As above-mentioned, VcINDY transport mechanism follows an elevator-type mechanism. The reason why the following two positions have been studied is because cation and substrate-binding sites in an elevator mechanism are supposed to be present in the protein's transport and scaffold domains. Prior to this section, amino acids included in the transport domain were presented and analysed.

To assess in the same way amino acids in the scaffold domain, V66A and T67A were tested. Thus, the elevator-type mechanism as VcINDY's way to transport substrate would be further corroborated by providing melting temperature shifts within these new mutants.

3.5.3.1. V66A

In this experiment, a valine was substituted with alanine, which means that the aliphatic chemical property of the location was maintained. V66 is located in the TM2 of the VcINDY structure.

Therefore, V66 should not interact with the substrate when the transporter is in the inward-facing state nor at the outward-facing state, but when the transporter is on an intermediate state between these two (*Figure 3.16*).
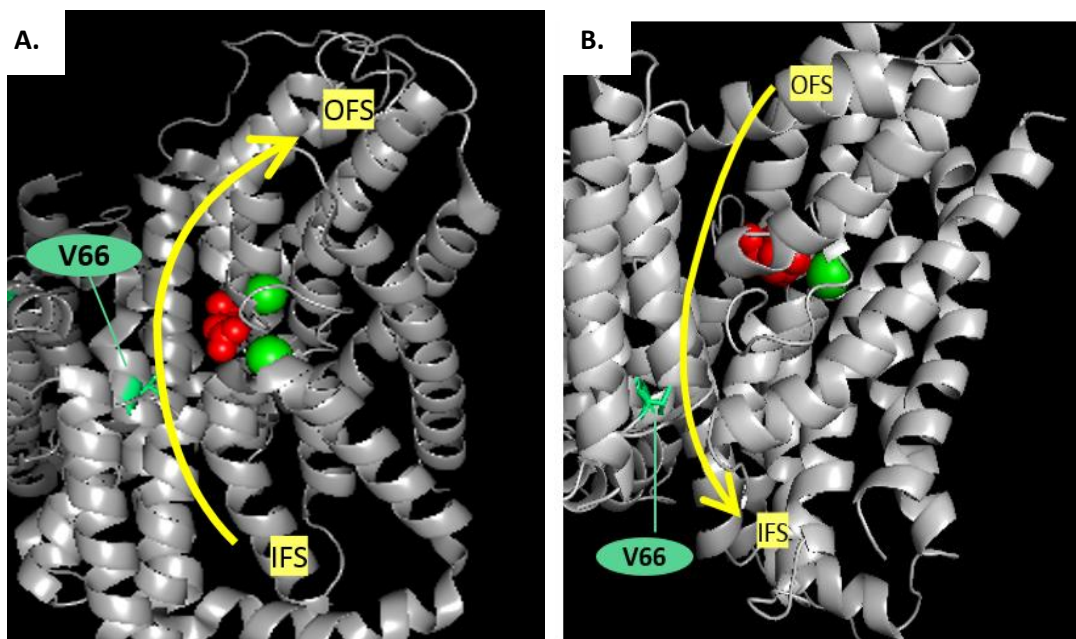
Figure 3.16: **Representation of V66 localization in a 3D VcINDY crystal structure.**

V66 location in a 3D model taken from a PyMOL at (**A**) VcINDY's inward-facing state from the crystal structure of Nie *et al.,* 2017, (**B**) VCINDY's outward-facing model based on Mancusso *et al.,*2012 crystal structure from Mulligan *et al.,*2016. V66 amino acid is marked in green in both conformations. Also, in both images, sodium cations are represented as green spheres and substrates as red spheres. The yellow arrow represents the path followed by the binding-site during the elevator-type transport cycle from IFS (inward-facing state) to OFS (outward-facing state), or vice versa.

The results from the CPM assay of V66A shown a similar pattern to VcINDY wild-type. All the compounds from the library generated higher stabilisation than when non-ligands were added to the solution besides oxalate (*Figure 3.17*). Still, oxalate trivial effect on stabilisation was not significant, which matches with what would be expected. Citrate effect on protein's stabilisation was significant but minimal with a ΔTm value of 0.3± 0.0002 °C *(Table 3.1)*.

Remarkably, succinate ΔTm was of 8 °C, same value found prior on wild-type. Thus, in a similar way, the rest of compounds also presented stabilisation values related to wild-type's prior findings *(Figure 3.17).* For V66A, succinate, fumarate and malate provoked the higher stabilization among all ligands, which is in line with the chain-length filter proposal as these three ligands have a chain of four carbons.

Yet, oxalacetate (4C) presented here a clear shift of 2 °C, double than wild-type (*Figure 3.17*). Another discrepancy with wild-type was the stabilisation effect of 5'-sulfosalisilic on V66A, which was only half from wild-type's (*Figure 3.17*). Icatonic acid generated a significant difference on V66A of 1.3 ± 0 °C (P-value 0.016). The same value for its effect was found for wild-type but without statistical support (*Table 3.1*).

Therefore, these results tie well with the previously presented on wild-type CPM assay, which it is not surprising since valine and alanine are similar amino acids. Values from the V66A study can be used to further corroborate and support the findings for VcINDY wild-type. In this experiment, the outcome found for 5'-sulfosalisilic acid (7C) correlated better with what could have been predicted accordingly to VcINDY carbon-length filter.

Besides, for V66A the stabilisation effect of the two other four-carbon compounds of the library, oxalacetate (4C) and icatonic acid (4C), were both statistically significant but still offer less stabilisation than other 4C-ligands tested. This supports that a ketone group as oxalacetate or a methylene group as icatonic acid at the second carbon affects the transport stability, while other carbon's groups such as a hydroxyl from malate do not affect as much.
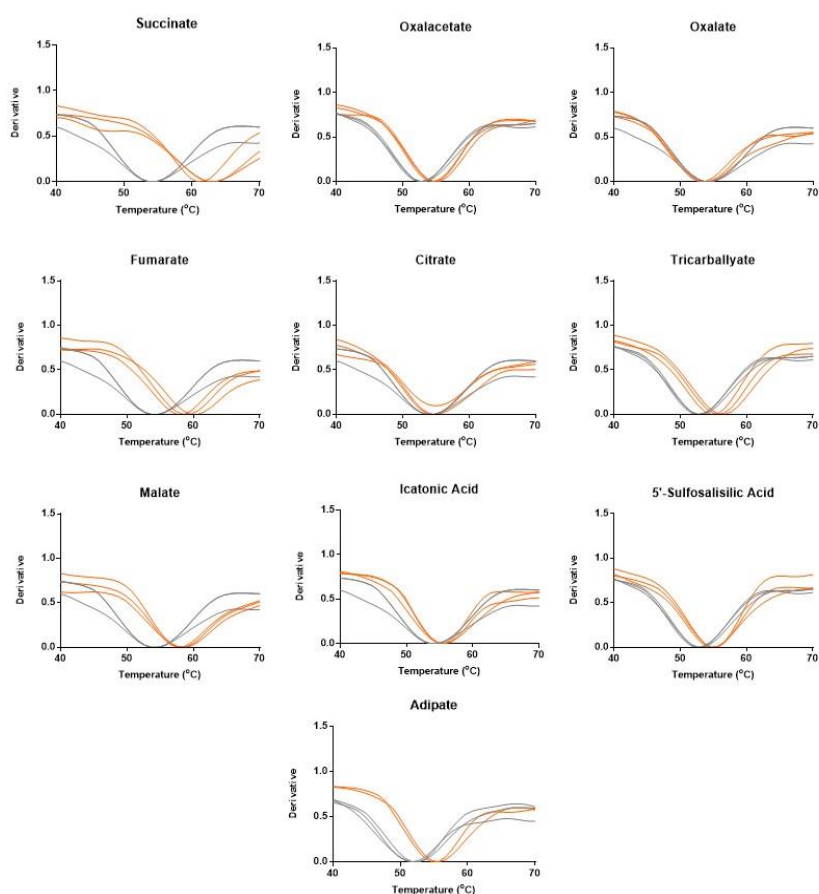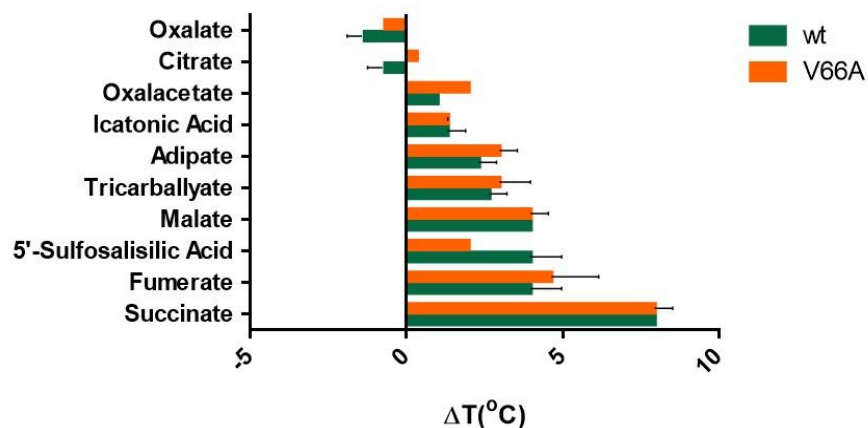
Figure 3.17: **10 compounds thermostability screen using VcINDY alanine mutant V66A.**

Average melting temperature shift (ΔTm) of VcINDY in the presence of each compound was determined by subtracting the VcINDY Tm in the absence of substrate from the Tm in the presence of the indicated compound. The results of the mutant (orange) are shown next to wild-type VcINDY outcomes for the same compound (green) for comparison. The bars shown are the average of triplicated datasets with their error bars represented SEM. In addition, below normalised melting curves graphs from the derivative of the untouched data of VcINDY V66A in 10 mM of the indicated compound present (orange) and in its absence (grey). Each line represents a single outcome of the triplicated data.

3.5.3.2. T67A

The threonine in position 67 on the sequence is found at the TM2 of the VcINDY structure. Its chemical properties include a hydroxylic side-chain. Since it is next to the V66, T67 relationship with the substrate is expected to be similar to V66 (*Figure 3.18*). However, some interesting findings differing from its neighbour position have been found.
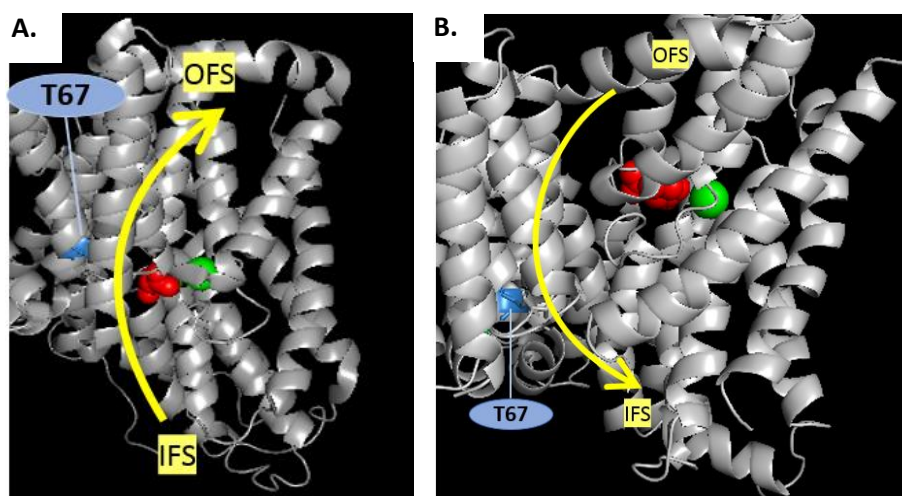

***Figure 3.18:* Representation of T67 localization in a 3D VcINDY crystal structure.**

T67 location in a 3D model taken from a PyMOL at (**A**) VcINDY's inward-facing state from the crystal structure of Nie *et al.,* 2017, (**B**) VCINDY's outward-facing model based on Mancusso *et al.,*2012 crystal structure from Mulligan *et al.,*2016. T67 amino acid is marked in dark blue in both conformations. Also, in both images, sodium cations are represented as green spheres and substrates as red spheres. The yellow arrow represents the path followed by the binding-site during the elevator-type transport cycle from IFS (inward-facing state) to OFS (outward-facing state), or vice versa.

In this experiment, compounds with four carbons in their chains gave the maximum stability (*Figure 3.19*). Succinate provoked the higher ΔTm of 8± 0.47 °C, followed by fumarate and malate with quite similar outcomes with approximately ΔTm of 4 °C. Tricarballyate and oxalacetate thermal shifts on T67A were almost identical to V66A, with ΔTm of 3± 0.68 °C and 2± 0.81 °C, respectively (*Table 3.1*).

Unexpectedly compared to prior results, the effect of 5'-sulfosalisilic acid on protein's stabilisation was negative. The destabilisation from 5'-sulsfosalisilic acid

was of -0.6 ± 0.81 °C (*Table 3.1*). Two more compounds from the library, together with 5'-sulfosalisilic acid, provoked a destabilisation when they were present (*Figure 3.19*). Oxalate effect was remarkable with a ΔTm of -5.3 ± 0.47 °C. Citrate, on the other hand, generated a ΔTm of 1.3± 0.47 °C, which is still larger than the one observed on VcINDY wild-type (*Figure 3.19*).
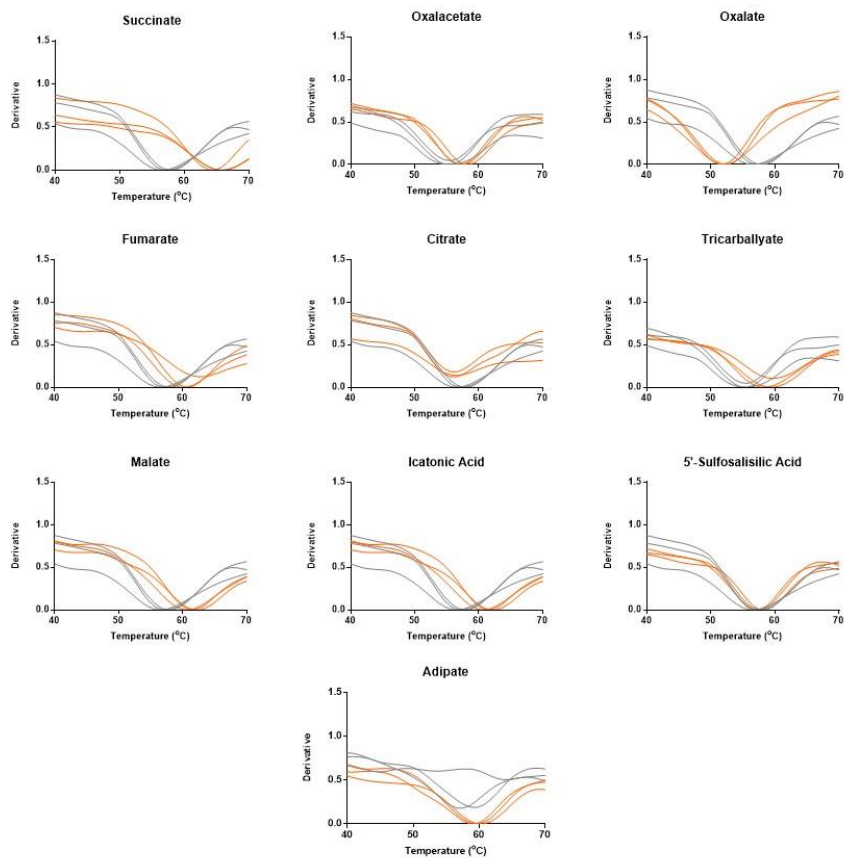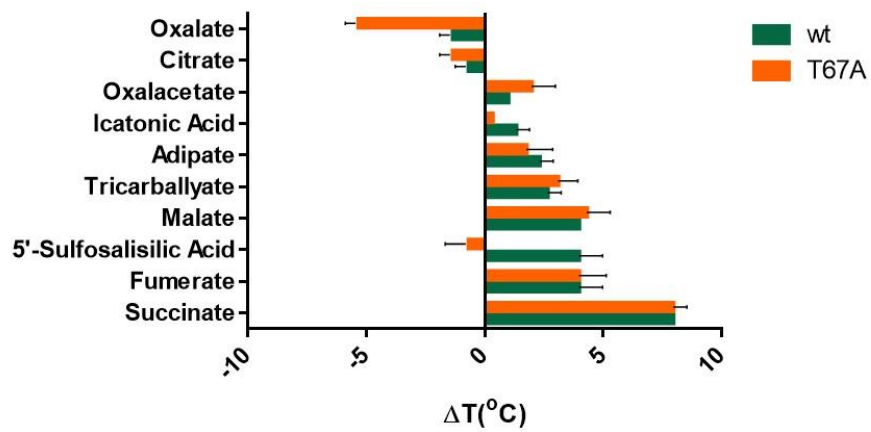
Average melting temperature shift (ΔTm) of VcINDY in the presence of each compound was determined by subtracting the VcINDY Tm in the absence of substrate from the Tm in the presence of the indicated compound. The results of the mutant (orange) are shown next to wild-type VcINDY outcomes for the same compound (green) for comparison. The bars shown are the average of triplicated datasets with their error bars represented SEM. In addition, below normalised melting curves graphs from the derivative of the untouched data of VcINDY T67A in 10 mM of the indicated compound present (orange) and in its absence (grey). Each line represents a single outcome of the triplicated data.

In general, these results are in keeping with previous CPM analysis of wild-type and V66A (*Table 3.1*). It seems that V66A and T67A would not cause a direct impact on the selectivity of four-carbon chain compounds. However, oxalacetate appeared to cause more stabilisation than wild-type, which means that it could be bound to the proteins more strongly in both mutants. The binding of 5'-sulfosalisilic acid in wild-type appeared to be as good as fumarate for its stabilisation effect. In T67A, the biding of 5'-sulfosalisilic acid seemed to not satisfy the protein's requirements marked for its destabilisation effect.

3.5.4. ASSESSING BINDING SELECTIVITY OF VcINDY MUTANTS OF THE OLIGOMERIZATION DOMAIN

The importance of the oligomerization domain is because of its function in connecting both protomers of VcINDY. Connections are described to happen between TM3, TM4, TM8 and, TM9. Mutations on these transmembrane helices could unfold as protein dynamics impediments, creating melting temperature shifts by affecting the structure of the protein, its transport mechanism and, perhaps, the binding selectivity of different compounds. Therefore, I96A, F100A, S290A, D319A, V322A and F326A were mutated to test if substrate selectivity has

a relationship with amino acids from the oligomerization domain. These amino acids are thought to interact distantly with the substrate at the outward-facing state of VcINDY as clear model structures display it (Mulligan *et al.*, 2016).

3.5.4.1. I96A

The first amino acid related to the oligomerization domain was I96A located at the TM4b of VcINDY structure. It is an isoleucine, which has similar aliphatic properties to alanine does, but it has a larger side-chain with four carbons instead of two.

The melting temperature of this mutant was equal to wild-type's with 53.57± 1.58 °C. Thus, the change from isoleucine to alanine did not affect protein's stability. As the protein folding for this mutant seemed stable and similar to wild-type's, a CPM assay was carried out to investigate amino acid involvement at the outward-facing state.

The selectivity for compounds with four-carbon chains was non-significant ΔTm for succinate, fumarate and oxalacetate (*Figure 3.20*). Only malate and icatonic acid melting temperature shifts were statistically significant with 3 ± 1.24 °C for malate and 1.3± 0 °C for icatonic acid (*Table 3.1*). In both cases, the selectivity for malate and icatonic acid were roughly lower than the ones observed on wild-type (*Figure 3.1*). Citrate and oxalate, two compounds with questionable stability effects on VcINDY, did not cause enough destabilisation effect to consider their melting temperature shift. The same outcome happened with adipate (*Table 3.1*). Tricarballyate and 5'-sulfosalisilic acid did stabilise I96A VcINDY but with a smaller ΔTm than on VcINDY wild-type (*Figure 3.20).*
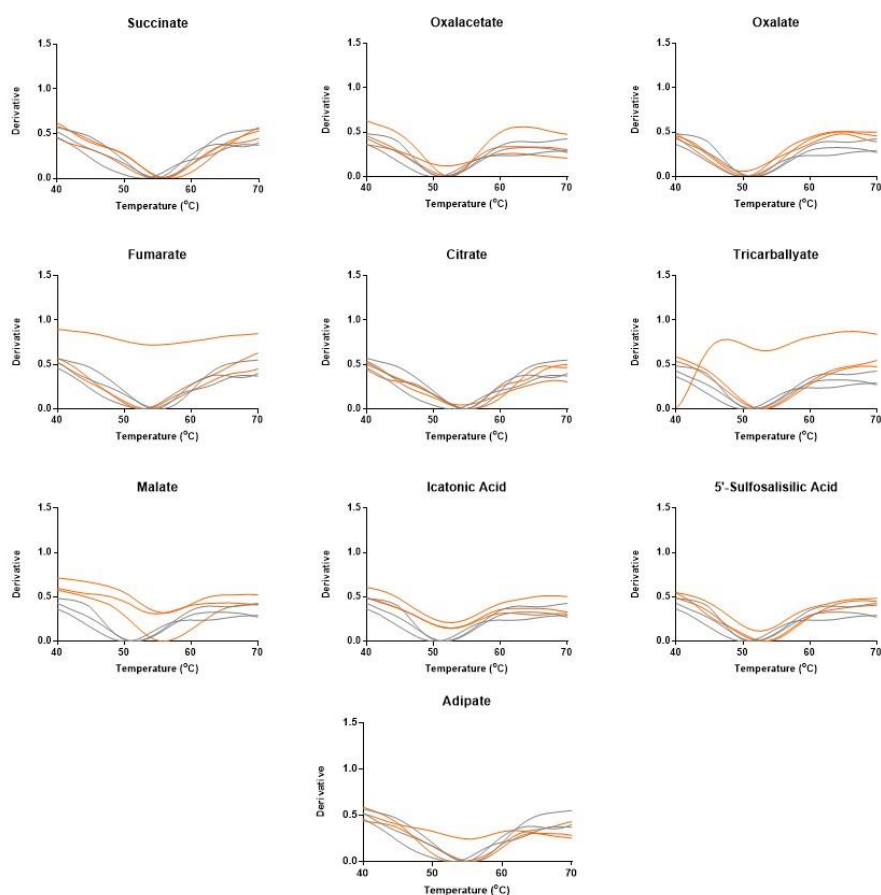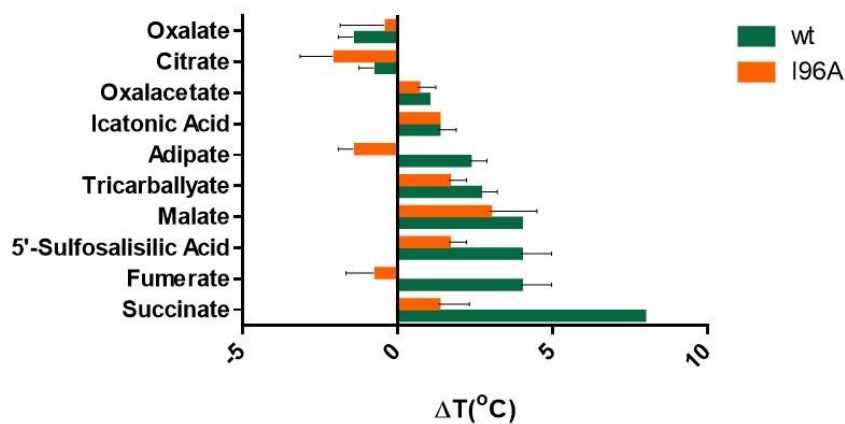
Figure 3.20: 10 compounds thermostability screen using VcINDY alanine mutant I96A.

Average melting temperature shift (ΔTm) of VcINDY in the presence of each compound was determined by subtracting the VcINDY Tm in the absence of substrate from the Tm in the presence of the indicated compound. The results of the mutant (orange) are shown next to wild-type VcINDY outcomes for the same compound (green) for comparison. The bars shown are the average of triplicated datasets with their error bars represented SEM. In addition, below normalised melting curves graphs from the derivative of the untouched data of VcINDY I96A in 10 mM of the indicated compound present (orange) and in its absence (grey). Each line represents a single outcome of the triplicated data.

Interestingly, this amino acid's side-chain would be facing the substrate in the outward-facing conformation of VcINDY according to simulations on PyMOL from the model described to be in the outward-facing state (*Figure 3.21*)(Mulligan *et al.*, 2016). Supporting that both conformations are present at equal rates in the solution, ΔTm represents differences of the specifically tested compound between the two conformations described for the protein. Therefore, differences from wild-type on substrate selectivity of this mutant occur due to recognition difference generated at the outward-conformation. In line with this idea, it can be assumed that there is some substrate selectivity discrepancy between the inward-facing state and the outward-facing state of the protein. Preference for four-carbon chains ligands seems to be at the inward-facing state, whereas, at the outward-facing conformation this preference seems less applicable.
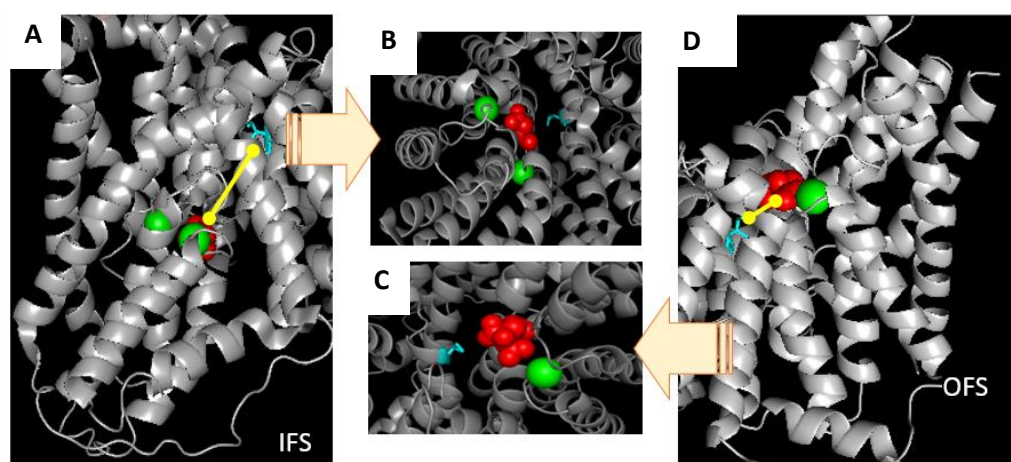

Figure 3.21: **Representation of I96 localization in a 3D VcINDY crystal structure.**

I96 location in a 3D model taken from a PyMOL at (**A**) VcINDY's inward-facing state from the crystal structure of Nie *et al.,* 2017, (**D**) VCINDY's outward-facing model based on Mancusso *et al.,*2012 crystal structure from Mulligan *et al.,* 2016. Images **B** and **C** show the same situation as A and D (*respectively*), but from an inside of the cell perspective. I96 amino acid is marked in cyan in both conformations. Also, in both images, sodium cations are represented as green spheres and substrates as red spheres. The yellow lines represent distance between the I96 and the substrate binding-site.

3.5.4.2. F100A

F100A is a mutant located at the TM4b of the VcINDY structure. The phenylalanine has an aromatic ring in its chemical structure (*Figure 3.22*). The melting temperature of the protein alone is 54.76± 1.59 °C, which matches with VcINDY wild-type melting temperature. Then again, the mutation in this position did not affect the overall protein stability. A CPM for F100A was performed with the library's ten compounds to see differences in substrate recognition.
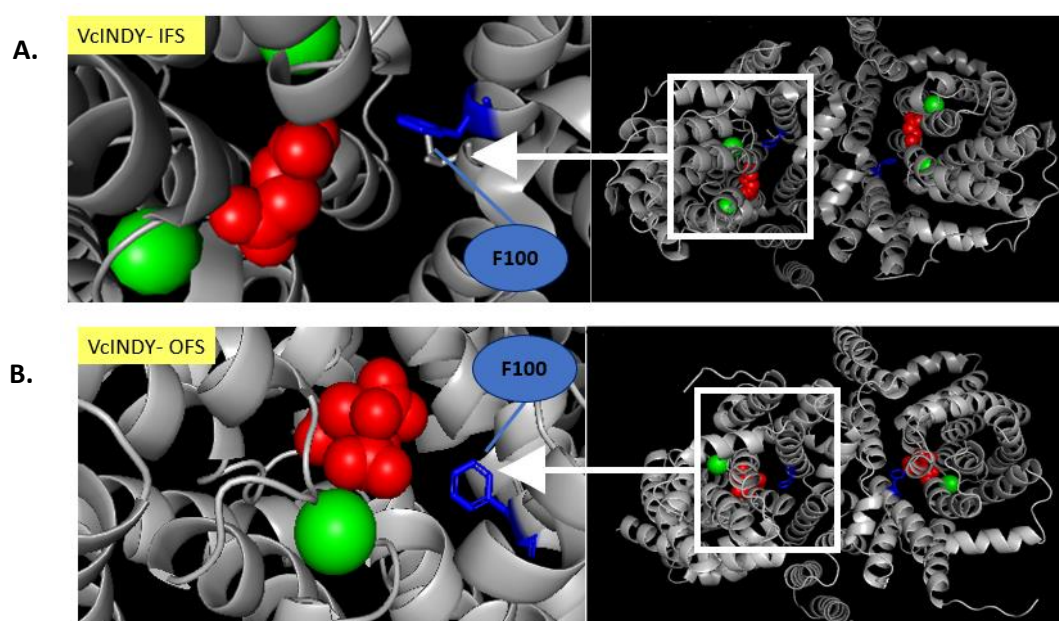
Figure 3.22: **Representation of 100 localization in a 3D VcINDY crystal structure.**

F100 location in a 3D model taken from a PyMOL at (**A**) VcINDY's inward-facing state from the crystal structure of Nie *et al.,* 2017, (**B**) VCINDY's outward-facing model based on Mancusso *et al.,*2012 crystal structure from Mulligan *et al.,* 2016. F100 amino acid is marked in blue in both conformations. Also, in both images, sodium cations are represented as green spheres and substrates as red spheres.

In F100A test, in the presence of succinate, ΔTm was significant but with half a thermal shit compared to wild-type succinate's influence (*Figure 3.23*). Despite this, other four-carbons, such as fumarate and oxalacetate, did not cause a significant ΔTm difference (*Table 3.1*). 5'-Sulfosalisilic acid influence on F100A stability resembled fumarate (*Figure 3.23*).

Remarkably, icatonic acid and malate did again show an increase in protein's stability. Icatonic acid stabilised F100A in the same way that succinate did (*Figure 3.23*). Remarkably in this experiment, malate's effect on the mutant stability was prominent with a ΔTm of 8.6± 0 °C. This value is slightly higher than the stabilisation effect of succinate on VcINDY wild-type (*Figure 3.23*).

Adipate is a six-carbon chain causing a destabilisation effect on F100A melting temperature (*Figure 3.23*). The ΔTm for adipate in this study was of -2.3 ± 0.47 °C. The same outcome for adipate was seen in I96A, a neighbour amino acid, but here the shift has statistical reinforcement (*Table 3.1*). Hence, succinate gets better bind to the mutant. The thermostability effect generated by malate and icatonic acid was noticeable compared to other mutants, although the reasons behind this effect are not clear.
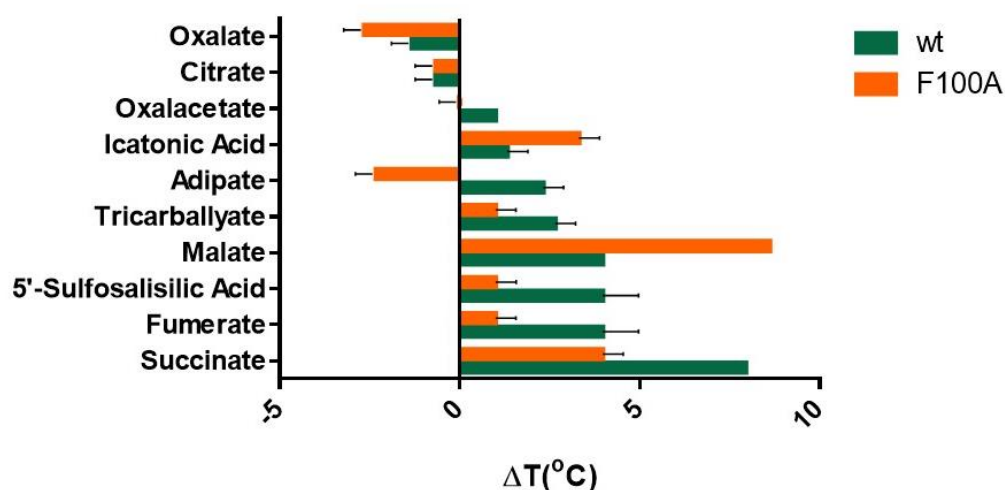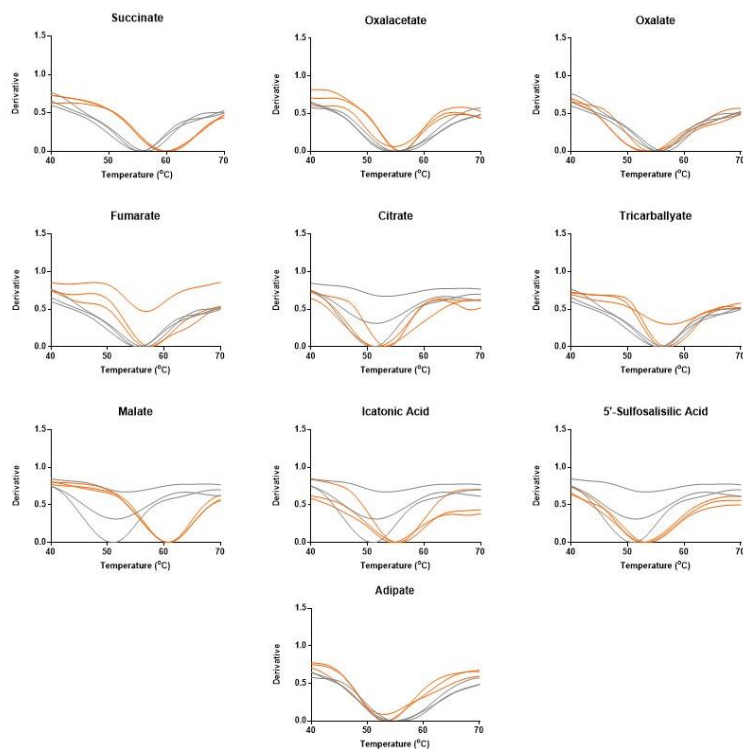

(Figure continues on next page)

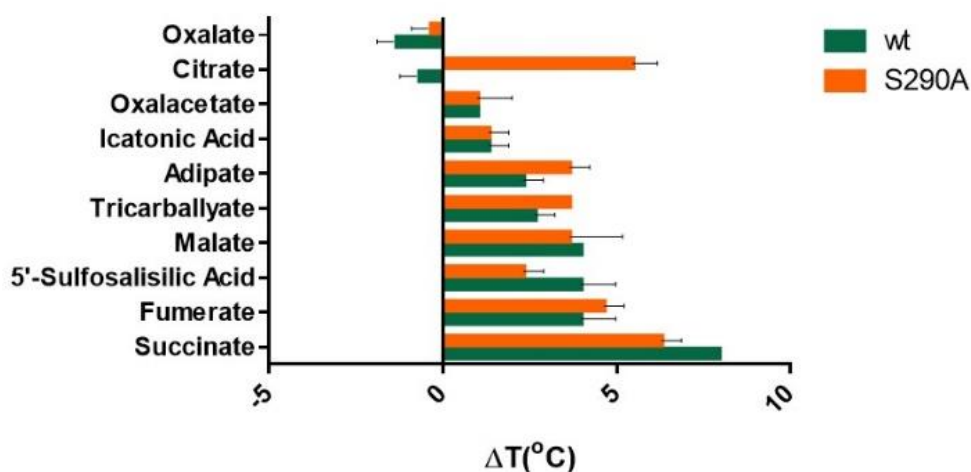***Figure 3.23:*** **10 compounds thermostability screen using VcINDY alanine mutant F100A.**

Average melting temperature shift (ΔTm) of VcINDY in the presence of each compound was determined by subtracting the VcINDY Tm in the absence of substrate from the Tm in the presence of the indicated compound. The results of the mutant (orange) are shown next to wild-type VcINDY outcomes for the same compound (green) for comparison. The bars shown are the average of triplicated datasets with their error bars represented SEM. In addition, below normalised melting curves graphs from the derivative of the untouched data of VcINDY F100A in 10 mM of the indicated compound present (orange) and in its absence (grey). Each line represents a single outcome of the triplicated data.

3.5.4.3. S290A

The amino acid in this position has a hydroxylic side-chain as chemical propriety from the serine. In this study, the serine has been mutated for the aliphatic alanine amino acid. The basal melting temperature of S290A was at 55.84± 2.15 °C roughly similar to wild-type (*Table 3.2*). A CPM assay to assess changes in substrate recognition was repeated as previously done for the other mutants.

In this experiment, all the outcomes came statistically significant, which means all compounds from the library generated a change by getting bound to the protein (*Table 3.2*). Oxalate, as a negative control, generated a small negative stabilisation effect on VcINDY.

Ligands with four-carbon chains stabilise S290A VcINDY with comparable ΔTm seen on wild-type. Compounds with more carbons such 5'-sulfosalisilic acid and adipate had distinct outcome than in wild-type (*Figure 3.24*). 5'-sulfosalisilic acid had less stabilisation effect but still positive with a ΔTm of 2.3± 0.47 °C (*Table 3.2*). Adipate a larger chain compound provoked a bigger ΔTm of 3.6± 0.47 °C than it did on VcINDY wild-type. However, despite this, the interesting finding in this experiment with S290A is citrate's stabilisation effect (*Figure 3.24*).
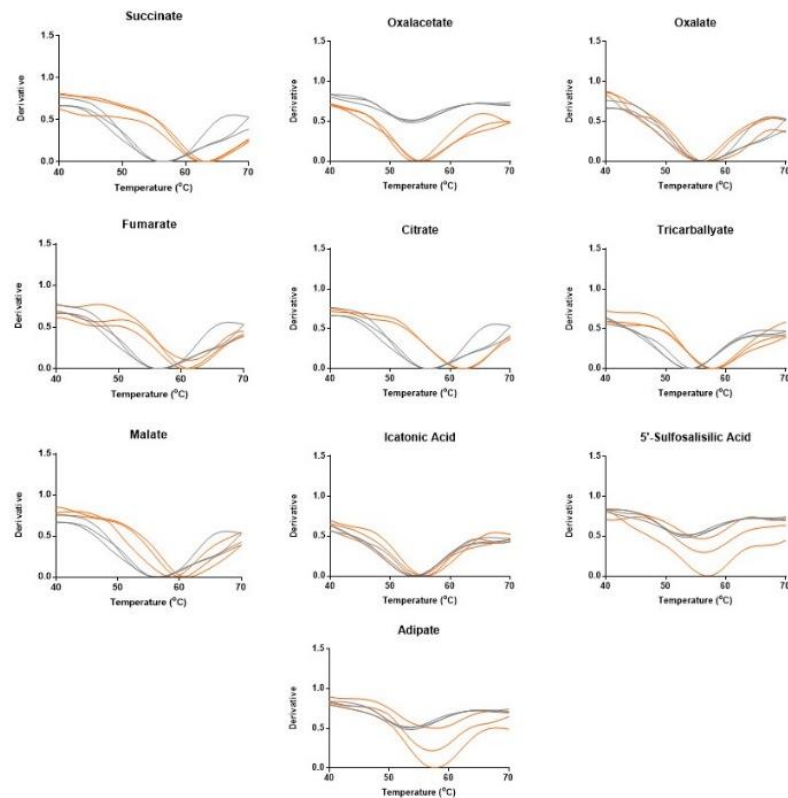

(Figure continues on next page)

Figure 3.24: **10 compounds thermostability screen using VcINDY alanine mutant S290A.**

Average melting temperature shift (ΔTm) of VcINDY in the presence of each compound was determined by subtracting the VcINDY Tm in the absence of substrate from the Tm in the presence of the indicated compound. The results of the mutant (orange) are shown next to wild-type VcINDY outcomes for the same compound (green) for comparison. The bars shown are the average of triplicated datasets with their error bars represented SEM. In addition, below normalised melting curves graphs from the derivative of the untouched data of VcINDY S290A in 10 mM of the indicated compound present (orange) and in its absence (grey). Each line represents a single outcome of the triplicated data.

When this serine was mutated to alanine, the citrate ligand could be bound to the protein creating the ΔTm of 5.4± 0.50 °C. Citrate it is supposed to be an inhibitor specific to the inward-facing state of VcINDY(Mancusso *et al.*, 2012). Hence, it is not a transported substrate. The S290 is predicted to be able to stay close to the substrate at the outward-facing state of VcINDY (*Figure 3.25*).

The results of citrate indicate the possibility for S290 to block citrate's binding. In tricarballyate case, the ΔTm was one of the highest for this compound along the study, with 3.6± 0 °C of melting temperature shift when tricarballyate was present.

This reinforces the idea of S290 being involved in not accepting compound with five-carbon chains at the outward-facing state.
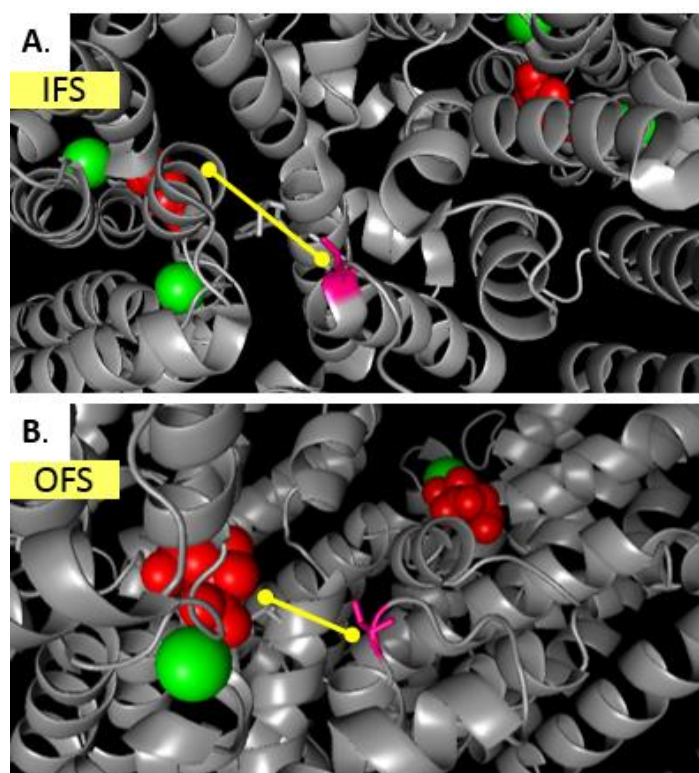

Figure 3.25: **Representation of S290 localization in a 3D VcINDY crystal structure.**

290 location in a 3D model taken from a PyMOL at (**A**) VcINDY's inward-facing state from the crystal structure of Nie *et al.,* 2017, (**B**) VCINDY's outward-facing model based on Mancusso *et al.,*2012 crystal structure from Mulligan *et al.,* 2016. S290 amino acid is marked in pink in both conformations. Also, in both images, sodium cations are represented as green spheres and substrates as red spheres. The yellow lines represent distance between the S290 and the substrate binding-site.

3.5.4.4. D319A

D319 is an amino acid located in between two transmembrane helixes, TM9a and TM9b from the oligomerization domain. Its chemical structure implicates acidic functional properties. Here, this group has been changed for an alanine. However, in this case, this mutation did affect protein's stability since the readings obtained following same measurements came poorly defined. For D319 an increase in sodium concentration of 150 mM was needed to obtain clearer

melting curves for the analysis (*Supplementary Figure 6.2.19*). The melting temperature afterward established for D319 was 51.26± 1.49 ℃.

A CPM assay was carried out, as it had been for the other mutants of the study. For this mutant, it is plausible to believe at this stage of understanding that D319 occupies an important position for the general protein stabilisation and perhaps for the transport mechanism. On observing images on PyMOL, D319 was seen to be near the binding site at the inward-facing state and, close to D319 belonging to the other protomer when VcINDY is found at the outward-facing state (*Figure 3.26*). Therefore, the proximity between the D319A of the two protomers would generate protein instability by repulsing forces.
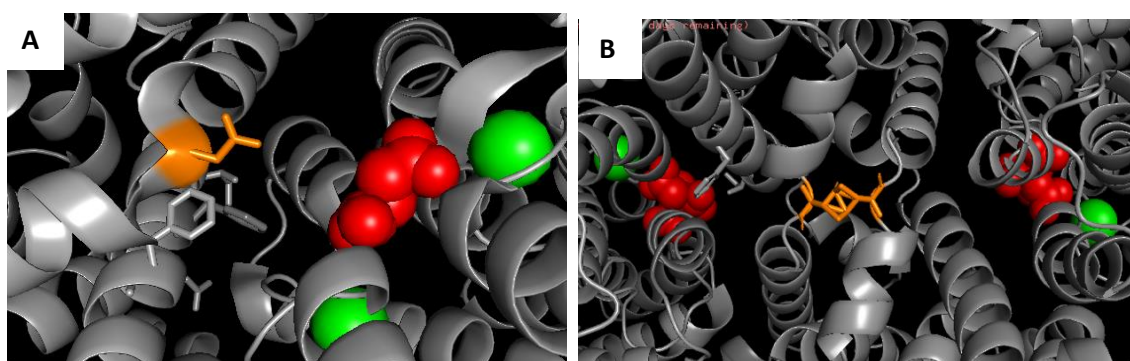

Figure 3.26: **3D close look at the D319 amino acid facing the substrate in the outward-facing state**

D319 location in a 3D model taken from a PyMOL at (**A**) VcINDY's inward-facing state from the crystal structure of Nie *et al.,* 2017, (**B**) VCINDY's outward-facing model based on Mancusso *et al.,*2012 crystal structure from Mulligan *et al.,* 2016. D319 amino acid is marked in orange in both conformations. Also, in both images, sodium cations are represented as green spheres and substrates as red spheres.

Oxalate and citrate did not influence any change on the melting temperature of D319A (*Figure 3.27). They are the only two compounds that did not affect the melting temperature of the mutant. Succinate, fumarate, malate and 5'-sulfosalisilic acid results keep in line with VcINDY wild-type findings by being the compounds with bigger stabilisation capacity (*Figure 3.27*). The ΔTm collected

from their data were: 8.6± 0.81 °C for succinate, 8± 3.38 °C for fumarate, 8.6± 0.81 °C for malate and 8.3± 0 °C for 5'-sulfosalisilic acid. Icatonic acid and oxalacetate, other four-carbon chain compounds, had a larger ΔTm than wild-type but still reduced in comparison with D319A previous four-carbon compounds changes (*Figure 3.27*). Besides, tricarballyate and adipate gave more stabilisation to D319A protein with a difference of 6± 0.47 °C and 6.3± 0.47 °C, respectively (*Table 3.2*).

The present study confirmed the findings of increased protein stability in augmentation of the present sodium concentration, as ΔTm were highly noticeable compared to wild-type. Wild-type analysis was carried out in the concentration of 50 mM, three times lower than the concentration used for D319A. This highlights the concept of sodium importance for substrate binding, indicating that both binding-site affect each other and are therefore cooperative The differences between wild-type and D319A result could be attributed to the effect on sodium and cannot be comparable, despite a parallel ΔTm pattern can be seen for both transporters.
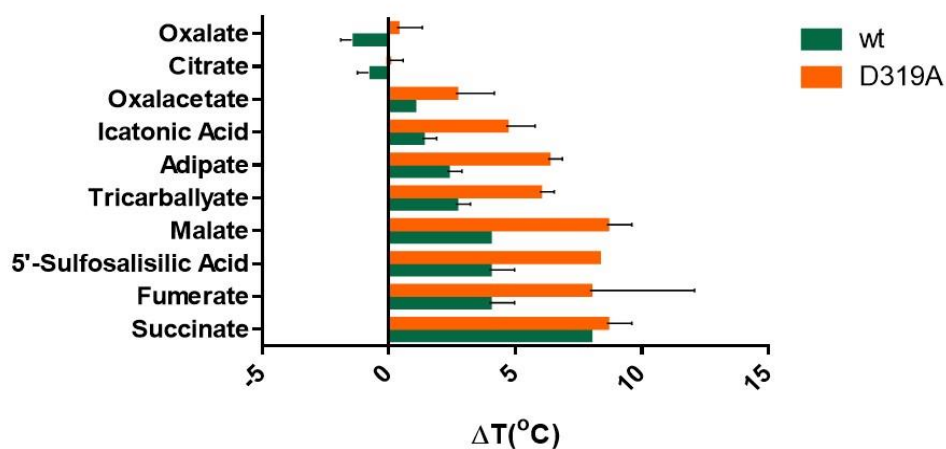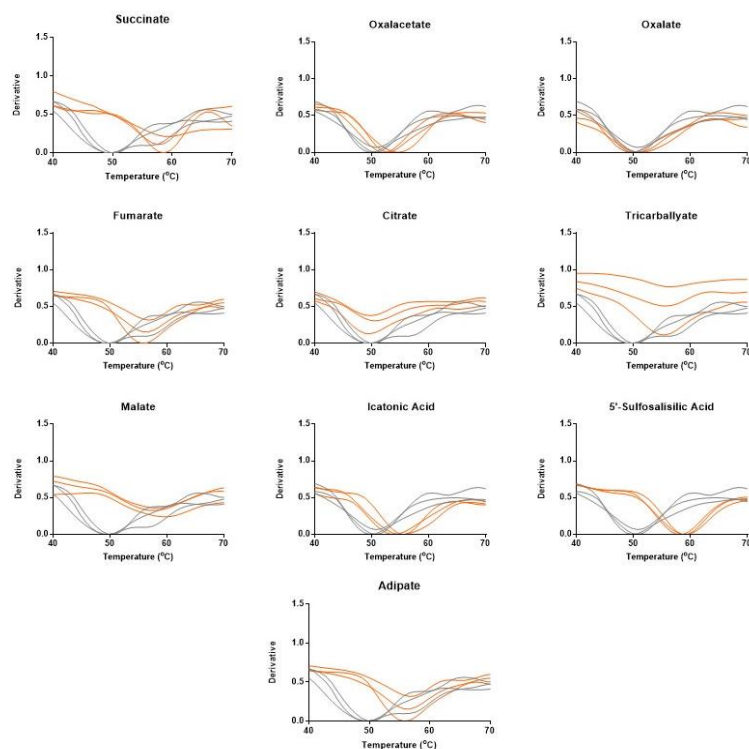

(Figure continues on next page)

Figure 3.27: **10 compounds thermostability screen using VcINDY alanine mutant D319A.**

 Average melting temperature shift (ΔTm) of VcINDY in the presence of each compound was determined by subtracting the VcINDY Tm in the absence of substrate from the Tm in the presence of the indicated compound. The results of the mutant (orange) are shown next to wild-type VcINDY outcomes for the same compound (green) for comparison. The bars shown are the average of triplicated datasets with their error bars represented SEM. In addition, below normalised melting curves graphs from the derivative of the untouched data of VcINDY D319A in 10 mM of the indicated compound present (orange) and in its absence (grey). Each line represents a single outcome of the triplicated data.

3.5.4.5. V322A

The valine of V322 has an aliphatic side-chain group. This amino acid has been described from the crystal structure to be at the TM9b, which belongs to the oligomerization domain (*Figure 3.28*). Hence, V322 possibly interacts with the substrate when it is being transported. The study of this position would reveal if substrate selectivity at some point of the transport gets influenced by V322. The baseline melting temperature obtained for V322A was of 50 ± 2.21 °C (*Table 3.2*), being lower than wild-type's without the presence of any compound.

The data gathered showed a general disability for the anionic compounds to stabilise V322A as they did on wild-type (*Figure 3.29*). In general, the experiment's outcomes lack statistical value. The difference with the substrate is not prominent enough when compared to the absence of ligand condition. Succinate provoked a unique significant shift equal to wild-type with 7 ±0.94 °C. Malate also provided extra stability to the VcINDY V322A protein when bound with a ΔTm of 3 ± 0.47 °C (*Table 3.2*).
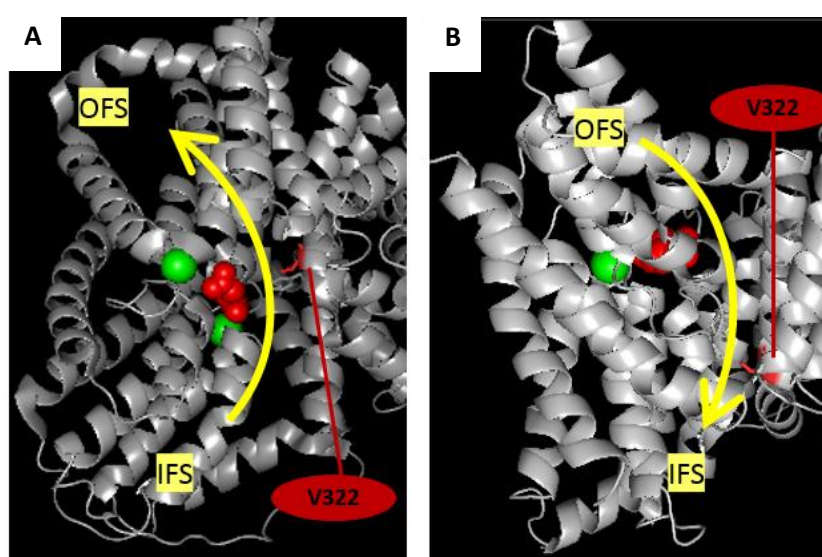

Figure 3.28: **Representation of V322 localization in a 3D VcINDY crystal structure.**

V322 location in a 3D model taken from a PyMOL at (**A**) VcINDY's inward-facing state from the crystal structure of Nie *et al.,* 2017, (**B**) VCINDY's outward-facing model based on Mancusso *et al.,*2012 crystal structure from Mulligan *et al.,*2016. V322 amino acid is marked in red in both conformations. Also, in both images, sodium cations are represented as green spheres and substrates as red spheres The yellow arrow represents the path followed by the binding-site during the elevator-type transport cycle from IFS (inward-facing state) to OFS (outward-facing state), or vice versa.

Overall, the alanine mutation at the 322 positions did not affect succinate and malate binding. However, any other compound of the library failed to provide stability to the mutant (*Figure 3.29*). Oxalate and citrate outcomes matched with what would be expected, as they did not provide stability in wild-type experiments. Icatonic acid, adipate and oxalacetate barely generated melting temperature shifts (*Figure 3.29*). So, the findings on V322A at least hint that V332A

does impact substrate selectivity by avoiding binding of compounds prior mentioned except succinate and malate.
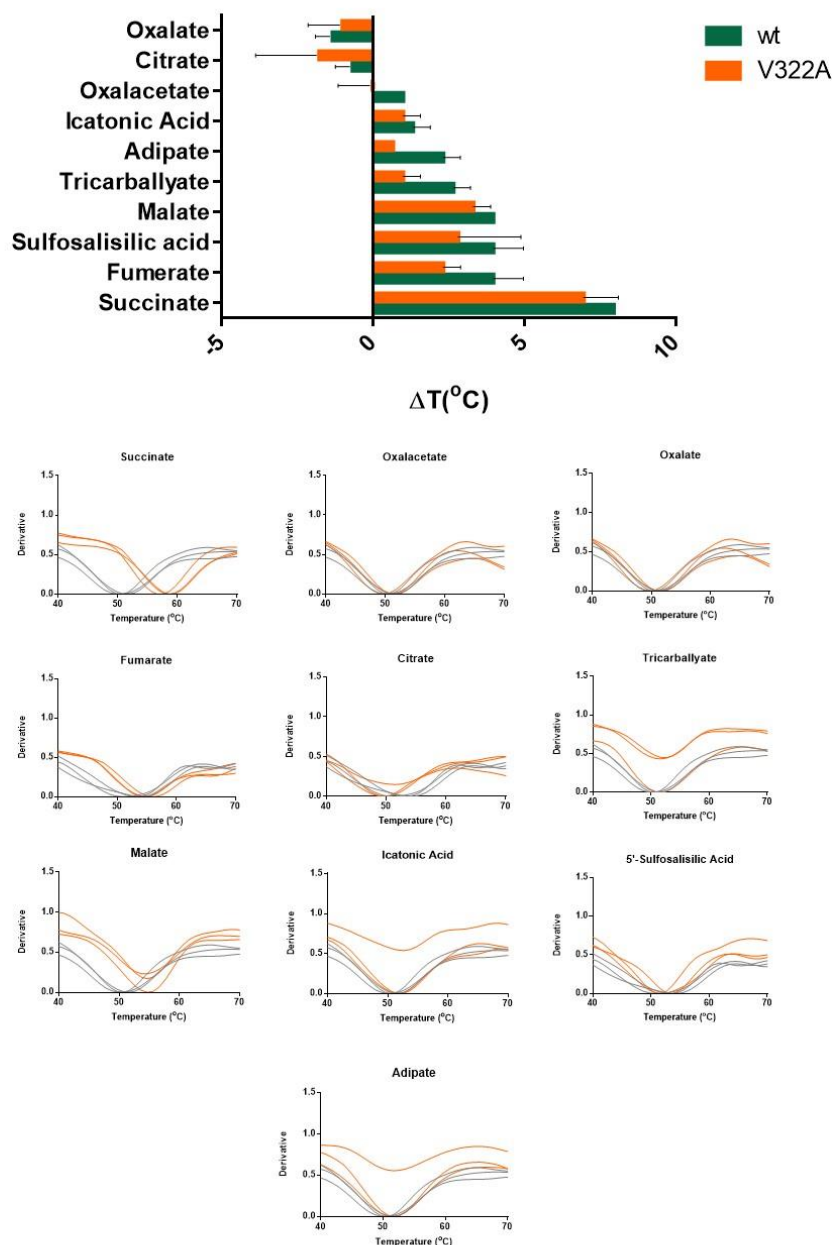

Figure 3.29: **10 compounds thermostability screen using VcINDY alanine mutant V322A.**

A) Average melting temperature shift (ΔTm) of VcINDY in the presence of each compound was determined by subtracting the VcINDY Tm in the absence of substrate from the Tm in the presence of the indicated compound. The results of the mutant (orange) are shown next to wild-type VcINDY outcomes for the same compound (green) for comparison. The bars shown are the average of triplicated datasets with their error bars represented SEM. In addition, below normalised melting curves graphs from the derivative of the untouched data of VcINDY V322A in 10 mM of the indicated compound present (orange) and in its absence (grey). Each line represents a single outcome of the triplicated data.

3.5.4.6. F326A

F326A is located at the TM8b of the VcINDY structure and the phenylalanine has an aromatic ring in its chemical structure. The melting temperature of the protein alone was 49.76± 1.43 °C, which indicates that VcINDY F326A is less stable than VcINDY wild-type. A CPM assay to test binding selectivity of ten compounds of the library was carried out as prior done to identify if F326A is involved in substrate selectivity, despite being far from the binding site *(Figure 3.30)*.
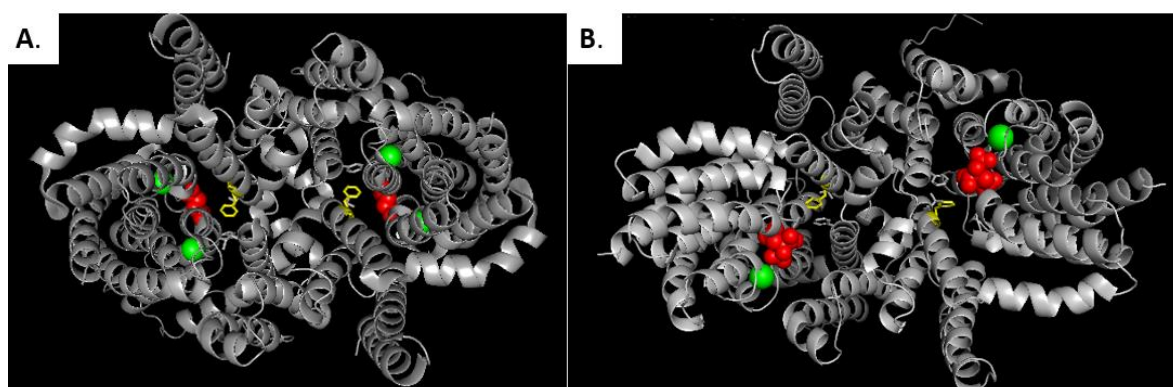

Figure 3.30: **Representation of 326 localization in a 3D VcINDY crystal structure.**

F326 location from the inside of the cell perspective in a 3D model taken from a PyMOL at (**A**) VcINDY's inward-facing state from the crystal structure of Nie *et al.,* 2017, (**B**) VCINDY's outward-facing model based on Mancusso *et al.,*2012 crystal structure from Mulligan *et al.,* 2016. F326 amino acid is marked in yellow in both conformations. Also, in both images, sodium cations are represented as green spheres and substrates as red spheres.

In this experiment, out of the compounds with four carbons in their chain, succinate gave the maximum stability with a higher ΔTm than it did on VcINDY wild-type (*Figure 3.31*). Succinate ΔTm provoked was of 8.9± 0.50 °C, followed by fumarate with quite similar outcomes than wild-type with approximately ΔTm of 5 ± 1.24 °C (*Table 3.2*). The thermal shifts for other four-chain compounds on F326A did not offer a significant ΔTm between conditions. For similar reasons, 5'-

sulfosalisilic acid, tricarballyate and, citrate would not be commented. However, adipate, a larger carbon chain compound, generated a ΔTm greater than the one saw on wild-type with 3.3± 1.24 °C (*Table 3.2*).

Unexpectedly, compared to any prior results, the effect of oxalate on protein's stabilisation was evident. The oxalate's stabilisation on F326A was 8.1 ± 1.87 °C (*Table 3.1*). On the oxalate raw data graphs, out of the three reading only two melting points matched with the substantial stabilisation increase (*Appendix B: Supplementary Figure 6.2.13*). Such effect on the melting temperature was not shared with any other compound from the library or any other mutant tested. Only succinate provided F326A with a parallel stabilisation (*Figure 3.31*). This F326A analysis found evidence for phenylalanine to rejects binding of short compounds such as oxalate (2C), while it preserves binding of the main substrate succinate and at the same time adipate (6C).
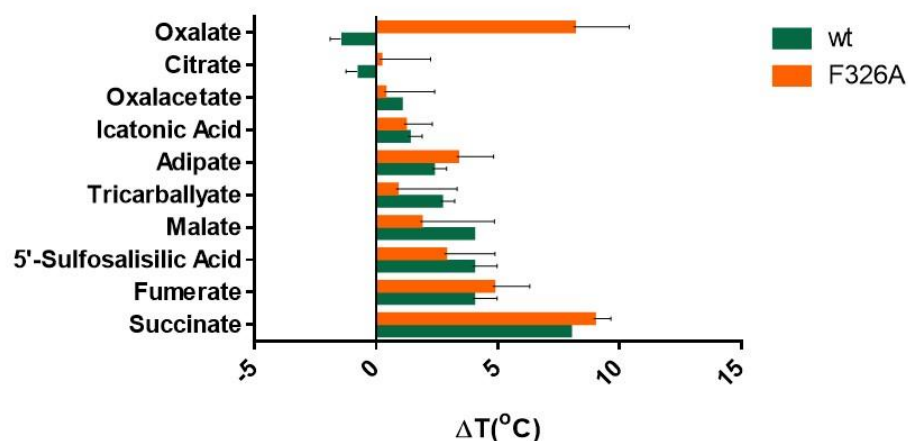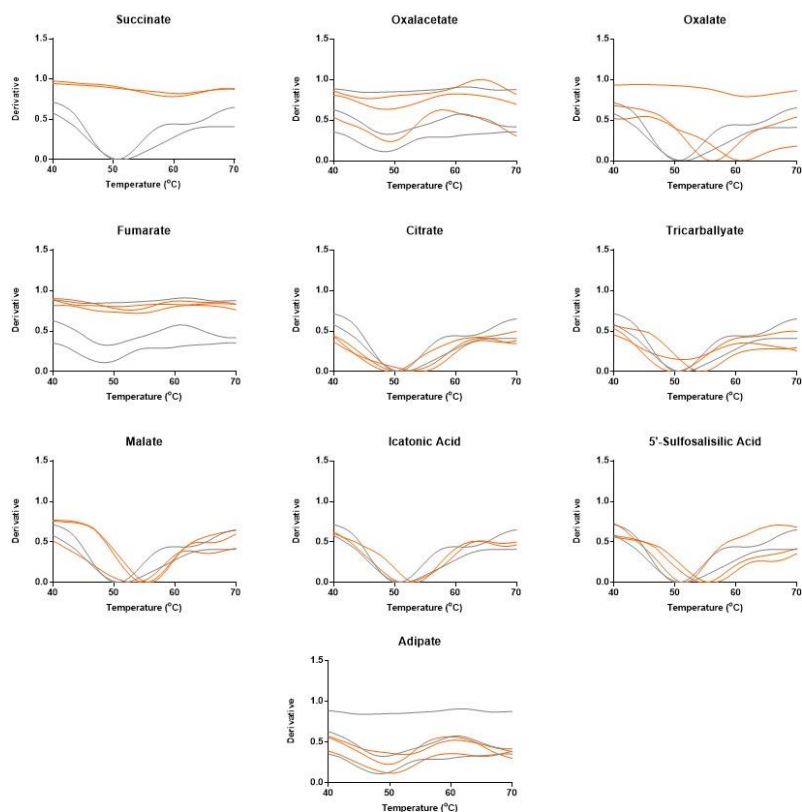

(Figure continues on next page)

Figure 3.31: **10 compounds thermostability screen using VcINDY alanine mutant F326A.**

Average melting temperature shift (ΔTm) of VcINDY in the presence of each compound was determined by subtracting the VcINDY Tm in the absence of substrate from the Tm in the presence of the indicated compound. The results of the mutant (orange) are shown next to wild-type VcINDY outcomes for the same compound (green) for comparison. The bars shown are the average of triplicated datasets with their error bars represented SEM. In addition, below normalised melting curves graphs from the derivative of the untouched data of VcINDY F326A in 10 mM of the indicated compound present (orange) and in its absence (grey). Each line represents a single outcome of the triplicated data.

3.6. EXAMINATION OF VcINDY SUBSTRATE RECOGNITION

CHANGES DEPENDING ON CATIONS

For further research to uncover which components could trigger substrate recognition, the influence of different anions on the binding site was studied. The sodium and substrate binding sites are situated close within the protein structure until the point where amino acids are shared between them. It would not be surprising if cation interactions bound to the described sodium-binding site could

yield variation in substrate selectivity. However, only the consequences of cation binding to DASS proteins within the transport mechanism have been investigated. Here, taking advantage of VcINDY well-characterised DASS transporter, study of sodium, lithium and potassium effect on substrate binding would be carried out.

3.6.1. ANION INFLUENCE ON SUCCINATE BINDING ON VcINDY

Sodium's importance in VcINDY transport, as well as other DASS transporters, is well-known (Mulligan *et al.*, 2014)(Inoue et al., 2002)(Inoue *et al.*, 2002)(Strickler *et al.*, 2009)(Hall and Pajor, 2007) (Sauer *et al.*, 2020). Sodium is capable of powering succinate transport in VcINDY, whereas, Li^+ is able to transport succinate but to a much lesser degree. Potassium, on the contrary, failed to provide VcINDY capacity to transport succinate (Mulligan *et al.*, 2014). Therefore, it seems that sodium binding provides VcINDY protein with higher stabilisation than any other cation.

To test how binding of different cations is directly coupled to substrate binding. First, the association between Na^+, Li^+ or K^+ and the stabilisation of VcINDY in the presence of its substrate, succinate, was used following a CPM assay.

The Tm offered by these three cations to VcINDY wild-type in the presence and absence of 10 mM succinate was evaluated (*Figure 3.32*). The relationship between sodium and succinate binding was first established. Then, lithium and potassium were tested in the same conditions to observe if variation in VcINDY stabilisation occurred in the presence of succinate.

In the concentration of 50 mM of each cation, stabilisation by sodium and lithium of VcINDY was almost identical with Tm of 56.66± 0.81 °C and 57.66± 0 °C,

respectively, whereas, a lower Tm of 52.35± 0.94 °C was found in the presence of K⁺. When observation of VcINDY's Tm in the presence of succinate the data presented some variance. Potassium's stabilisation effect was lower than previously with a Tm of 51.36± 0.47 °C (*Figure 3.32*). Therefore, potassium did not show any significance change on VcINDY Tm in the presence of the substrate as expected. However, a shift on the Tm was perceptible in sodium and lithium experiments.

In the presence of 50 mM of lithium, Tm was 60.30± 0.47 °C, approximately 2.6 °C higher than in the absence of succinate. In the case of sodium, in the same concentration, Na⁺ provided VcINDY with a much higher stabilisation when succinate was present. The VcINDY Tm in the presence of sodium and succinate was 64.61 ± 0 °C, generating the stabilisation effect of almost 8 °C.
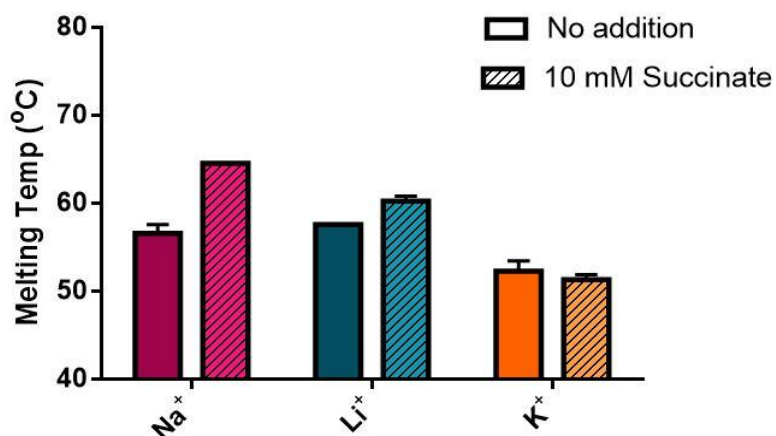

Figure 3.32: **Differences in succinate binding depending on cation interactions.**

Succinate-induced stabilisation effect on VcINDY by sodium (pink), lithium (blue) and potassium (orange). Two conditions were tested in the presence of 50 mM of each cation: 10 mM of succinate (filled lines) and non-succinate added (blank). The data presented are the melting temperatures obtained in each experiment shown as the average from triplicate datasets and the error bars represent SEM.

From the data collected, it could be suggested that sodium cation has the ability to stabilise the protein in a specific way that the two other cations of the study are unable to. A key finding emerged from the observation of Li$^+$ thermostability effect on VcINDY, which demonstrates two things. First, VcINDY can generate a similar amount of bonds with lithium that it does with sodium since Li$^+$ thermostability effect was very similar to Na$^+$. Second, it highlights that little is known about the effects of these two cations on substrate binding since lithium can stabilise VcINDY by itself, but it barely gives a higher stabilisation when succinate is present. This might imply that Li$^+$ causes an effect on substrate selectivity not identical to sodium, despite forming the same number of bonds.

3.6.2. COMPOUND SCREEN WITH VcINDY WILD-TYPE INFLUENCED BY NA$^+$ SUBSTITUTION REVEAL DIFFERENCES IN LIGAND'S SELECTIVITY

From the previous findings, it seems that Na$^+$ is essential for substrate interactions by generating succinate-induced stability not replicated by lithium or potassium. Hence, and as previously suggested, sodium creates local allosteric interaction with VcINDY that would facilitate substrate to get bound more easily to the protein (Mancusso *et al.*, 2012). On the contrary, despite lithium gets bound to the protein, it probably fails to enhance succinate-induced binding as sodium does.

To further test changes in substrate selectivity depending on the cation bound to VcINDY, the effect of lithium and potassium with other ligands from the library of the study were exploded. Following a CPM assay, as done previously for the alanine mutants, the relationship between cations and ligands was analysed by

observation of melting temperature shifts. If VcINDY increased stability in the presence of substrate and sodium is due to unique sodium allosteric interactions, a non-increase of VcINDY melting temperatures compared to wild-type would be expected in the presence of lithium and potassium.

Tables indicating the ΔTm for each cation and ligand tested may be found in Appendix B (*Supplementary Figure 6.2.19*). Raw untouched data from the CPM-test for Li^+ and K^+ can also be found in *Figure 6.2.17* and *6.2.18* (respectively) in the appendix chapter.

3.6.2.1. Potassium effect on substrate selectivity

The effect on substrate selectivity caused by potassium was decided to be investigated. Potassium K^+ was reported here by observation of the Tm to unsuccessfully promote succinate binding and in other studies to be unable to support succinate transport in VcINDY (Mulligan *et al.*, 2014). Thus, potassium is expected to do not be suited to allow the binding of ligands to get bound to VcINDY. To confirm this, VcINDY wild-type CPM assay was carried out in the presence of 1 % DDM, 50 mM K^+, and 2 mg/ml of protein, in addition to the absence or presence of 10 mM of a compound of the study.

The results gathered from testing K^+ shown that no compound stabilised VcINDY wild-type in the presence of 50 mM potassium (*Figure 3.33*). All the ΔTm resulted from the screen of the ten different compounds were negative, which means that VcINDY was even less stable when a compound was added to the solution. The melting temperature shifts varied significantly except succinate, fumarate and malate, from which ΔTm did not differ from the baseline of the control condition.

The results of the 50 mM K$^+$ CPM assay go beyond the findings of its insufficient succinate-induction stabilisation to any other compound tested. Potassium has a larger size than sodium which could be the reason behind its inadequacy to promote binding of substrates to the binding site of the protein.
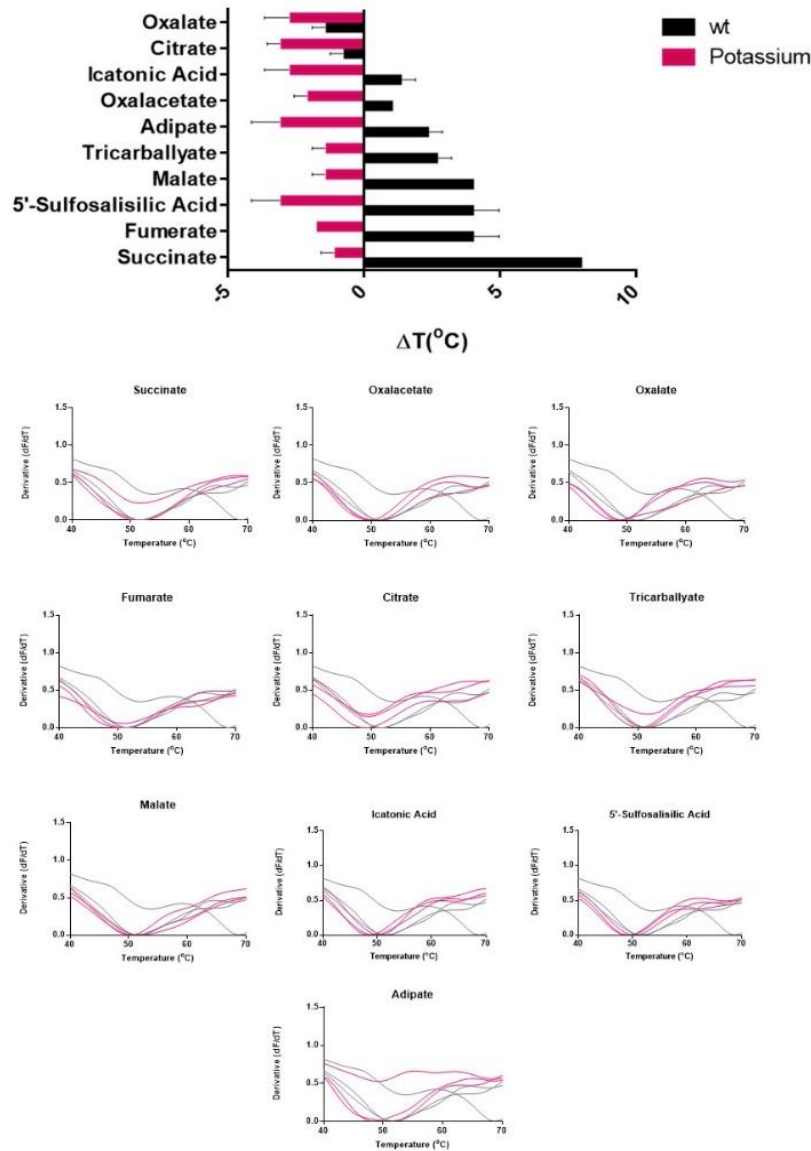

Figure 3.33: **10 compounds thermostability screen using VcINDY wild-type in the presence of potassium cation.**

Average melting temperature shift (ΔTm) of VcINDY in the presence of each compound was determined by subtracting the VcINDY Tm in the absence of substrate from the Tm in the presence of the indicated compound (all in the presence of 50 mM K$^+$). The bars shown are the average of triplicated datasets with their error bars represented SEM. In addition, below normalised melting curves graphs from the derivative of the untouched data of VcINDY in 10 mM of the indicated compound present (pink) and in its absence (grey). Each line represents a single outcome of the triplicated data. This experiment was only one day.

3.6.2.2. Lithium effect on substrate selectivity

Li$^+$ catalysed succinate transport poorly in VcINDY but, as prior confirmed, it gets somehow specifically bound to the VcINDY transporter (*Figure 3.32*). We speculate that sodium enhances substrate binding by the intervention of allosteric forces, which triggers the protein to follow an induced-fit mechanism to adequate substrates at the binding-site. However, so far only succinate recognition has been reported in VcINDY in the presence of sodium and lithium.

In order to cast some light on this proposed induced-fit mechanism more ligands should be studied to approach the cations and substrates relationship. Thus, a CPM assay with the compounds from the library in the presence of Li$^+$ was carried out.

The binding of lithium to the protein and its repercussions on substrate binding was observed (*Figure 3.34*). First, in the presence of 50 mM of lithium, lithium stabilised VcINDY with a Tm 57.6± 0 ^{o}C, which showed that lithium interacted and generated bonds specifically with the transporter. In the test with ligands, the ΔTm in the presence of succinate was significant but with less VcINDY stabilisation compared to wild-type succinate's influence in the presence of sodium, as well as 5'-sulfosalisilic acid. Fumarate, a similar molecule to succinate bound, did not provoke a significant ΔTm difference so it will not be commented further (*Figure 3.34*).

Other four-carbons molecules such oxalacetate stabilised more VcINDY in the presence of lithium than sodium, with an almost significant ΔTm of 2 ^{o}C (*Figure 3.34*). Malate showed a ΔTm of 2.98± 1.4 ^{o}C, whereas, icatonic acid presented the

same ΔTm with both cations. Molecules with five-carbon chains such as tricarballyate showed the same stabilisation effect with lithium than when sodium was present. Citrate stabilisation effect in the presence of Li$^+$ was surprisingly positive. Finally, out of the ten molecules, oxalate and adipate did not offer VcINDY a significant stabilisation, which means that they did not get bound to the transporter.

From the results, evidence from lithium effect on substrate recognition suggests that Li$^+$ provides citrate, tricarballyate, oxalacetate, malate and icatonic acid with enough stability forces, while it fails to generate a fitting binding site to the main stabilising compounds reported in the presence of sodium such as other 4C-molecules and 5'-sulfosalisilic acid.

From these findings, it could be speculated that lithium's stability effect on the transporter is due to whether the molecules have a functional group. Despite sodium provides generally more stabilisation to the transporter indicated by larger ΔTm when comparing conditions, lithium could be able to imitate sodium's effect when substrates have a functional group in 2C or 3C of their structure. On the contrary, with compounds that own a linear carbon-chain such as succinate, fumarate and adipate, Li$^+$ would not be able to build allosteric changes as adequate as sodium does. To support this, it could be possible that Li$^+$ smaller size brings better fitting to additional groups of the scaffold-carbon chains of the ligands. Therefore, lithium could be able to change substrate selectivity and sodium-succinate interaction it is not unique although, sodium binding leads to better substrate recognition.
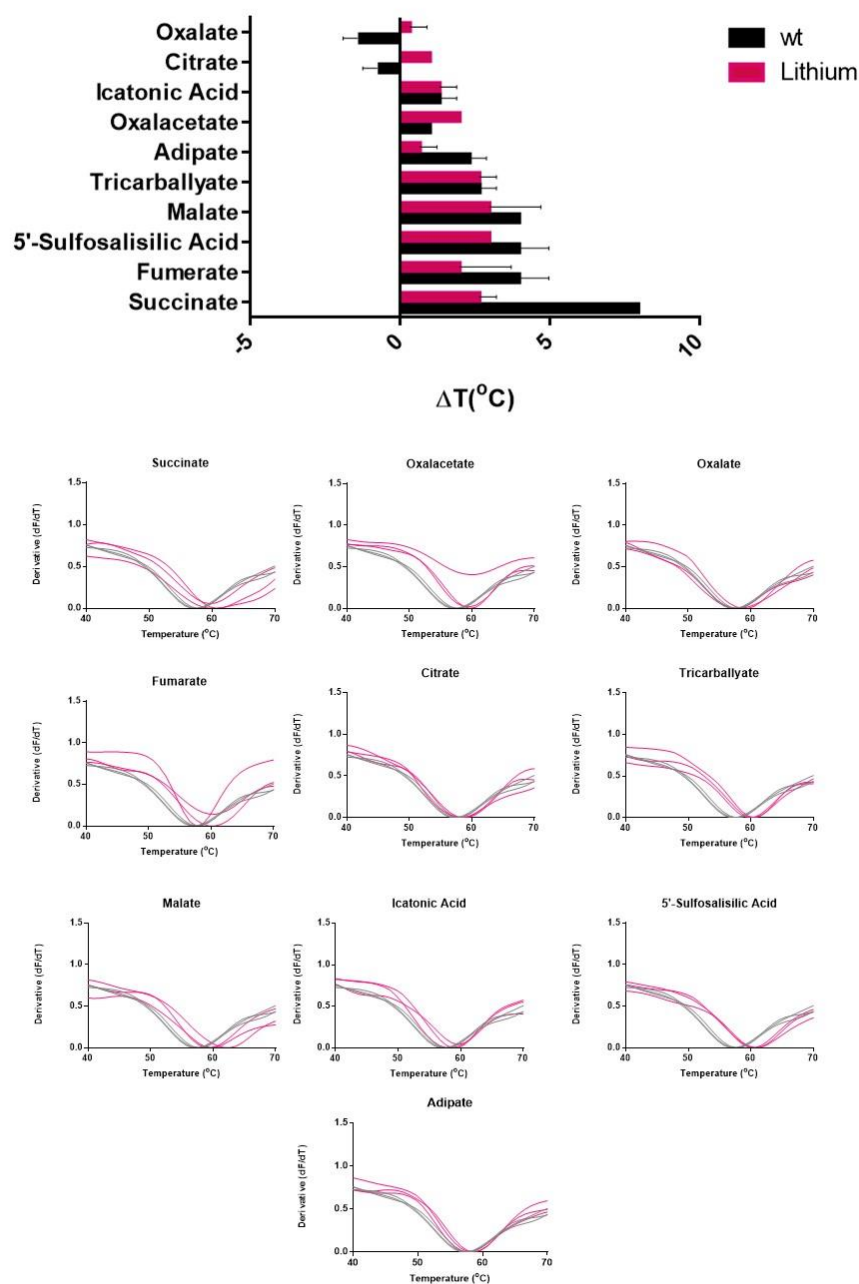
Figure 3.34: **10 compounds thermostability screen using VcINDY wild-type in the presence of lithium cation.**

Average melting temperature shift (ΔTm) of VcINDY in the presence of each compound was determined by subtracting the VcINDY Tm in the absence of substrate from the Tm in the presence of the indicated compound (all in the presence of 50 mM Li$^+$). The bars shown are the average of triplicated datasets with their error bars represented SEM. In addition, below normalised melting curves graphs from the derivative of the untouched data of VcINDY in 10 mM of the indicated compound present (pink) and in its absence (grey). Each line represents a single outcome of the triplicated data.

CHAPTER 4: DISCUSSION

In this project, a series of thermostability-based binding assays were used to gain comprehension of substrate and cations interactions in VcINDY transporters. VcINDY is used as a DASS model since it was at the moment the only DASS member with a solved crystal structure (Nie *et al.*, 2017). While this research was being carried out, the LaINDY transporter's structure was published (Sauer *et al.*, 2020).

DASS transporters are very dynamic, holding some functional and sequence differences between members, but they all converged together due to their important physiological roles (Pajor, 1999) (Pajor, 2006)(Knauf *et al.*, 2006) (Pajor, 2014) (Lu, 2019). Several knock-down gene studies have proved their relevance among different species (Fei *et al.*, 2004)(Rogina and Helfand, 2013). Specifically, studies on the SLC13 mammalian family have highlighted members as approaching medical targets for the treatment of cancer, diabetes and obesity and other metabolic-related diseases (Birkenfeld *et al.*, 2011)(Bergeron *et al.*, 2013)(Huard *et al.*, 2015).

Focusing on monitoring transport has been so far the main approach in the study of DASS transporters. Within an elevator-type mechanism, VcINDY exposes the substrate alternatively to the extracellular or the cytosolic side with two known different conformations: outward-facing state (OFS) and inward-facing state (IFS), respectively (Mulligan *et al.*, 2016). Developing state-dependent inhibitors requires an understanding of the distribution of the protein's conformational

states. Hence, it is important to clearly understand the mechanism from which these proteins operate to develop effective inhibitors. To this goal, it is equally vital to determine the factors for substrate recognition and the rules proceeding cation and substrate-specific interactions.

Here, with a high-throughput method and screening of multiple ligands with different VcINDY alanine mutants, we ought to identify protein-ligand binding demands and give some further insights into VcINDY substrate recognition variation throughout the elevator-type transport (*Figure 4.0*).
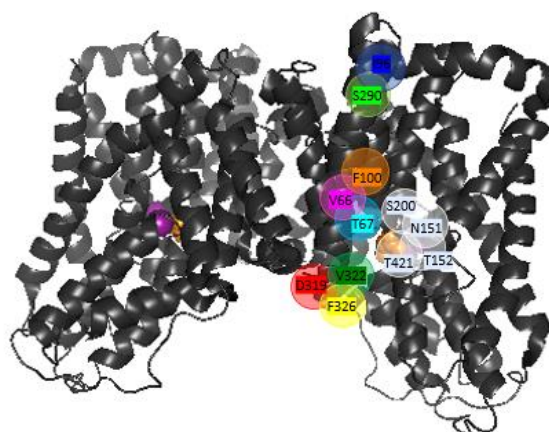

Figure 4.0: **View of the selected amino acids of the study in the VcINDY inward-facing state conformation.**

Detailed crystal structure of succinate molecule (orange) bound at the binding site (PDB 5UL7) from (Nie et al.,2017). Na+ ions are purple spheres. The relative position of the amino acids mutated to alanine are marked in colours: yellow (F326), red (319), green dark (V322), light blue (T67), pink (V66), orange (F100), light green (S290) and dark blue (I96) and amino acids in the transport domain are all painted in white (N151, T152, S200 and T421).

These work findings hint participation of amino acids belonging to the scaffold and oligomerization domain in implementing secondary substrate filters, while amino acids belonging to the transport domain seem to carry the chain-length filter into effect. Further analysed residues in VcINDY structure could also infer differences in substrate selectivity accordingly to the conformation adopted by the transporter. Finally, other positions are suggested for the first time to have potential mechanistic roles in the elevator-type mechanism of VcINDY.

Therefore, substrate-binding events in isolation have been carried out to study specific transporter's residues. Using the same approach, cation binding effects on substrate recognition have also been pursued. Such results indicate that interactions with sodium are indeed necessary for allowing substrate binding in a way that lithium cannot reproduce. However, a variation in binding these two cations could give rise to differences in substrate selectivity.

4.1. SUBSTRATE BINDING SELECTIVITY IS SHARED BETWEEN DIFFERENT VcINDY STRUCTURAL COMPONENTS

4.1.1. ACCOUNT FOR VcINDY BROAD LIGAND RECOGNITION

In this study, the understanding of VcINDY interactions with ligands has been exploded. With site-directed mutagenesis and a functional assay based on the thermostability of VcINDY, the prerequisites of ligands to be recognized by the transport have been revealed thanks to the structural knowledge of the transporter.

Optimal successful binding, seen by a large increase in the protein's thermostability, happens when compounds have four carbons and non-extra carboxyl groups, only two carboxyl groups at each side of the carbon-chain (succinate and fumarate) (*Figure 3.9*). Therefore, based on the results, a ligand requirement to ascertain successful interaction within the binding site is the presence of two carboxylate groups.

Variations can be tolerated by the transporter when carboxylic groups are located at the second carbon of dicarboxylates (oxaloacetate, icatonic acid and malate). Binding of tricarboxylates with bulky groups at the third carbon (tricarballyate) is

also accepted by the transporter. Hence, VcINDY tolerates additional functional groups when they can be oriented out (towards binding site opening) in a way that the protein can stabilise them as the citrate VcINDY crystal structure displays (Nie *et al.*, 2017)(Mancusso *et al.*, 2012).

These findings support the notion that VcINDY prefers C4 and C5-tri/dicarboxylates, which would be due to their optimal length to interact fully with the carboxylate recognition regions of the transporter, known as the SNT motifs (Mulligan *et al.*, 2014)(Mancusso *et al.*, 2012). This would explain why shorter compounds like oxalate, which despite having carboxylic regions on each side of the molecule, fail to provide stability to VcINDY. Once more, the best compound length to fulfil interaction accomplishment for these SNT motifs seems to be four-carbon compounds. Compounds with five carbons can also fit in but offering fewer interactions given the lesser stabilisation effect seen.

However, in our data citrate did not offer stability to the protein. At the pH 7.5 of the experiment, the citrate's predominant state is deprotonated with three negative charges, whereas succinate only has two (Mulligan *et al.*, 2014). Since VcINDY is susceptible to negatively charged molecules such as glutamate, we argue that the lack of citrate binding is due to VcINDY rejection of citrate's fully Pro-S negatively charge carboxylate (Mulligan et al., 2014)(Nie et al., 2017). Similarly, the tricarballyate state would also be mainly deprotonated. The reasons behind its better stability effect on the transporter remain unclear since its molecular structure is very similar to citrate's but without the hydroxyl group on

the third carbon. Surprisingly, adipate (6C) and 5'-sulfosalisilic acid (C7) compounds offered stabilisation (*Figure 3.9*).

In the adipate case, we believe that the absence of additional functional groups allows the compound to be flexible inside the binding-site. In a similar way, the benzene ring of 5'-sulfosalisilic acid compresses the molecule in a way that can fit inside the binding site and get bound thanks to its extreme carboxylic group. This way, the previous hypothesis of ligand's requirement to interact with the two carboxylic recognition regions of VcINDY is supported if the molecules present the right size.

In addition, results of the SNTAAA VcINDY displayed the relevance of at least the SNT motif at the HPin structure since non-ligand could offer stabilisation when the three present amino acids were mutated with an alanine. It seems that VcINDY substrate selectivity is largely related to the binding accomplishment of the two SNT motifs. Implementing discrimination of any compound that does not have the correct dicarboxylate distance or cannot adapt.

Importantly, these motifs are considered the fingerprint of the Na^+-dependent tri/dicarboxylate transporters family (Mancusso *et al.*, 2012). They are almost fully conserved in the DASS family (Vergara-jaque *et al.*, 2012). This implicates that VcINDY binding selectivity could be common in the DASS family. In fact, the dicarboxylate length dependence has been observed in transport competition assays for other DASS transporters (Mulligan *et al.*, 2014) (Kekuda *et al.*, 1999)(Burckhardt *et al.*, 2005).

4.1.2. RELEVANCE OF THE SNT MOTIF AND OTHER RELATED TRANSPORT DOMAIN AMINO ACIDS

Since a molecular chain-length filter could rule ligands' binding, specific residues from the binding-site were tested to test their involvement in such a filter. An individual amino acid of the SNT motif tested in this study showed that its role is indeed crucial. The results of N151 imply a very important role of the amidic group to recognise ligands (*Figure 3.12*).

No compound from the library of this study could stabilize the protein when N151 was mutated to an alanine. The 5'-sulfosalisilic acid was an exception generating a small increase in stability. We believe that its positive effect is well justified as 5'-sulfosalisilic acid contains only one carboxylic group that could still be bound to SNT at the HPout while the sulphur group, at the other side of the molecule, could form interactions without the need of the amide functional group of 151.

The importance of N151 gets further reinforced by the information provided of the crystal structure. N151 forms bonds with the carboxylate group of succinate as well as the sodium in Na1 (Nie *et al.*, 2017).

The T152 amino acid is located at the HP1 next to N151. T152 forms a bond with the carboxylic group of succinate as N151 does (Nie *et al.*, 2017). In our Thermofluor assays results for its mutant, citrate presented a modest stabilisation in a similar way that happens for N151A (*Figure 3.13*). In the Mancusso *et al.*, crystal structure, the residues of 151 and 152 generate H-bound with the terminal citrate's carboxylate group providing stabilisation. The interpretation of our results suggests that T152 has a role in implementing the molecular chain rule but

not as much as N151, while both share stabilisation of the ligand's bulky groups with H-bounds. In normal conditions, N151 and T152 are responsible for avoiding the binding of deprotonated citrate.

The results of these two binding-site involved mutants support their vital functions and add modest specificity roles for N151 and T152. When N151 is mutated to alanine in VcINDY, the transport capacity gets impaired, and succinate binding is reduced (Nie *et al.*, 2017). In NaDC3, mutants of amino acids related to the binding-site also affect transport function. Some of these mutants are NaDC3^{N144} (VcINDY N151), NaDC3^{T145}(VcINDY T152), NaDC3^{T253} (VcINDY S200) and NaDC3^{T527} (VcINDY 421), which have been tested in our CPM-assays (Schlessinger *et al.*, 2014). Hence, it is wise to believe that other critical related amino acids contribute to the SNT motif selectivity role.

4.1.3. MECHANISTIC ROLES OF S200 AND T421

More amino acids belonging to the transport domain appeared to be required for the binding of ligands. S200 and T421 are located at the L5a-b and L10a-b (respectively). Interestingly, they both showed increased stability in the absence of succinate when mutated to alanine (*Figure 3.8*) (Nie *et al.*, 2017).

From the published structural information, S200 interacts with N151 stabilising it by the formation of H-bonds. T421 does the same but binding to N378 at the other SNT motif at the HPout (Nie *et al.*, 2017). Despite not being described to interact directly with the substrate, we believe that their participation in ligand binding could go beyond the formation of the described H-bonds from the crystal structure.

The melting temperature baseline found for S200A was 62.32 ± 1.64 °C, equal to the succinate binding effect on VcINDY wild-type (*Figure 3.8*). In most cases, the presence of ligands for S200A destabilised the transport or did not offer any change in the melting point (*Figure 3.14*). T421A melting temperature baseline was not as substantial as S200A, but the results in the presence of ligands matched S200A findings (*Figure 3.15*). For its similar position in the VcINDY structure and similar destabilisation effects in the ligand's presence, we proposed that T421 carries out a comparable action to S200.

We speculate that S200 and T421 residues are involved in keeping the binding site opened at the IFS, increasing binding site exposure (*Figure 1.4-A*). While, when mutated to alanine and after sodium binding, S200A and T421A can adopt a conformation where the binding site is less exposed to the external medium (*Figure 4.1-B)*. The adopted conformation will give the ability to increase hydrophobic interactions within the protein. Thereby, enhancing protein's thermostability at a higher level than binding water molecules could do. Hence, the differences in stability between wild-type in comparison to these two alanine mutants could be explained by the lesser ability of water molecules to help protein's stability.

Following this line of thought, ligands' presence would block S200A and T421A shift to a more stable conformation. Ligands can be bound to the protein and form bonds with the alanine in 200 and T421 positions. Hence, the mutated VcINDY can change conformation when sodium gets bound, but not in the ligands' presence.

Finally, the negative effect seen in the presence of ligands can be explained by the interplay of more binding-site amino acids (*Figure 1.4-C*).

Alanine mutations in 200 and T421 would disrupt the possibility to create H-bonds with the asparagine of the SNT motifs. Consequently, N151 and N378 are unable to get stabilised in the optimal position to recognise ligands' carboxylic groups. The inability to stabilise the optimal position of the binding-site SNT motifs would explain the negative stability effect seen for these two alanine mutants in sodium and ligand's presence.
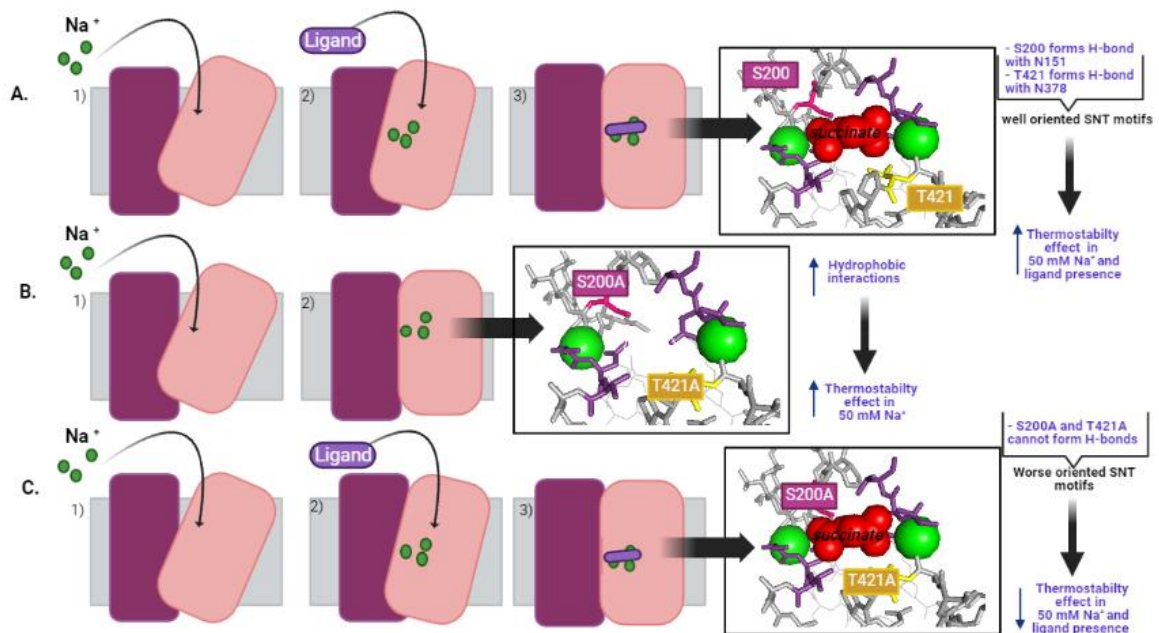
***Figure 4.1*: Schematic representation of sodium and ligand binding in VcINDY wild-type, T421A and S200A.**

The sequence of events according to the Thermofluor assay protocol is represented as follows; (**1**) Sodium ions are added first and get bound to VcINDY, increasing the transporter's stability. (**2**) The selected ligand is added to the solution. (**3**) The ligand binds to VcINDY. At the end of each sequence, a theoretical representation of the binding-site from close view is exposed created with PyMOL and the crystal structure from (Nie et al.,2017). The expected binding-site situation according to S200 and T421 ability to form bonds is represented in **A)** wild-type in the presence of sodium and ligand. **B)** VcINDY mutant S200A and T421A in the presence of only sodium. **C)** VcINDY mutant S200A and T421A in the presence of sodium ions and ligand. The ligand is a succinate represented in red spheres. Na+ ions are shown in green sphere. The T421 amino acid is coloured yellow and S200 in pink. The SNT motifs are both coloured in purple. (Created with BioRender.com)

An alternative explanation could be the adaptation of one specific conformation with more bonds possibly formed, such as a unique inward-facing state that is more stable than others in experiment conditions (50 mM Na$^+$). Therefore, the high stability and the destabilisation effects would be due to mere conformational changes, not involving these mutants' specific roles and binding events.

In other transporters using an elevator-type mechanism such as Glt$_{tk}$ and Glt$_{ph}$, an arginine occupies the substate-binding site in the absence of substrate to stabilize the protein (Jensen *et al.*, 2013)(Verdon *et al.*, 2014). Whereas, in VcINDY, there is no mechanism or amino acid described to stabilise DASS protein's apo-state (Nie *et al.*, 2017). Nie *et al.,* proposed that VcINDY could act as a water carrier to neutralise the vacant substrate-binding site in the absence of it and sodium. Both sodium and substrate-binding sites are solvents accessible in the inward-facing state. Water molecules would be enough to compensate for the empty-transporter's intrinsic charge so it can switch conformations again from the inward-facing state to the outward-facing state (Zeuthen et al., 2016).

VcINDY has a serine in position two hundred while other SLC13 members have a threonine. Both amino acids are hydroxylic supporting the hypothesis of their possible shared role in keeping the binding site open at the inward-facing state. The hydroxylic properties of the serine would be enough to bind water molecules strongly until VcINDY's residual charges in its apo state got compensated. In support of this hypothesis, alanine mutations of NaDC3 in T253 (VcINDY^{T200}) exhibit suppressed transport. Mutations in NaDC3^{T527} (VcINDY ^{T421}) also displayed disrupted transport (Nie *et al.*, 2017). However, the conservation of T421 among

SLC13 is different between NaC and NaS. In respective positions to VcINDY[T421], NaC transporters have also a threonine, while NaS transporters have an arginine (*Figure 4.2*). Conservation of the threonine only among NaC transporters could indicate that T421 is more relevant for di/tri-carboxylates recognition than S200, while it carries the mentioned mechanistic role.
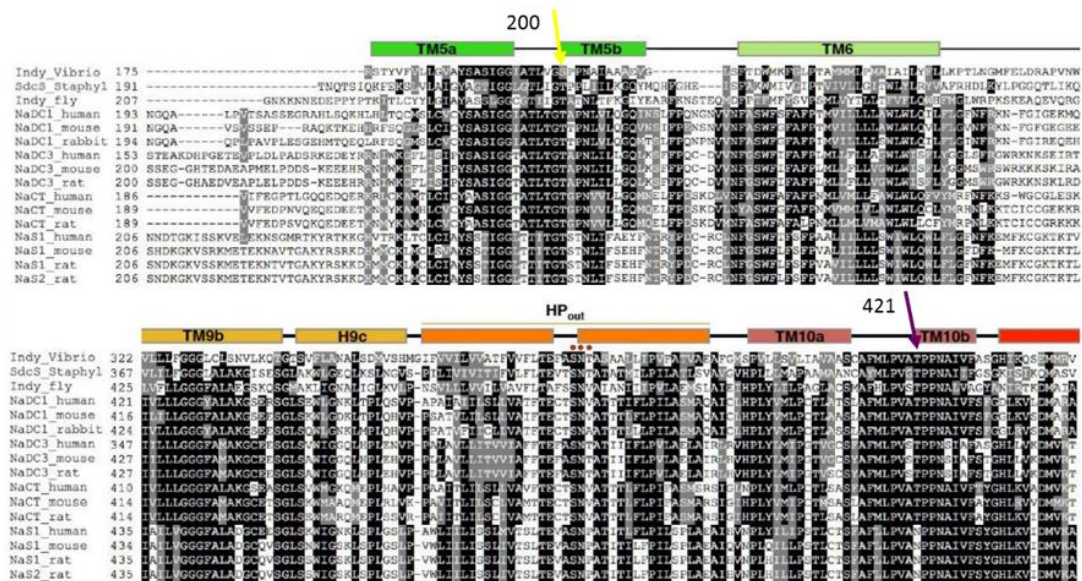

Figure 4.2: T421 and S200 conservation in the DASS family according to a sequence alignment of VcINDY and its homologues.

Secondary structures of the protein from the knowledge of the 2012 crystal structure are marked above the sequence alignment. T421 and S200 are marked with a purple and yellow arrow respectively. The SNT motifs are marked in dots. The image is a fragment of the full image shown in *Figure 1*.3 (*Chapter 1*), which was taken from (Mancusso *et al.,* 2012).

In conclusion, T421 and S200 roles could implicate changes in mechanistic forces. Such forces would at its turn provide a better substrate-binding site fit for substrates, which would utterly apply substrate's selection.

T421 and S200 do not only draw attention to their possible roles in binding events but also to a new hypothesis development for a novel mechanistic movement involving these two positions. This idea is developed in section 4.2.3 since we believe T421 and S200 hypothetical roles are linked to sodium-binding.

4.1.4. SCAFFOLD AND OLIGOMERIZATION AMINO ACIDS PARTICIPATION IN IMPLEMENTING SUBSTRATE SELECTIVITY

The study described here has been very valuable in identifying amino acids that affect substrate interactions that would not be predicted from the structure of VcINDY. Our CPM assays are shown for the first-time implication of amino acids in the scaffold and oligomerization domains involved in substrate selectivity. Specifically, we suggest V66, T67, F100 and V322 implement a second selectivity refinement filter.

The V66A and T67A are two amino acids located at TM2 situated at a middle position in the VcINDY structure (Nie *et al.*, 2017). According to the actual VcINDY known conformations, V66 and T67 are proportionally distant from the binding site in VcINDY's inward-facing conformation and outward-facing conformation (Nie *et al.*, 2017)(Mulligan *et al.*, 2016) (*Figure 4.3*).
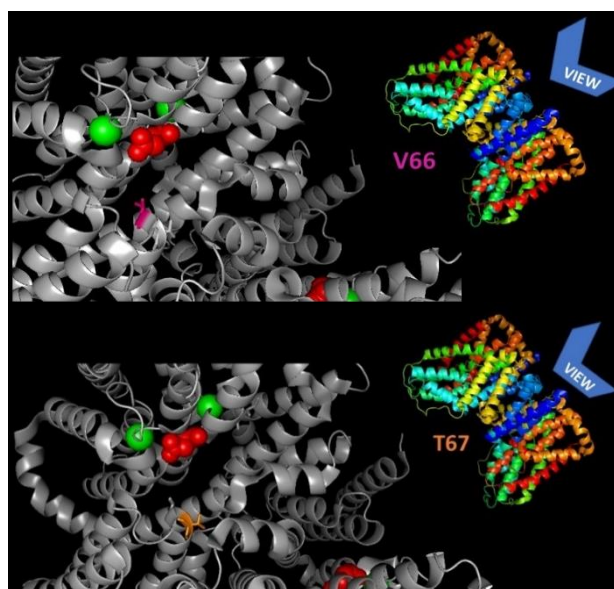
Figure 4.3V66 and T67 position in VcINDY crystal inward-facing state structure.

Images show the crystal structure of VcINDY inward-facing state. The whole protein at the right has been coloured according to the chains of the protein and indicates the view from which the amplified image was taken to have a clearer vision of the amino acids. V66 is indicated in pink and T67 in orange. Images made with PyMOL, Crystal structure from (Nie *et al.*, 2017).

Hence, it is plausible to believe that at some point, along with the movement of the binding site during transport, these two amino acids can contact the substrates, possibly at half-way of the VcINDY described elevator-movement.

From the CPM- results, T67A of the scaffold domain did not affect the binding of the principal 4C-molecules (succinate, fumarate and malate) (*Figure 3.19*). However, an alanine in that position rejected the binding of 5'-sulfosalisilic acid. Yet, other ligands expressed slighter better binding capacity when T67 was mutated to alanine. V66A that conserves the aliphatic amino acid side-chain produced a similar outcome. The ligand 5'-sulfosalisilic acid offered half of the stabilisation seen for VcINDY wild-type, while other 4C-dicarboxylic compounds stabilised V66A effectively (*Figure 3.17*). Thus, they did not exercise any binding modification of 4C-compounds as alanine did not change succinate, fumarate and malate thermostability capacity. We suggest T67 and V66 to be responsible for the possible binding of 5'-sulfosalisilic acid by enhancing the stabilisation of its molecular ring. We also believe T67 and V66 involvement in adding some resistance for ligands with additional functional groups such as methylene or carbon groups, except for hydroxyl groups as malate did get bound to those two alanine mutants.

Variation in other VcINDY alanine mutants and ligand interactions have also been observable for F100A and V322A (*Figure 3.23*) (*Figure 3.29*). These two amino acids belong to the oligomerization domain. Both amino acids are located around the middle part of the protein facing the transport domain from the structural information (Mancusso *et al.*, 2012)(Nie *et al.*, 2017). Nonetheless, they seem to

be closer to the substrate binding-site when the transporter is in its inward-facing state (*Figure 4.4*) (Nie *et al.*, 2017).

Interestingly, the stabilisation effect of malate in F100A was higher than succinate's effect in wild-type. Yet, succinate only generated half of its normal expected effect, equal to icatonic acid in the mutant (*Figure 3.23*). We argue that the phenylalanine in such a position blocks interaction for ligands owning additional functional groups at the second carbon of the scaffold molecule. Similarly, V322 could also participate in such a function because only succinate and malate could get bound to the mutated VcINDY, as seen for V66, T67 and F100 (*Figure 3.29*). All results showed that succinate and fumarate stabilisation effect were barely affected by alanine changes, whereas malate and other compounds with carbon groups attached to their scaffold were negatively affected.
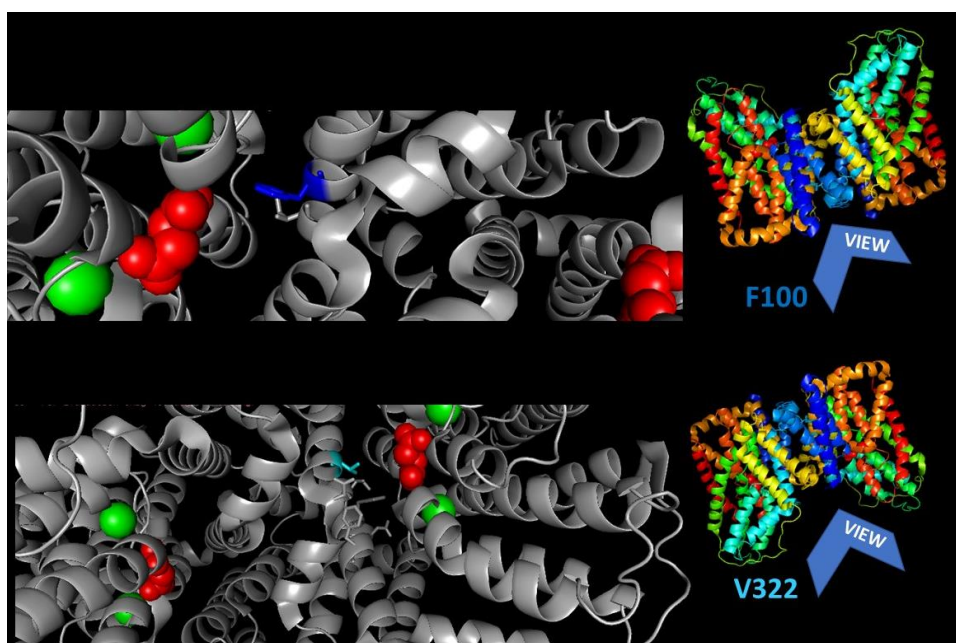
Figure 4.4: F100 and V322 position in VcINDY crystal inward-facing state structure.

Images show the crystal structure of VcINDY inward-facing state. The whole protein at the right has been coloured according to the chains of the protein and indicates the view from which the amplified image was taken to have a clearer vision of the amino acids. F100 is indicated in dark blue and V322 in cyan. Images made with PyMOL, Crystal structure from (Nie *et al.*, 2017)

So, V66, T67, F100 and V322, could be responsible for the evidence found in transport assays by implementing a ligand selectivity refinement (Mulligan *et al.*, 2014). In those studies, fumarate, malate and succinate are always more efficiently transported than any other compounds. Succinate is the most effectively transported substrate, followed by fumarate and then malate (Mulligan *et al.*, 2014). However, the difference in malate's, succinate's and fumarate's transport rates has not been explained regarding the transporter's structure. V66, T67, F100 and V322 could aid recognition of simple dicarboxylates while making it more difficult for dicarboxylates with additional functional groups to interact and thereby, reducing their transported efficiency.

The overall idea of some amino acids involved in the binding of substrates, and non-related directly to the transport domain, is a requirement for the elevator-type transport to happen as suspected (Mulligan *et al.*, 2016). In a 2020 paper, the acquisition of an intermediated conformation was proven in sodium binding, triggering a shift in conformations (Mulligan, 2020). They called it the yet-undefined-conformation, which involved amino acids belonging to the oligomerization and scaffold domain located in the middle of the structure. In support of our previous thoughts, all four tested amino acids are indeed located within the described gap where the binding-site moves back and forth between the IFS and OFS (Nie *et al.*, 2017)(Mulligan *et al.*, 2016)(Mulligan, 2020).

4.1.5. PHENYLALANINE PROPERTIES OF F326 INVOLVED IN OXALATE'S REJECTION

F326A was another tested amino acid that belongs to the protein's oligomerization domain, and it is closer to the binding site in the protein's inward-facing state (Nie *et al.*, 2017). The alanine change in such a position did not affect the binding of succinate, fumarate or other related 4C-compounds (*Figure 3.31*). It neither affected the binding of adipate with its larger size. However, oxalate (C2-dicarboxylate) stabilisation was similar to succinate's stabilisation for the same mutant.

Significant stabilisation effect of oxalate has barely been obtained in any other VcINDY mutant or wild-type. As speculated, we believe that oxalate has a short-carbon chain that prevents it from reaching the two necessary SNT regions in the VcINDY structure. It was introduced to the study as a negative control since it was not reported to be a transported substrate (Mulligan *et al.*, 2014).

To gain some comprehension, we believe that F326 of TM9b is responsible for rejecting oxalate binding. Phenylalanine owns a bulky side-chain due to its aromatic ring that could easily invade one portion of the binding-site, preventing oxalate's binding. When phenylalanine was mutated for alanine, with a much smaller side-chain, oxalate could offer a remarkable stabilisation effect non-seen before. But more importantly, F326 allowed other compounds such as 4C-dicarboxylates to still interact with the protein. The reason behind 4C-dicarboxylates' ability to get bound to F326A remains unclear. Perhaps, F326 can

interfere with some ligands binding while not affecting the SNT carboxylic recognition motifs.

In SLC13 transporters, two different amino acids are found in F326 respective positions: NaC transporters have a leucine, while NaS has a valine (Mancusso *et al.*, 2012). In both families the small aliphatic amino acid in that position would not be able to block anything due to its size. Out of the DASS characterised proteins, only the VcINDY orthologue SdcS transporter shared the phenylalanine in a respective position (*Figure 4.5*). In SdcS succinate-competitive transport assays by the presence of other compounds, oxalate did not inhibit succinate transport (Hall and Pajor, 2007). However, there is a lack of further evidence to approve F326 role.
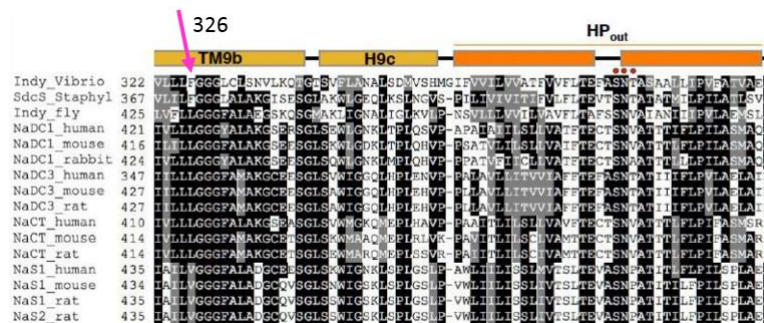
Figure 4.5: **V326 conservation in the DASS family according to a sequence alignment of VcINDY and its homologues.**

Secondary structures of the protein from the knowledge of the 2012 crystal structure are marked above the sequence alignment. V326 is marked with a pink arrow. The image is a fragment of the full image shown in *Figure 1.3*(*Chapter 1*), which was taken from (Mancusso *et al.,* 2012).

4.1.6. VcINDY DISPARITY OF SUBSTRATE RECOGNITION BETWEEN THE INWARD-FACING STATE AND THE OUTWARD-FACING STATE

The particular location of two tested mutants in this study could be key to demonstrate substrate selectivity differences between the two known conformations of VcINDY, according to the OFS VcINDY model. These two mutants

are I96A and S290 from TM4b and TM8, respectively. They are predicted to interact with the binding-site when the transporter is in its outward-facing state but not in its inward-facing state (Mulligan *et al.*, 2016). Their position appears displayed far away from the succinate in the VcINDY crystal structure (Nie *et al.*, 2017). However, variation in ligands binding has been reported for I96A and S290A. Therefore, we believe those visible discrepancies in these mutants' CPM-results are partly differing between the inward-facing state and outward-facing state ability to bind the ligand.

In I96A results, 4C-compounds did not offer VcINDY stabilisation or at least they did not in a comparable manner to wild type (*Figure 3.20*). Important substrates as fumarate and succinate did not generate a significant thermal shift in their presence. But, binding of 4C-molecules with additional functional groups in the second carbon offered interaction with the mutated transporter.

Thus, I96 could be important to preserve the capacity of binding 4C-compounds at the outward-facing state, above other compounds such as compounds with additional bulky groups with five carbons in their scaffold (tricarballyate), bulky by themselves or with a larger number of carbons (5'-sulfosalicylic acid and adipate) or with additional groups at the second carbon of their carbon-chain (icatonic acid and malate).

On the other hand, 4C-compounds stabilised S290A in a similar way seen in wild-type. Thus, indicating that S290 did not affect 4C-compounds selectivity.

Interestingly, citrate offered to S290A a significant positive stabilisation, equally to succinate's (*Figure 3.24*). Citrate is detailed described to interact with the protein

at the inward-facing state (Mancusso *et al.*, 2012). However, nothing has been said about its ability to be bound at the outward-facing conformation. S290A results suggested that due to the presence of a S290 serine, citrate probably cannot be bound to the specific OFS conformation.

In the SLC13 family, NaCT transporters are known to have citrate as their preferable substrate. The mNaCT has a threonine in a respective position to VcINDY^{S290} (Mancusso *et al.*, 2012). On the other hand, NaDC1 and NaDC3 are mainly 4C-dicarboxylates that can transport citrate but in a lesser way. All NaDC1 and NaDC3 own a serine in S290 respective position supporting the serine function (*Figure 4.6*).
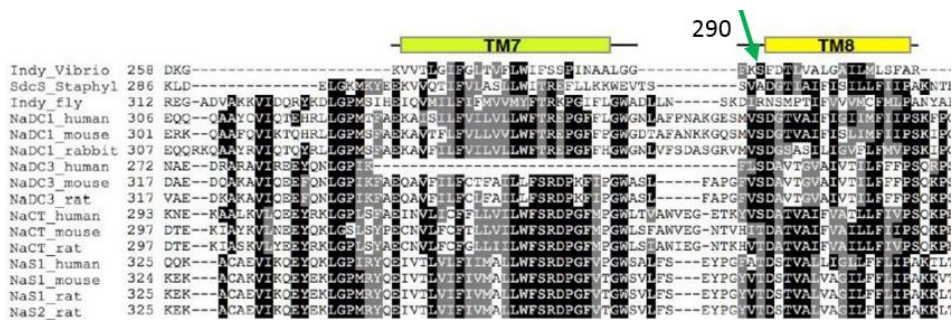
Figure 4.6: **S290 conservation in the DASS family according to a sequence alignment of VcINDY and its homologues.**

Secondary structures of the protein from the knowledge of the 2012 crystal structure are marked above the sequence alignment. S290 is marked with green arrow. The image is a fragment of the full image shown in *Figure 1.*3 (*Chapter 1*), which was taken from (Mancusso *et al.,* 2012).

Yet, the proposal main limitation is the lack of certainty of the outward-facing state of the transport since it is all based on the VcINDY predicted OFS model. Recently, a crystal structure from an INDY transporter from *Lactobacillus acidophilus* in its outward-facing state has been published (Sauer *et al.*, 2020). LaINDY's outward-facing state structure seemed to agree with VcINDY predicted outward-facing state (Mulligan *et al.*, 2016). An alternative explanation could be that the changes presented happened because alanine mutations were indifferent

from the adapted conformation of the transporter. However, the idea of substrate selectivity difference depending on the state of the transport is not absurd.

VcINDY prefers 4C-dicarboxylates at the outward-facing state to transport them inside the cell to obtain energy in the Krebs cycle. This biologic concept matches fully with the results obtained for I96A. The isoleucine is only preserved in the orthologue SdcS from *Staphylococcus aureus* (*Figure 4.7*).
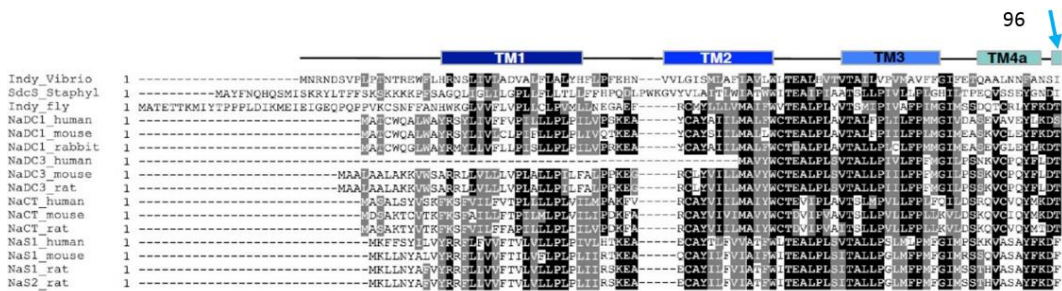

Figure 4.7: **I96 conservation in the DASS family according to a sequence alignment of VcINDY and its homologues.**

Secondary structures of the protein from the knowledge of the 2012 crystal structure are marked above the sequence alignment. I96 is marked with blue arrow. The image is a fragment of the full image shown in *Figure 1*.3 (*Chapter 1*), which was taken from (Mancusso *et al.,* 2012).

Substrate selectivity studies on SdcS highlight its preference for 4C-compounds with terminal dicarboxylate groups. It also detected transporter interactions susceptibility for compounds with substitutions at the substrate C-2 and C-3 positions (Hall and Pajor, 2007). Following this biological reasoning, citrate could signal that they already have enough compounds to generate energy. Hence, it can be bound to the inward-facing state but not in the outward-facing.(Mancusso *et al.*, 2012).

In general, these two mutants' results go beyond previous reports showing that differences in ligands selectivity between VcINDY states could exist.

4.1.7. MECHANISTIC ROLE OF D319 FOR THE MOVEMENT OF THE DOMAINS DURING THE CONTINUOUS ELEVATOR-TYPE MECHANISM

Another finding was the initial instability for D319A. Out of the mutants of the study, D319A required several tests until adequate baseline stabilisation was accomplished to carry on with the CPM-ligand's binding test. Consequently, the thermal shifts for this mutant were exceptionally higher compared to wild-type but similar to it when ignoring the sodium stabilisation effect.

D319 stays in contact with the binding site at the inward-facing state (Nie *et al.*, 2017). The displayed distance in the crystal structure between these amino acids and the substrate would be too large to infer any effect on selectivity. Indeed, this mutation's CPM-assay results came equal to what was seen in wild-type (*Figure 3.27*).

Hence, two conclusions can be drawn from the D319 results. First, it highlights the power of sodium cations in promoting protein stabilisation and enhancing substrate interactions (Mulligan *et al.*, 2014). Secondly, D319 could be important for elevator-type transport preserving structure during movement.

Given D319 structural position and initial instability when mutated to alanine we propose a mechanistic role for this amino acid. We believe that D319 could act as a buffer to stop the transport domain from getting too much unattached to the other domains of the protein and thereby, ensure a good outward-facing conformation.

As displayed in the VcINDY outward-facing state model, the amino acid D319 from one monomer meets the D319 from the other monomer forming the dimer (*Figure 4.8-A*)(Mulligan *et al.*, 2016). At physiological (pH 7.5-8), the aspartic acid in D319 is negatively charged and therefore, it repells the other negative charged D319. This repulsion would limit the movement of the transporter when it is switching to the outward-facing state (*Figure 4.8-B*). The presence of an uncharged alanine in those positions would avoid such an effect. This idea could be an explanation for the lack of stability found for the mutant (*Figure 27*).
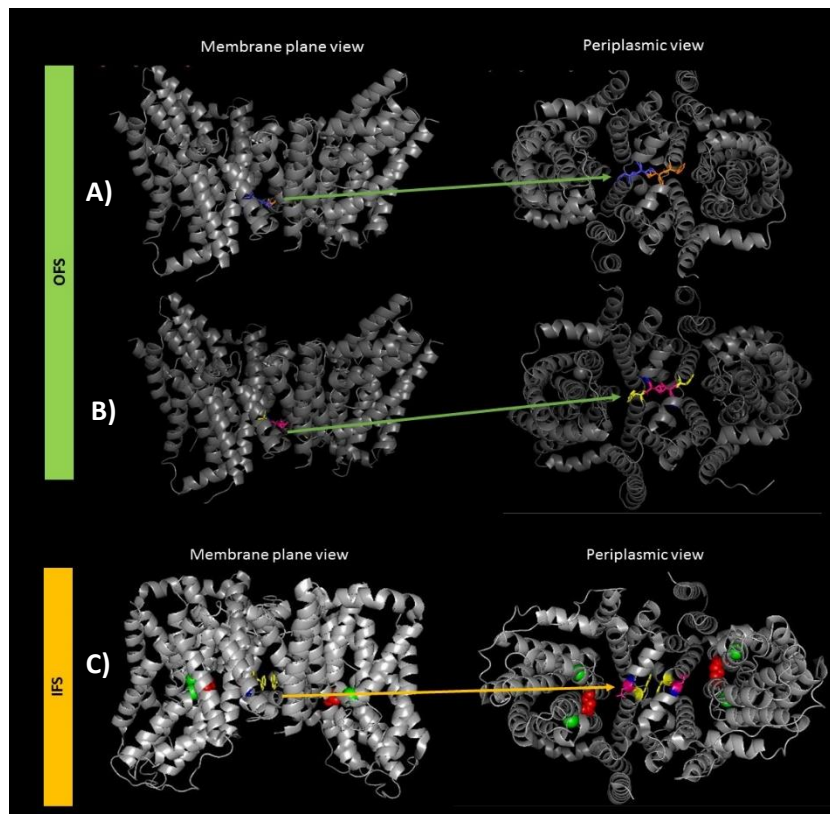
Figure 4.8: Description of D319 plausible interactions between monomers in VcINDY dimeric structure.

VcINDY outward-facing model (dark grey-A and B) and crystal inward-facing (light grey-C) proteins are shown from the membrane plane and periplasmic view. **A)** The A-D-W set of amino acids from each monomer of the dimer are coloured in different colours: blue (monomer 1) and orange (monomer 2) at the outward-facing state of VcINDY. The position acquired by A318 (blue), D319 (pink), W320 (yellow) is shown in the **B)** outward-facing state (OFS), **C)** inward-facing state (IFS). In the OFS, the aspartic acids from the monomers are close, which could create repulsion forces, while at the IFS arginine's are facing opposite directions.

However, the aspartic acid in 319 is not conserved among the DASS family *(Figure 4.9)*. All SLC13 members have a proline in such a position. Proline is an aliphatic amino acid similar to alanine that would not own any specific at physiological pH. The amino acid proline is normally found at the end of secondary structures, in this case at the end of the H9a, where it can influence the conformation of the protein structure by affecting the preceding residue. Interestingly, the proline's effect on conformation constraints on the residue preceding it to have a more valued consequence (Macarthur and Thornton, 1991). In a previous position to proline, DASS members have a lysine which is a basic amino acid. Hence, in physiological pH conditions, lysine would be charged positively offering the same proposed role as D319 but caused by positive charge repulsion instead of negative.
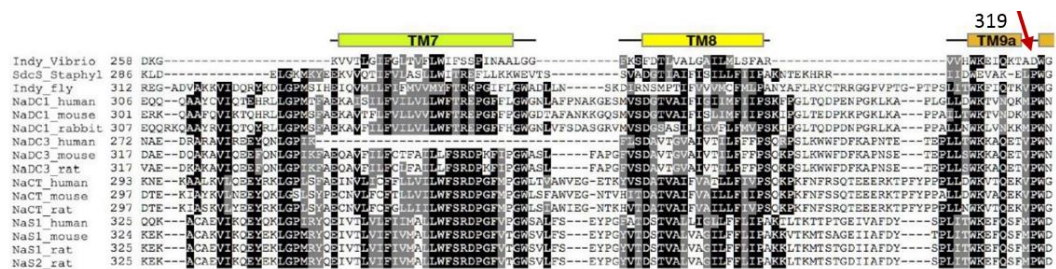
Figure 4.9: **D319 conservation in the DASS family according to a sequence alignment of VcINDY and its homologues.**

Secondary structures of the protein from the knowledge of the 2012 crystal structure are marked above the sequence alignment. D319 is marked with red arrow. The image is a fragment of the full image shown in *Figure 1.*3 (*Chapter 1*), which was taken from (Mancusso *et al.,* 2012).

Alternatively, it could simply mean that alanine's alky groups form interactions between them when mutated. D319 is located outside the protein structure where the formation of such types of interactions could disrupt the overall transporter's stability.

Nevertheless, the relevance of specifically charged amino acids around those positions can be drawn by these mutant's findings. Relevant specific charged amino acids have been proven important in the relative structure of DASS proteins such as H4c and probably H9c. Positively charged amino acids in those structures were reported crucial for the elevator-type mechanism and the interaction with other proteins (Khamaysi *et al.,* 2020).

Overall, the relevance of D319 in the transporter movement could be ice-breaking for further questions to emerge. But since it is the first time such a mechanistic role is proposed, the possibility for it to be true warrants further investigation. Crosslinking methodologies targeting D319 could prove useful to establish the role of this residue between VcINDY monomers. Since the possibility of amino acids in the VcINDY structure owning strictly mechanic positions is sensible, there is a need for clearer information on D319 before confirming the suggested role further.

4.2. CATION BINDING REPERCUSSIONS IN SUBSTRATE SELECTIVITY

4.2.1. SODIUM AND LITHIUM ELECTROCHEMICAL FORCES PLAYING IN SUBSTRATE RECOGNITION

The majority of the DASS transporters catalyse transport using sodium cation (Pajor *et al.,* 1995)(Inoue *et al.,* 2002)(Hall and Pajor, 2007) (Strickler *et al.*, 2009). The electrochemical gradient dependence of sodium is a common feature of the members of this family. VcINDY is described as a Na$^+$-dependent transporter (Mulligan *et al.*, 2014). However, as with some other members, succinate

transport has been carried out in the presence of other cations such as lithium (Mulligan *et al.*, 2014). Even though sodium action in DASS transporters is known and sodium binding requirements have been assumed, little is known about the consequences of its binding to the transporters.

The observation of isolated binding of sodium without any substrate or ligand has been shown in this study. The results presented here provide a basis for the sodium effect on substrates interactions in VcINDY. The main conclusion that can be drawn from these findings is that sodium does not need preliminary molecules to be able to bind to the transporter. This is in accordance with the proposed order of binding events followed by other members of the DASS family (Yao and Pajor, 2020). Hence, sodium binding is essential to allow the following binding of substrate.

Importantly, our results also provide evidence for lithium to be able to bind in a similar way to sodium (*Figure 3.32*). Li^+ provides VcINDY with 57.66± 0 ^{o}C in the absence of succinate, very similar to the 56.66± 0.81 ^{o}C provided by sodium. This indicates that sodium and lithium generate a similar amount of bonds within the protein, interacting equally well with it. However, lithium presented discrepancies compared to the sodium-binding effect in the presence of succinate.

While sodium seems to generate a high-quality binding-site fit for succinate, lithium cannot generate the same effect. This demonstrates that the sodium effect is more than just a mere play of electrostatic attraction forces near the binding site caused by its binding. Sodium is thought the get bound first and trigger a

change in conformation to a state that is intermediate between the two described confirmations for VcINDY (Mulligan, 2020).

The intermediate conformation preceded the substrate-binding event as it allows the transporter to acquire a better organisation for substrate recognition and binding. Hence, the lesser Li$^+$ ability to stabilize VcINDY suggests that lithium would fail to promote the needed conformational change to an intermediate state, where succinate binding is more favourable. This matches well with the poor demonstrated Li$^+$ capacity to transport succinate when substituting sodium gradient in liposome-based transport assays (Mulligan *et al.*, 2014).

Interestingly, this idea could aid explanation in substrate selectivity differences in lithium or sodium presence.

4.2.2. SODIUM AND LITHIUM TRIGGER SEPARATE SUBSTRATE RECOGNITION

Broadly translated, our findings indicate that lithium can trigger different substrate selectivity from sodium (*Figure 3.34*). Library compounds with different carboxyl groups such as citrate, tricarballyate, malate and icatonic acid seem to offer higher or similar stabilisation in the presence of lithium and sodium. Whereas fumarate and succinate, which are the well-known substrates for VcINDY, offered significant stabilisation only in the presence of sodium but not lithium.

We believe that such results could be explained due to lithium failure to promote the necessary changes to aid the protein adaptation of a less solvent-exposed binding-site. Li$^+$ cannot firmly bind known substrates but allows binding of

molecules with extra functional carbon-groups, keeping the transporter with an opening binding site that allows stabilisation of bulky groups facing the outside.

These results appeared consistent with the previously mentioned idea: lithium keeps the protein in a position where the binding site is open to any side of the membrane. In contrast, a unique driven movement of the transporter occurs in the binding of sodium. The structural shift brings the binding site to the inside. The transport will then adopt a new undetermined conformation enhancing the overall stabilisation of VcINDY.

To give further insight into Li^+ and Na^+ differences, we suggest that a better interaction ability of the transporter with the substrate, once the intermediated state is achieved, lays partially on two pairs of amino acids. The amino acids involved are S200 with N151 from the SNT of the HPin, and T421 with N378 from the SNT of the HPout.

Hence, we believe that sodium binding will narrow the gap between the pairs so an H-bound can be formed. The H-bonds formation would help rearrange the binding site, concretely the SNT motifs, which can now interact better with the substrates' carboxylic groups. On the contrary, lithium binding will have a lesser effect connecting the two pairs of amino acids. Li^+ would fail to allocate the carboxylic recognition regions in the optimal position. The same problem will happen for potassium since its large size will separate even more the gap between S200-N151 and T421-N378. This gives a better explanation of Li^+ inability to enhance succinate transport as much as sodium.

4.2.3. AMINO ACIDS RELATED TO THE BINDING SITE COULD MARK CHANGES AT THE TRANSPORTER APO STATE

When relating the previous data with the proposed mechanistic roles for S200 and T421, we have a step further in understanding VcINDY's transport dynamics. As argued before, the mechanistic roles for S200 and T421 imply a change in the binding-site formation involving mainly positions of the amino acids of the SNT motif. On the other side, sodium binding is thought to shift one specific conformation to another yet-undetermined middle state along the transport cycle. Here, we have come across an idea that may be considered a promising explanation for transport dynamics and explain the differences seen in cations selectivity.

This novel notion presented involve cation binding and the play of the mentioned amino acids (*Figure 4.10):*

In the outward-facing conformation (OFS), the protein binds sodium to Na1 and Na2. The electrochemical forces of sodium generated S200 to get closer to N151 (and the same happens for T421 and N378). Therefore, the formation of H-bonds would accommodate the SNT motif to the right orientation. Besides small changes in the binding site, cations' binding will also help the protein achieve a slightly different state.

In such state, the binding site would be more separated from the medium and, therefore, more stable for the substrate-binding event. By binding the appropriate substrate, larger structural changes will be triggered. Then, the transporter will eventually switch the conformational state from OFS to IFS. As described by Sauer

et al., the appropriate carboxylates will have to carry two negative charges that would compensate for the two positive charges from the sodium already bound to the transporter. Only this way, the positive charge of the binding-site (provided by sodium) is neutralised and the proteins' domains are more likely to move to pass the membrane environment (Sauer *et al.*, 2020).

In the inward-facing state (IFS), the substrate will be released first followed by sodium (Mancusso *et al.*, 2012)(Nie *et al.*, 2017). The exit of sodium from the transporter will separate the distance between S200-N151 and T421-N378. By increasing the gap distance between the paired amino acids, the formed H-bonds will break. The amino acids will get back to their initial positions as they are supposed to be in the transporter's apo state. All these changes will inform that the transporter is empty, so conformational changes will occur to avoid destabilisation caused by solubilisation of the binding site kept open.

As proposed by Nie et al., we also agree that water molecules would be responsible for compensating the empty transporter's slight charge in its inward-facing state. In fact, S200 and T421 are hydroxylic amino acids that have been freed so they can form new bonds with water molecules.

Once the transporter charge is neutralised, it can switch again between conformations from IFS to OFS. At the outward-facing state by binding a minimum of two sodium cations, the described cycle will start again.
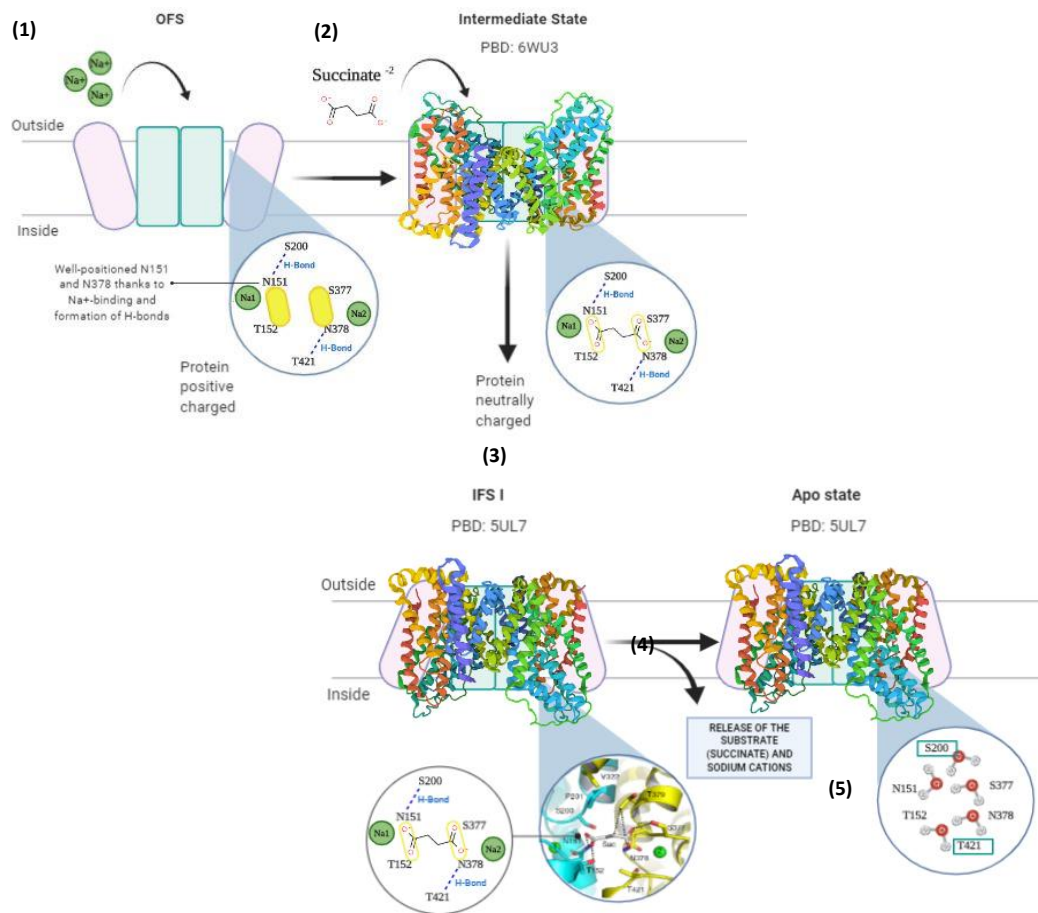
Figure 4.10: Representation of VcINDY transport mechanistic connection to binding-site amino acids S200, N151, N378 and T421.

In the OFS, VcINDY binds sodium (1). The binding of sodium allows the proximity between the pairs of amino acids N1521-S200 and N378-T421. Formation of H-bonds will occur, stabilising the SNT regions into an appropriate orientation. An intermediate state where substrate can bind will be acquired simultaneously (2). By succinate binding switch from OFS to IFS will happen (3). Then, in the IFS, the substrate and sodium will be released (4), and all amino acids will get back to their initial positions. In the transporter's apo state water molecules would be responsible for compensating the charge of the transporter by getting bound to S200 and T421 (5). Once the transporter charge is neutralised, it can switch again between conformations from IFS to OFS (step between 5-1). (Created with BioRender.com)

This novel idea of amino acids of the binding site involvement as signals between charged or uncharged transporter states matches previous mechanistic descriptions of DASS elevator-type transport.

An important question associated with this novel mechanism is which specific structural changes allow a switch between conformations? The comparison of the crystallised IFS conformation with the obtained cryo-EM IFS with substrate still bound revealed that amino acid P422 was moved up to 1.5 A° (Sauer *et al.*, 2020). Although the cause of this movement has not been described, we believe that it is caused by the movement of its neighbour T421, in support of our initial thoughts. In the same paper, besides T421 other necessary movements were described throughout the study of cryo-EM new VcINDY states' structures. Also, sodium was indicated to be responsible for letting the transporter know that it was fully loaded via electrostatic effects (Sauer *et al.*, 2020). From our data, we like to suggest that, besides sodium influence, changes in S200-N151 and T421-N378 interactions play a relevant role as well. Our proposal just adds the play of amino acids from the binding site as first signals since the release of sodium and substrate must be acquired to have an empty transporter.

It is sensible to imply that these conserved amino acids in the binding-site start the cascade movements to change conformation in DASS transporters. Hence, due to sodium and these amino acids movements, more structural modifications are bound to happen until the shift between conformations is possible.

4.3. CONCLUSION

In conclusion, it would appear that the findings on CPM analysis lead to the following conclusions. Using thermostability-based assays, the initial statement of the existence of specific amino acids related to the binding site or in the action mechanism by which variation in substrate recognition occurs has been tested. On this basis, the results imply positive involvement of new residues of the VcINDY structure in the binding event of ligands and more.

First, as it was already known, VcINDY is a secondary active transporter with a preference for four di/tri-carboxylates (Mulligan *et al.*, 2014). However, our data confirm that it has a broad tolerance towards other carboxylic compounds. The wide ligand selectivity variety could be explained according to the conformational state adopted by VcINDY, the interplay of oligomerization and scaffold amino acids on the binding site, and finally, cation binding forces readjusting essential amino acid's positions.

The findings of this project could broaden the present knowledge of VcINDY sodium and substrate interactions. They have also helped to address clear rules of ligands binding in the VcINDY bacterial DASS transporter. This is very much the key component in future attempts to overcome the first steps towards developing effective inhibitors. Besides, the CPM Thermofluor assays represent a quick, high-throughput and reproducible method. Such technique has allowed screening different compounds with VcINDY mutants by performing many melting curves along with the study.

However, this work must be held accountable for its limitations. One of those is the inability to discern between interaction generated at the transporter's binding-site to any other allosteric site present in the structure. The CPM-assays do not have either the resolution to discern between the structural basis of the study's compound. This makes it complicated when explaining why some get bound when similar molecules do not (e.g., citrate and tricarballyate).

Another potential restriction is concerning the origin of the stabilisation effect. The increase in stability could be due to the binding of the ligand to VcINDY or adaptation of one specific-single high-stable conformation. The inward-facing state of VcINDY kept an adequate, stable conformation to be crystallised (Nie *et al.*, 2017)(Mancusso *et al.*, 2012). Therefore, due to mutations in the protein structure, we argue that a higher stability outcome in some CPM assays might be due to adaptation of the inward-facing state over any other states.

In addition to this point, one assumption is that the two conformations of VcINDY are present in the solution at similar rates. However, it is possible that some specific alanine mutations may oblige transporters to stay in a particular conformation. A benefit that could come from this would be the study of one specific mutant that confines VcINDY in a solid outward-facing state facilitating crystallisation such as we speculate happens for F326A.

Overall, future investigations are necessary to validate the kinds of conclusions that can be drawn from this study. Development of transport assays could fruitfully attain a selection of substrates from ligands. Transport assays would also

help to determine the affinity of the identified substrates given that CPM-interactions may not be representative for substrates binding affinity. The creation of double mutants or mutants with the same chemical properties could be useful to determine if the suggested roles of some residues in this study are accurate, according to the amino acid properties. Studies targeting one specific VcINDY conformation in vesicles could prove useful to identify changes in selectivity due to mere conformational changes. Finally, if future research is conducted in more realistic settings such as nanodiscs, imitating the lipid composition of the bacterial transporter, the corroboration of some proposed mechanistic effects could be verified. All of it is desirable to be addressed in future work along with tips of ligands that allow prediction of future DASS inhibitors.

In summary, studying VcINDY to approach SLC13 family members understanding could be a great platform for further research (Willmes and Birkenfeld, 2013)(Lu, 2019). It is difficult to arrive at any conclusions concerning true specific-binding site interactions with this screening analysis focusing only on shifts in thermostability. The obtention of the VcINDY bacterial transporter's crystal structure in the outward-facing state or other unknown middle conformations could fully lend support to any unfolding discoveries.

Nonetheless, we have provided a good starting point with several ideas to consider in future research questions. If the appealing suggested interplay in the regulation of the VcINDY mechanism by T421 and S200 holds certain, it would be a step toward understanding the DASS transporter mechanism at their yet puzzling apo state.

REFERENCES

Alexandrov, A. I., Mileni M, Chien EY, Hanson MA, Stevens RC. (2008) 'Ways & Means Microscale Fluorescent Thermal Stability Assay for Membrane Proteins', *Structure,* 16(3): 351–359. doi: 10.1016/j.str.2008.02.004.

Bergeron, M. J. *et al.* (2013) 'Molecular Aspects of Medicine SLC13 family of Na + -coupled di- and tri-carboxylate / sulfate', *Molecular Aspects of Medicine*, 34(2-3): 299–312. doi: 10.1016/j.mam.2012.12.001.

Birkenfeld, A. L. Lee HY, Guebre-Egziabher F, *et al.* (2011) 'Article Deletion of the Mammalian INDY Homolog Mimics Aspects of Dietary Restriction and Protects against Adiposity and Insulin Resistance in Mice', *Cell Metab*, 5;14(4);184–195. doi: 10.1016/j.cmet.2011.06.009.

Bosshart, P. D. and Fotiadis, D. (2020) *Secondary Active Transporters*. *Springer International Publishing*. Volume 92. doi: 10.1007/978-3-030-18768-2.

Burckhardt, B. C. *et al.* (2005) 'Substrate specificity of the human renal sodium dicarboxylate cotransporter , hNaDC-3 , under voltage-clamp conditions', *American Journal of Physiology. Renal physiology, 288(4);F792–F799.* doi: 10.1152/ajprenal.00360.2004.

Chen, Xiangmei *et al.* (1999) 'Molecular and functional analysis of SDCT2, a novel rat sodium-dependent dicarboxylate transp*orter', J. Clin. Investigation.* 103(8); 1159–1168.

Chen, J. S., Reddy, V., Chen, J. H., Shlykov, M. A., Zheng, W. H., Cho, J., Yen, M. R., & Saier, M. H., Jr (2011) `Phylogenetic characterization of transport protein superfamilies: superiority of Superfamily Tree programs over those based on multiple alignments´, *Journal of molecular microbiology and biotechnology*, *21*(3-4); 83–96. doi: 10.1159/000334611

Colas, C., Pajor, A. M., & Schlessinger, A. (2015) 'Structure-Based Identification of Inhibitors for the SLC13 Family of Na(+)/Dicarboxylate Cotransporters' *Biochemistry*, 54(31);4900–4908. doi: 10.1021/acs.biochem.5b00388.Structure.

Colas, C., Schlessinger, A. and Pajor, A. M. (2017) 'Mapping Functionally Important Residues in the Na + /Dicarboxylate Cotransporter, NaDC1'. *Biochemistry*, *56*(33), 4432–4441. doi: 10.1021/acs.biochem.7b00503.

Crichton, P. G. *et al.* (2015) 'Trends in Thermostability Provide Information on the Nature of Substrate, Inhibitor, and Lipid Interactions with Mitochondrial Carriers', *The Journal of biological chemistry,* 290(13);8206–8217. doi: 10.1074/jbc.M114.616607

Dawson, P. A., Steane, S. E. and Markovich, D. (2005) 'Impaired memory and olfactory performance in NaS i -1 sulphate transporter deficient mice', *Behavioural brain research*, *159*(1); 15–20. doi: 10.1016/j.bbr.2004.09.020.

Drew, D. and Boudker, O. (2016) 'Shared Molecular Mechanisms of Membrane Transporters', *Annual review of biochemistry*, *85*; 543–572. doi: 10.1146/annurev-biochem-060815-014520.

Faham, S., Watanabe, A., Besserer, G. M., Cascio, D., Specht, A., Hirayama, B. A., Wright, E. M., & Abramson, J. (2008). The crystal structure of a sodium galactose transporter reveals mechanistic insights into Na+/sugar symport. *Science (New York, N.Y.)*, *321*(5890); 810–814. doi: 10.1126/science.1160406

Fei, Y., Liu, J. C., Inoue, K., Zhuang, L., Miyake, K., Miyauchi, S., & Ganapathy, V. (2004). Relevance of NAC-2, an Na+-coupled citrate transporter, to life span, body size and fat content in Caenorhabditis elegans. The Biochemical journal, 379(Pt 1),; 191–198. doi: 10.1042/BJ20031807

Fitzgerald, G. A., Mulligan, C. and Mindell, J. A. (2017) 'A general method for determining secondary active transporter substrate stoichiometry', *eLife*, *6*, (e21016); 1–15. doi: 10.7554/eLife.21016.

Forrest, L. R. and Rudnick, G. (2010) 'The rocking bundle: a mechanism for ion-coupled solute flux by symmetrical transporters', *Physiology (Bethesda, Md.)*, *24*,; 377–386. doi: 10.1152/physiol.00030.2009.

Girard, J. P., Baekkevold, E. S., Feliu, J., Brandtzaeg, P., & Amalric, F. (1999) 'Molecular cloning and functional analysis of SUT-1 , a sulfate transporter from human high endothelial venules'. *Proceedings of the National Academy of Sciences of USA*, *96*(22);12772–12777. https://doi.org/10.1073/pnas.96.22.12772

Hall, J. A. and Pajor, A. M. (2007) 'Functional Reconstitution of SdcS , a Na$^+$-Coupled Dicarboxylate Carrier Protein from Staphylococcus aureus', *Journal of bacteriology*, *189*(3); 880–885.880–885. doi: 10.1128/JB.01452-06.

Ho, H. T., Ko, B. C., Cheung, A. K., Lam, A. K., Tam, S., Chung, S. K., & Chung, S. S. (2007) 'Generation and characterization of sodium- dicarboxylate cotransporter-deficient mice', *Kidney international*, 72 (1); 63–71. doi: 10.1038/sj.ki.5002258.

Huard, K. *et al.* (2015) 'Optimization of a Dicarboxylic Series for in Vivo Inhibition of Citrate Transport by the Solute Carrier 13 (SLC13) Family', *Journal of medicinal chemistry*, *59*(3); 1165–1175. doi: 10.1021/acs.jmedchem.5b01752

Hutchison, J. M., Lu, Z., Li, G. C., Travis, B., Mittal, R., Deatherage, C. L., & Sanders, C. R. (2017) 'Dodecyl- β -melibioside Detergent Micelles as a Medium for Membrane Proteins', Proteins. *Biochemistry*, *56*(41);5481–548. doi: 10.1021/acs.biochem.7b00810.

Inoue, K. *et al.* (2002) 'Structure, Function, and Expression Pattern of a Novel Sodium- coupled Citrate Transporter (NaCT) Cloned from Mammalian Brain', *The Journal of biological chemistry,* 277(42); 39469–39476. doi: 10.1074/jbc.M207072200.

Inoue, K., Zhuang, L., & Ganapathy, V. (2002). ´Human Na$^+$ -coupled citrate transporter: primary structure, genomic organization, and transport function´.

Biochemical and biophysical research communications, *299*(39); 465–471.doi: 10.1016/s0006-291x(02)02669-4

Jardetzky, O. (1966) `Simple Allosteric Model for Membrane Pumps´. *Nature* 211;969–970. doi: 10.1038/211969a0

Jensen S, Guskov A, Rempel S, Hänelt I, Slotboom DJ. (2013) 'Crystal structure of a substrate- free aspartate transporter', *Nat Struct Mol Biol* 20(10):1224–6. doi: 10.1038/nsmb.2663.

Khamaysi, A., Aharon, S., Eini-Rider, H., & Ohana, E. (2020). A dynamic anchor domain in slc13 transporters controls metabolite transport. *The Journal of biological chemistry*, *295*(24);8155–8163. doi: 0.1074/jbc.RA119.010911.

Karpowich, N. K., & Wang, D. N. (2008). `Structural biology. Symmetric transporters for asymmetric transport´ *Science (New York, N.Y.)*, *321*(5890); 781–782. doI. 10.1126/science.1161495

Kekuda, R., Wang, H., Huang, W., Pajor, A. M., Leibach, F. H., Devoe, L. D., Prasad, P. D., & Ganapathy, V. (1999) 'Primary Structure and Functional Characteristics of a Mammalian Sodium-coupled High Affinity Dicarboxylate Transporter ', *The Journal of biological chemistry*, *274*(6); 3422–3429274. doi: 10.1074/jbc.274.6.3422

Knauf, F., Mohebbi, N., Teichert, C., Herold, D., Rogina, B., Helfand, S., Gollasch, M., Luft, F. C., & Aronson, P. S. (2006). 'The life-extending gene Indy encodes an exchanger for Krebs-cycle intermediates', *The Biochemical journal*, *397*(1); 25–29. doi: 10.1042/BJ20060409.

Langefeld, C. D., Palmer, N. D., Zhong, M., Roh, B., Lewis, J. P., Wing, M. R., Pandya, H., Freedman, B. I., Langefeld, C. D., Rich, S. S., Bowden, D. W., & Mychaleckyj, J. C. *et al.* (2008) 'Genomics Heterogeneity in gene loci associated with type 2 diabetes on human chromosome', *Genomics*, *92*(4); 226–234. doi: 10.1016/j.ygeno.2008.06.004.

Lee, S., Kesby, J. P., Muslim, M. D., Steane, S. E., Eyles, D. W., Dawson, P. A., & Markovich, D.(2007) 'Hyperserotonaemia and reduced brain serotonin levels in NaS1 sulphate transporter null mice', *Neuroreport*, *18*(18); 981–1985. https://doi.org/10.1097/WNR.0b013e3282f22998

Li, Z., Li, D., Choi, E. Y., Lapidus, R., Zhang, L., Huang, S. M., Shapiro, P., & Wang, H (2017) 'Silencing of solute carrier family 13 member 5 disrupts energy homeostasis and inhibits proliferation of human hepatocarcinoma cells', *The Journal of biological chemistry* 292(14); 13890–13901. doi: 10.1074/jbc.M117.783860.

Lu, M. (2019) 'Structure and Mechanism of the Divalent Anion / Na + Symporter', (Figure 1), *International journal of molecular sciences*, *20*(2); 1–12. doi: 10.3390/ijms20020440.

Macarthur, M. W. and Thornton, J. M. (1991) 'Influence of Proline Residues on Protein Conformation', *Journal of molecular biology*, *218*(2); 397–412. doi: 10.1016/0022-2836(91)90721-h

Mancusso, R. *et al.* (2012) 'Structure and mechanism of a bacterial sodium-dependent dicarboxylate transporter', *Nature. Nature Publishing Group*, *491*(7425); 622–626. doi: 10.1038/nature11542.

Markovich, D. (2012) `Sodium-Sulfate / Carboxylate Cotransporters (SLC13)´, *Current topics in membranes, 70*, 239–256. doi: 10.1016/B978-0-12-394316-3.00007-7.

Markovich, D. and Aronson, P. S. (2007) 'Specificity and Regulation of Renal Sulfate Transporters'. *Annual review of physiology*, *69*; 361–375. doi: 10.1146/annurev.physiol.69.040705.141319.

Markovich D, Murer H. (2004) 'The SLC13 gene family of sodium sulphate / carboxylate cotransporters', *Plugers Arch- Eur J Physiol*, 447(5); 594–602. doi: 10.1007/s00424-003-1128-6.

Mulligan, C., Fitzgerald, G. A., Wang, D. N., & Mindell, J. A. (2014) 'Functional characterization of a Na^+ -dependent dicarboxylate transporter from Vibrio cholerae', *The Journal of general physiology*, *143*(6); 745–759. doi: 10.1085/jgp.201311141.

Mulligan, C., Fenollar-Ferrer, C., Fitzgerald, G. A., Vergara-Jaque, A., Kaufmann, D., Li, Y., Forrest, L. R., & Mindell, J. A.. (2016) 'The bacterial dicarboxylate transporter VcINDY uses a two-domain elevator-type mechanism', *Nature Publishing Group*. Nature Publishing Group, 23(3); 256–263. doi: 10.1038/nsmb.3166.

Mulligan, C. (2020) 'Substrate-dependent accessibility changes in the Na^+-dependent C4-dicarboxylate transporter, VcINDY, suggest differential substrate effects in a multistep mechanism'. (Unpublished paper-bioRxiv server).

Nie R., Stark, S., Symersky, J., Kaplan, R. S., & Lu, M. (2017). `Structure and function of the divalent anion/Na^+ symporter from Vibrio cholerae and a humanized variant ´, *Nature communications*, 8; 1-10 doi: /10.1038/ncomms15009.

Pajor, A. M. (1999) 'Sodium-coupled transporters for Krebs cycle intermediates´. *Annual review of physiology*, 61; 663–682. doi: 10.1146/annurev.physiol.61.1.663

Pajor, A. M. (2006) 'Molecular properties of the SLC13 family of dicarboxylate and sulfate transporters', *Pflugers Archiv : European journal of physiology*, *451*(5); 597–605. doi: 10.1007/s00424-005-1487-2.

Pajor, A. M. (2014) 'Sodium-coupled dicarboxylate and citrate transporters from the SLC13 family', *Pflugers Archiv : European journal of physiology*, *466*(1); 119–130. doi: 10.1007/s00424-013-1369-y.

Pajor A. M. (1995). `Sequence and functional characterization of a renal sodium/dicarboxylate cotransporter´. *The Journal of biological chemistry*, *270*(11); 5779–5785. doi: 10.1074/jbc.270.11.5779.

Pantoliano, M. W., Petrella, E. C., Kwasnoski, J. D., Lobanov, V. S., Myslik, J., Graf, E., Carver, T., Asel, E., Springer, B. A., Lane, P., & Salemme, F. R. (2001). `High-density miniaturized thermal shift assays as a general strategy for drug

discovery´. *Journal of biomolecular screening*, *6*(6); 429–440. doi: 10.1177/108705710100600609.

Prakash, S. *et al.* (2003) 'The ion transporter superfamily', *Biochimica et biophysica acta*, 1618 (1); 79–92.79–92. doi: 10.1016/j.bbamem.2003.10.010.

Rogina, B. and Helfand, S. L. (2013) 'Indy mutations and Drosophila longevity', *Frontiers in genetics*, *4*; 1–8. doi: 10.3389/fgene.2013.00047.

Roth, A. *et al.* (2020) 'Substrate binding modulates the conformational kinetics of the secondary multidrug transporter LmrP', pp. 1–24. (Unpublished paper- bioRxiv server)

Sárvári, M., Kalló, I., Hrabovszky, E., Solymosi, N., Tóth, K., Likó, I., Molnár, B., Tihanyi, K., & Liposits, Z. (2014) 'Estradiol Replacement Alters Expression of Genes Related to Neurotransmission and Immune Surveillance in the Frontal Cortex of Middle-Aged ', *Endocrinology*, *151*(8); 3847–3862. doi: 10.1210/en.2010-0375.

Sauer, D. B., Trebesch, N., Marden, J. J., Cocco, N., Song, J., Koide, A., Koide, S., Tajkhorshid, E., & Wang, D. N. (2020) 'Structural basis for the reaction cycle of DASS dicarboxylate transporters', *eLife*, 3; 1–28. doi: 10.7554/eLife.61350

Schlessinger, A., Sun, N. N., Colas, C., & Pajor, A. M. (2014) 'Determinants of Substrate and Cation Transport in the Human Na^+-Dicarboxylate Cotransporter NaDC3', *The Journal of biological chemistry*, *289*(24); 16998–17008. doi: 10.1074/jbc.M114.554790.

Shi, Y. (2013) 'Common Folds and Transport Mechanisms of Secondary Active Transporters'. *Annual review of biophysics*, *42*; 51–72. doi: 10.1146/annurev-biophys-083012-130429.

Simino, J. *et al.* (2009) 'Variants on Chromosome 6p22 . 3 Associated With Blood Pressure in the HyperGEN Study : Follow-Up of FBPP Quantitative Trait Loci', *American Journal of Hypertension*. Nature Publishing Group, 24(11); 1227–1233. doi: 10.1038/ajh.2011.140.

Strickler, M. A. *et al.* (2009) 'Biochimica et Biophysica Acta Functional characterization of a Na^+-coupled dicarboxylate transporter from Bacillus licheniformis', *BBA - Biomembranes*. Elsevier B.V., 1788(12); 2489–2496. doi: 10.1016/j.bbamem.2009.10.008.

Verdon, G., Oh, S., Serio, R. N., & Boudker, O. (2014) 'Coupled ion binding and structural transitions along the transport cycle of glutamate transporters', *eLife*, 1–23. doi: 10.7554/eLife.02283.

Vergara-jaque A., Fenollar-Ferrer, C., Mulligan, C., Mindell, J. A., & Forrest, L. R A. *et al.* (2012) 'Family resemblances : A common fold for some dimeric ion-coupled secondary transporters', *The Journal of general physiology*, *146*(5); 423–434. doi: 10.1085/jgp.201511481.

Willmes, D. M. *et al.* (2018) 'The longevity gene INDY (I ' m N ot D ead Y et) in metabolic control : Potential as pharmacological target', *Pharmacology and Therapeutics*. Elsevier, 185(10); 1–11. doi: 10.1016/j.pharmthera.2017.10.003.

Willmes, D. M., & Birkenfeld, A. L. (2013) 'The Role of INDY in Metabolic Regulation´, *Computational and structural biotechnology journal*, *6*; 1-8 doi: 10.5936/csbj.201303020

Yan, N. (2013) 'Structural advances for the major facilitator superfamily (MFS) transporters', *Trends in Biochemical Sciences*. Elsevier Ltd, 38(3); 151–159. doi: 10.1016/j.tibs.2013.01.003.

Yao, X. and Pajor, A. N. A. M. (2020) 'The transport properties of the human renal Na$^+$ - dicarboxylate cotransporter under voltage-clamp conditions', *American journal of physiology. Renal physiology*, *279*(1);F54–F64. doi. 10.1152/ajprenal.2000.279.1.F54

Zeuthen, T., Gorraitz, E., Her, K., Wright, E. M., & Loo, D. D. (2016) 'Structural and functional significance of water permeation through cotransporters'. *Proceedings of the National Academy of Sciences of the USA* 113(44); E6887–E6894. doi: 10.1073/pnas.1613744113.

6. APPENDIX

In this section, supplementary figures and data for a better understanding are provided. The appendix is classified into two sub-sections, Appendix A and Appendix B.

In **Appendix A** the figures provided are from other sources and related to the introduction (Sections 1 of the thesis). In **Appendix B** original data generated during this study can be found unless indicated otherwise.

6.1. APPENDIX A
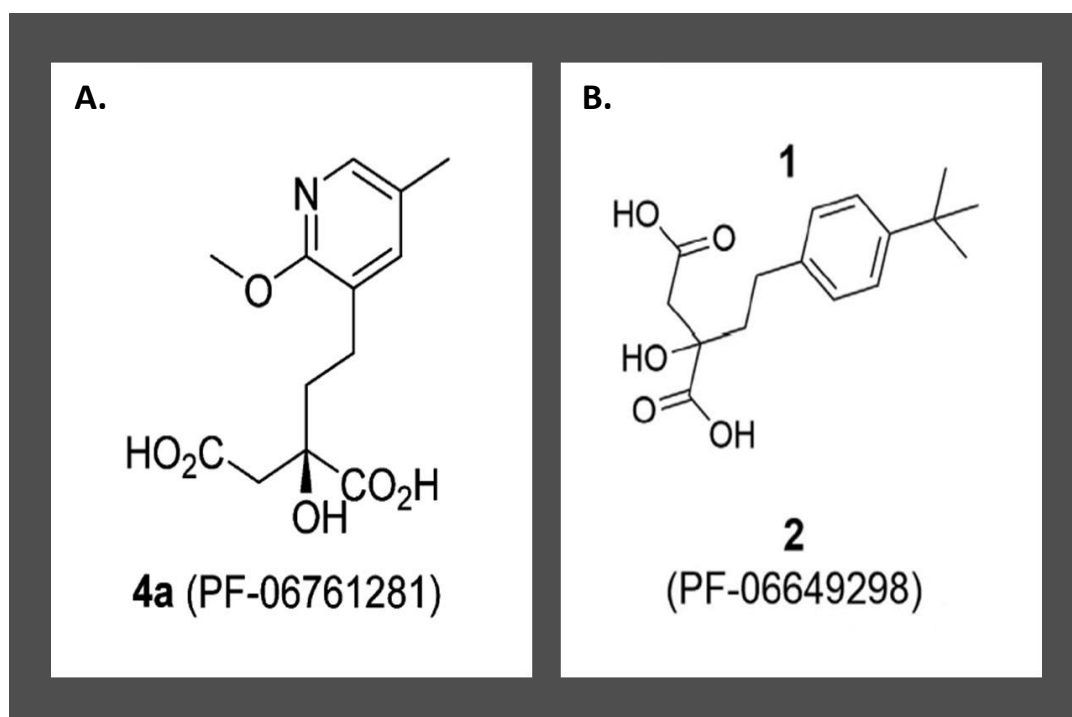
Figure 6.1.1: **INDY protein inhibitors' molecular structure.**

A) Molecular representation of an INDY inhibitory compound 4a. **B)** Molecular representation of an INDY inhibitory compound 2.
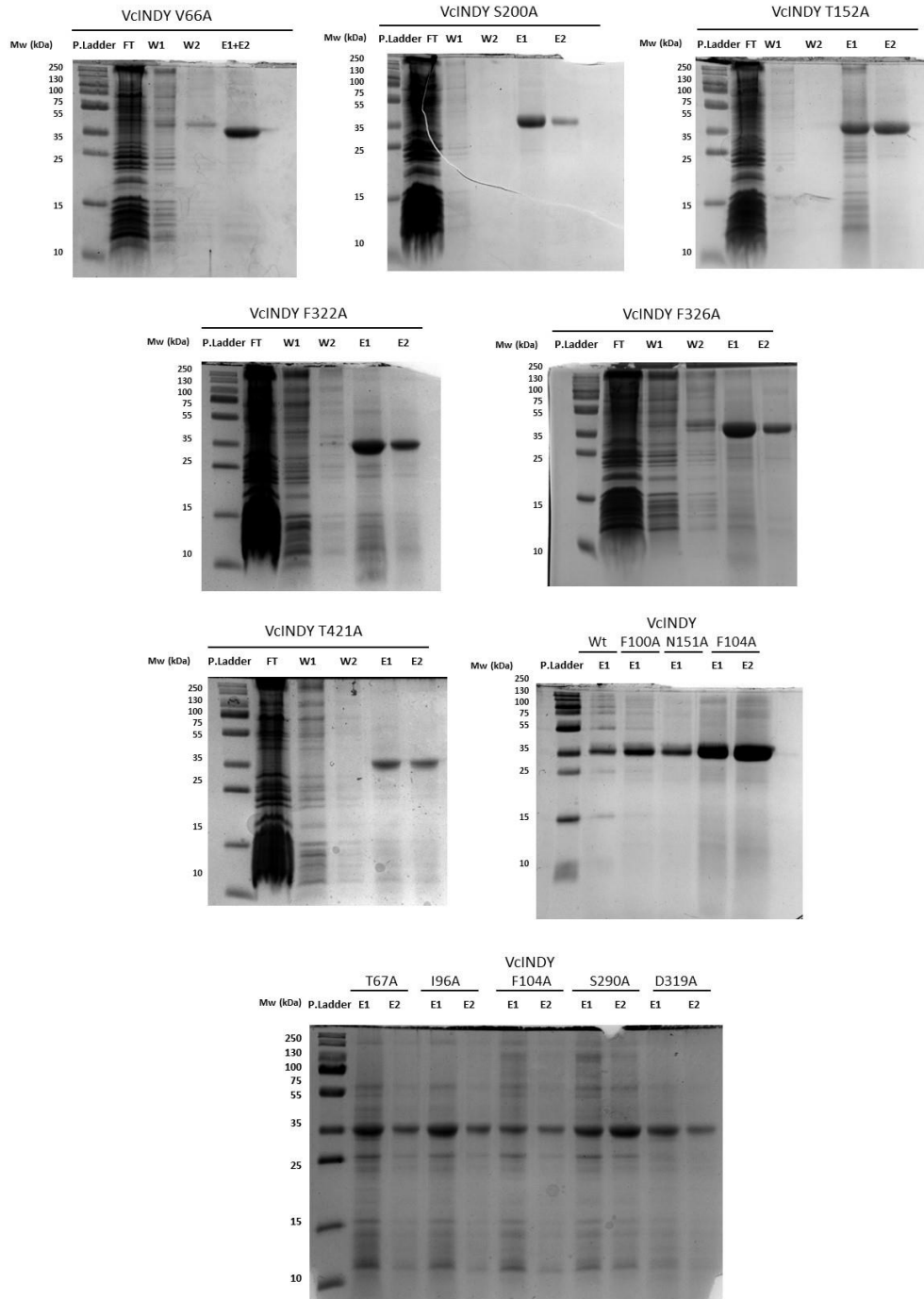
***Figure 6.2.1*: SDS-PAGE gels from all the alanine mutants of the study.**

Purification outcomes of VcINDY proteins on SDS-page gels used in this project. In order: first column is the protein ladder (P. Ladder), Flow-through (FT), Wash buffer one (W1), Wash buffer two (W2), Elution buffer one (E1) and Elution buffer two (E2). Columns of E1 and E2 with a band at 35kDa indicate presence of VcINDY protein. In **gels 1,2,3,4,5** and **6** proteins V66A, S200A, T152A, V322A, F326A and T421A are presented individually and respectively. The elution solutions of VcINDY wild-type, F100A, N151A and F104A are presented in **gel 7**. F104 was purified before acknowledging a default in its mutation sequence. Hence, it was dropped out the study. The left VcINDY alanine mutants were visualised in **gel 8** as the previously explained.

A.

B.

C.
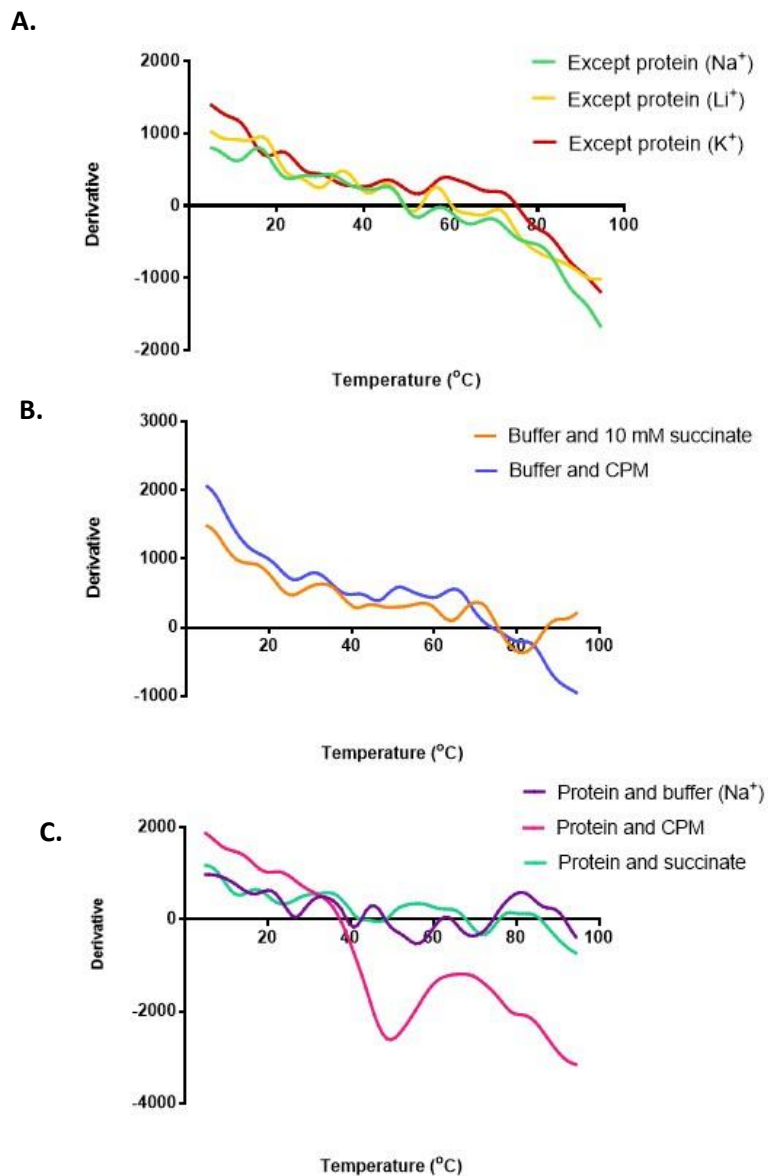
***Figure 6.2.2*: Calibration controls for the CPM assay.**

Graphs represent the derivative curve in different conditions to evaluate the CPM principle. **A)** Melting curves of the CPM was conducted with the presence of CPM,10 Mm of succinate, buffer without VcINDY protein. Three buffers with different cation were tested; lithium (green), sodium (yellow) and potassium (red) **B)** Melting curves of CPM assays in the conditions of buffer with succinate (orange) or CPM (blue) only **C)** Melting curves obtained in the presence of : protein and buffer (purple), protein and succinate (turquoise) and, protein and CPM (pink). Only the experiment where protein and CPM were present in the solution gave a melting curve. Absence of melting curves in any other case proved that CPM assays are a reliable technique. Only one measure was taken for condition.

- SUCCINATE
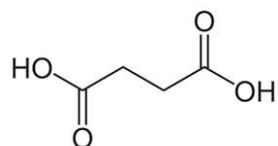
- FUMARATE
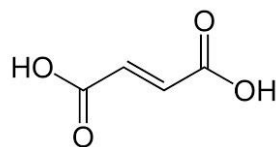
- ICATONIC ACID
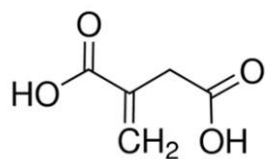
- OXALACETATE
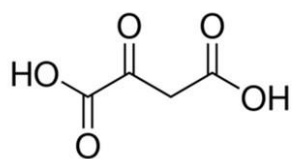
- 5'-SULFOSIALICYLIC ACID
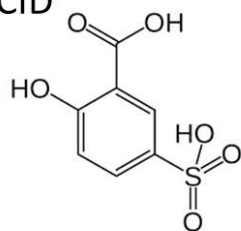
- MALATE
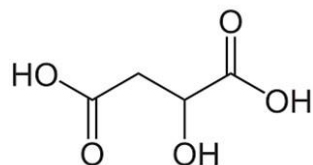
- OXALATE
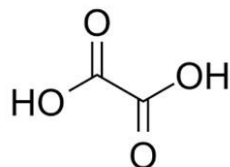
- ADIPATE
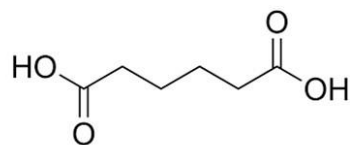
- TRICARBALLYIC ACID
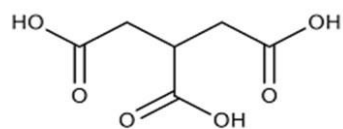
- CITRATE
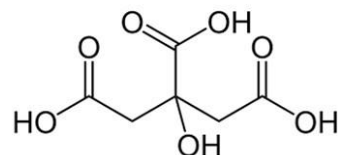
Figure 6.2.3: **Molecular structure from the study library compounds.**

Molecular structures were obtained from sigma company on sigmaaldrich.com

Here the untouched charts from the derivative of the fluorescence read in CPM assays for each VcINDY transporter tested would be displayed. It is important to remark here that graphs would always be shown in the same format; *dark green lines* are for readings with substrate present, which would be specifically indicated, and *light green lines* represent baselines. In some cases, repetitions were needed, so it could be more than one baseline graph for protein tested.
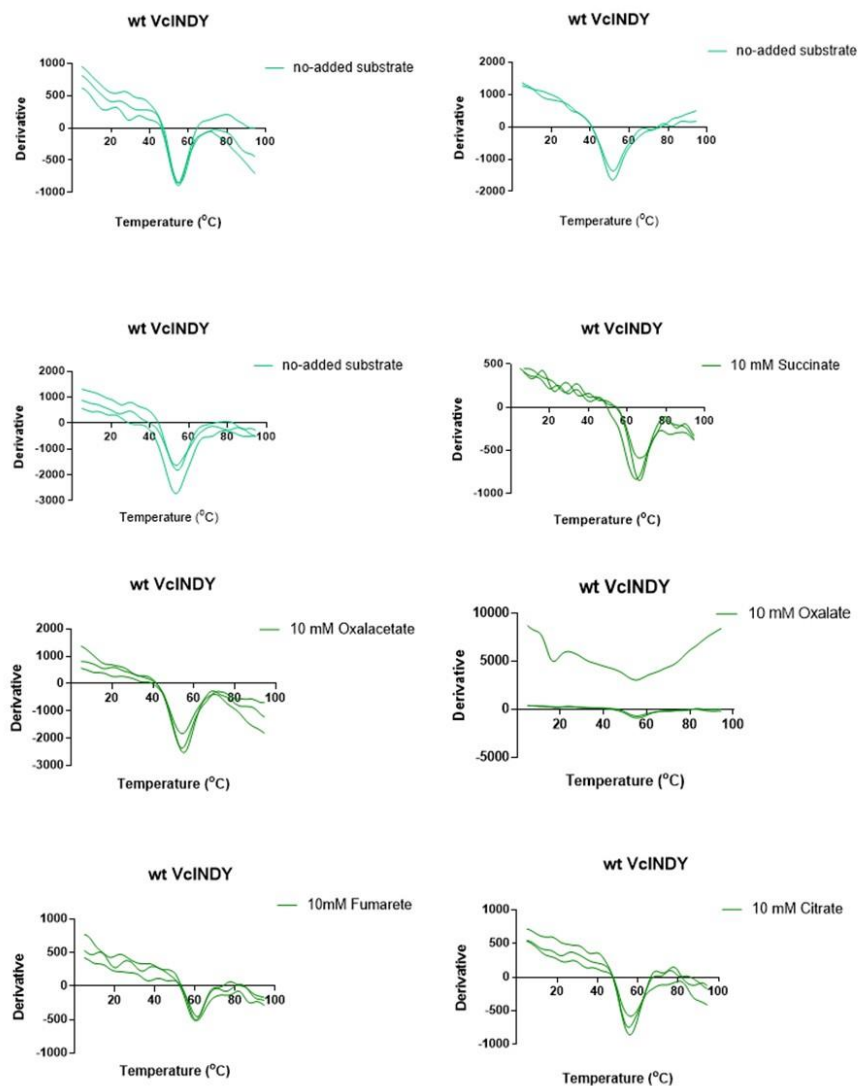
Figure 6.2.4: Continued
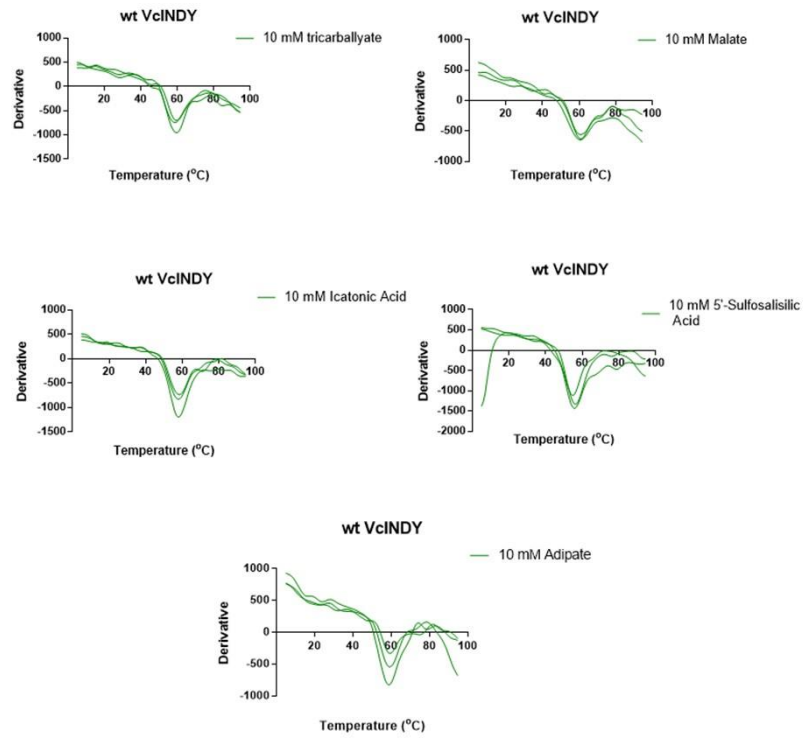
Figure 6.2.4: CPM assays of VcINDY wild-type
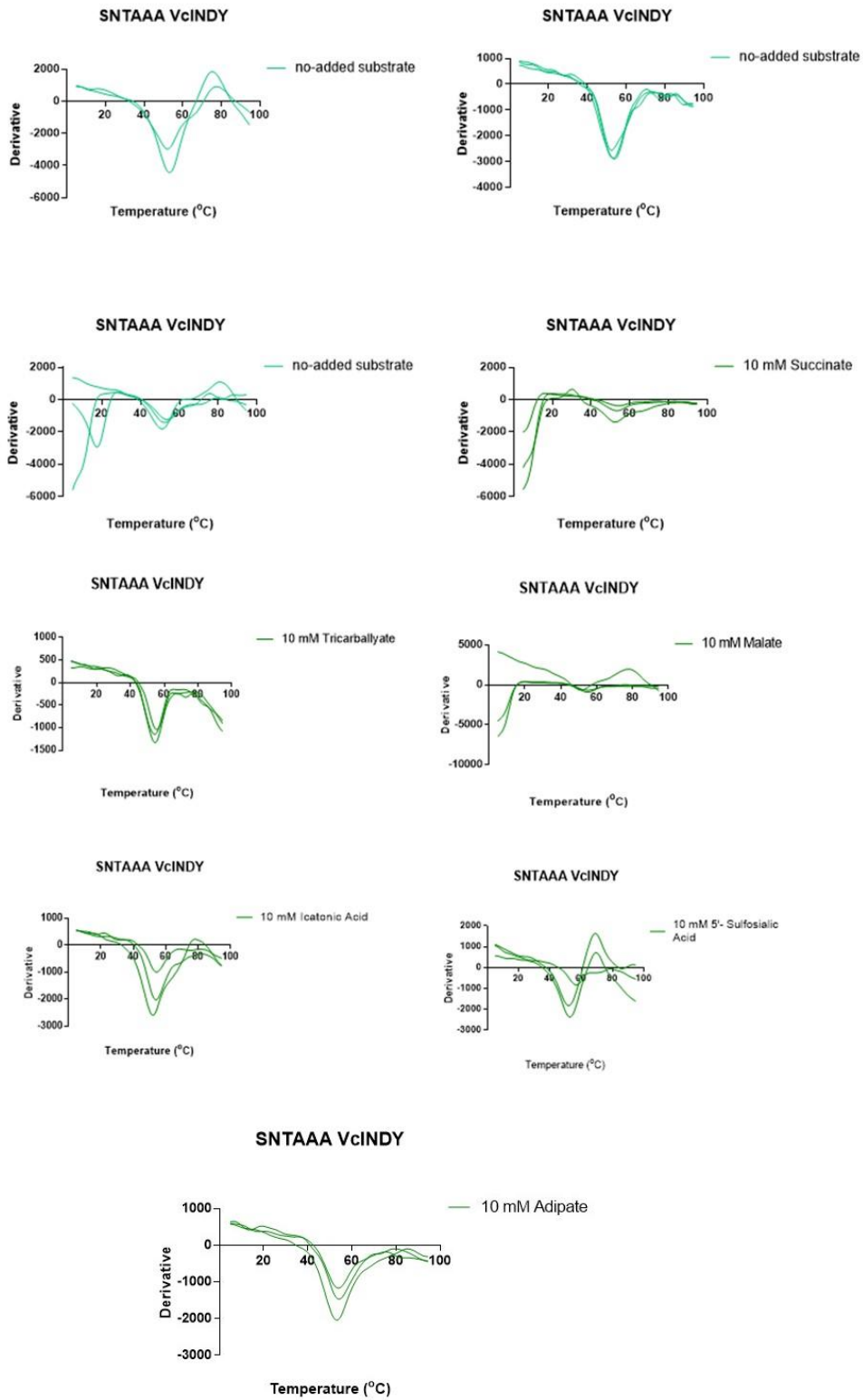
Figure 6.2.5: CPM assays of SNTAAA VcINDY
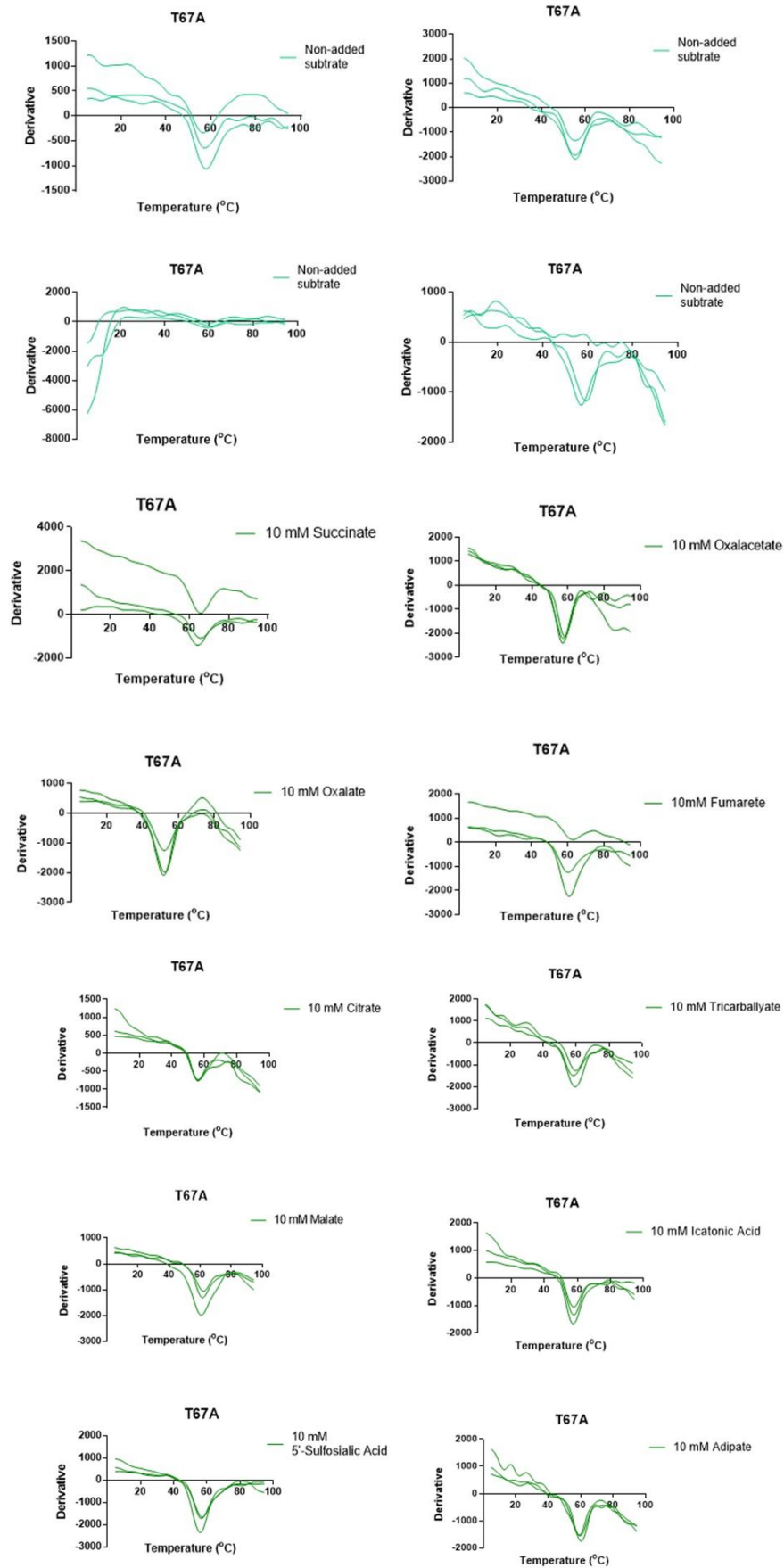
Figure 6.2.7: CPM assays of T67A VcINDY
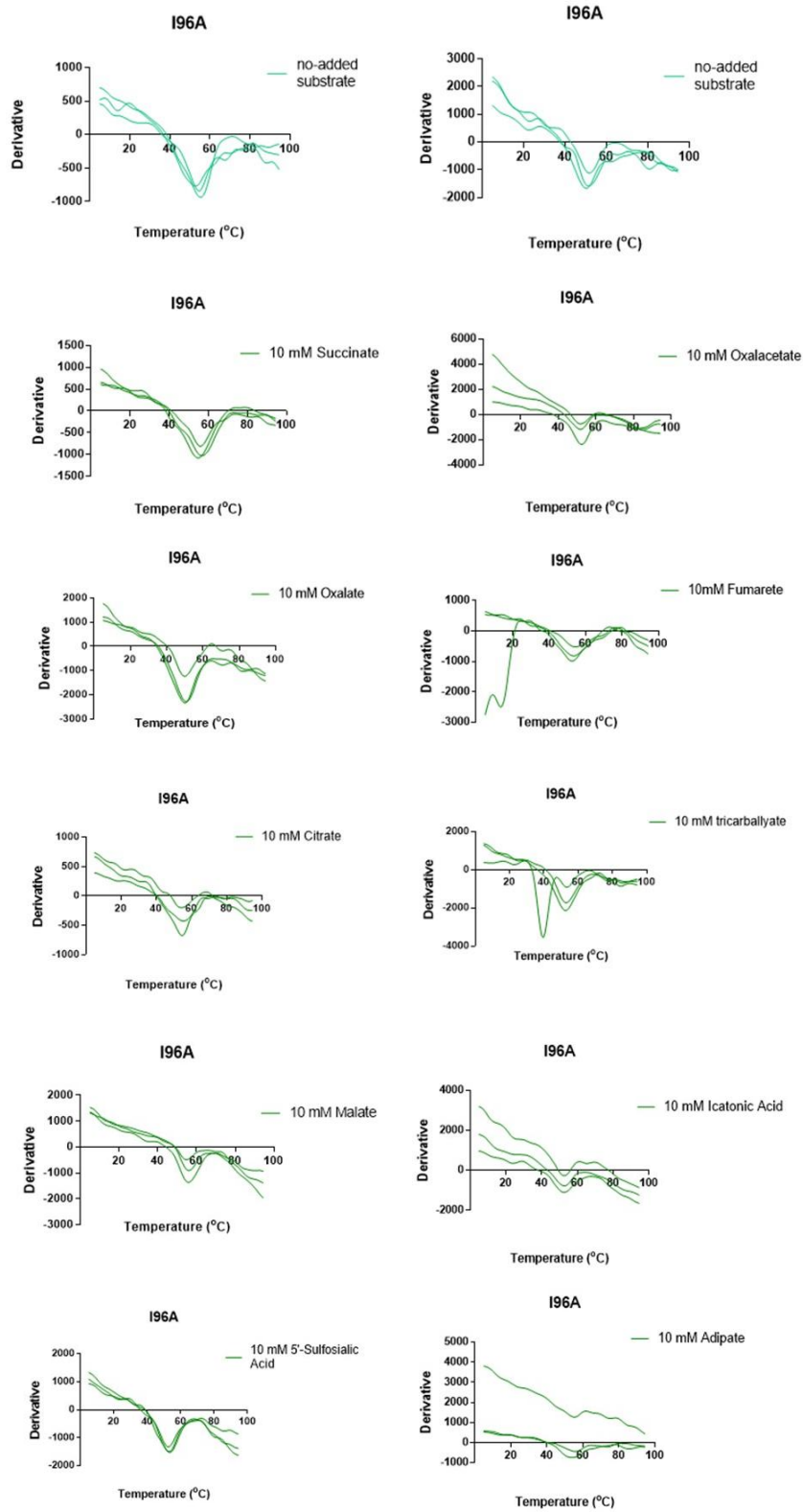
Figure 6.2.8: CPM assays of I96A VcINDY
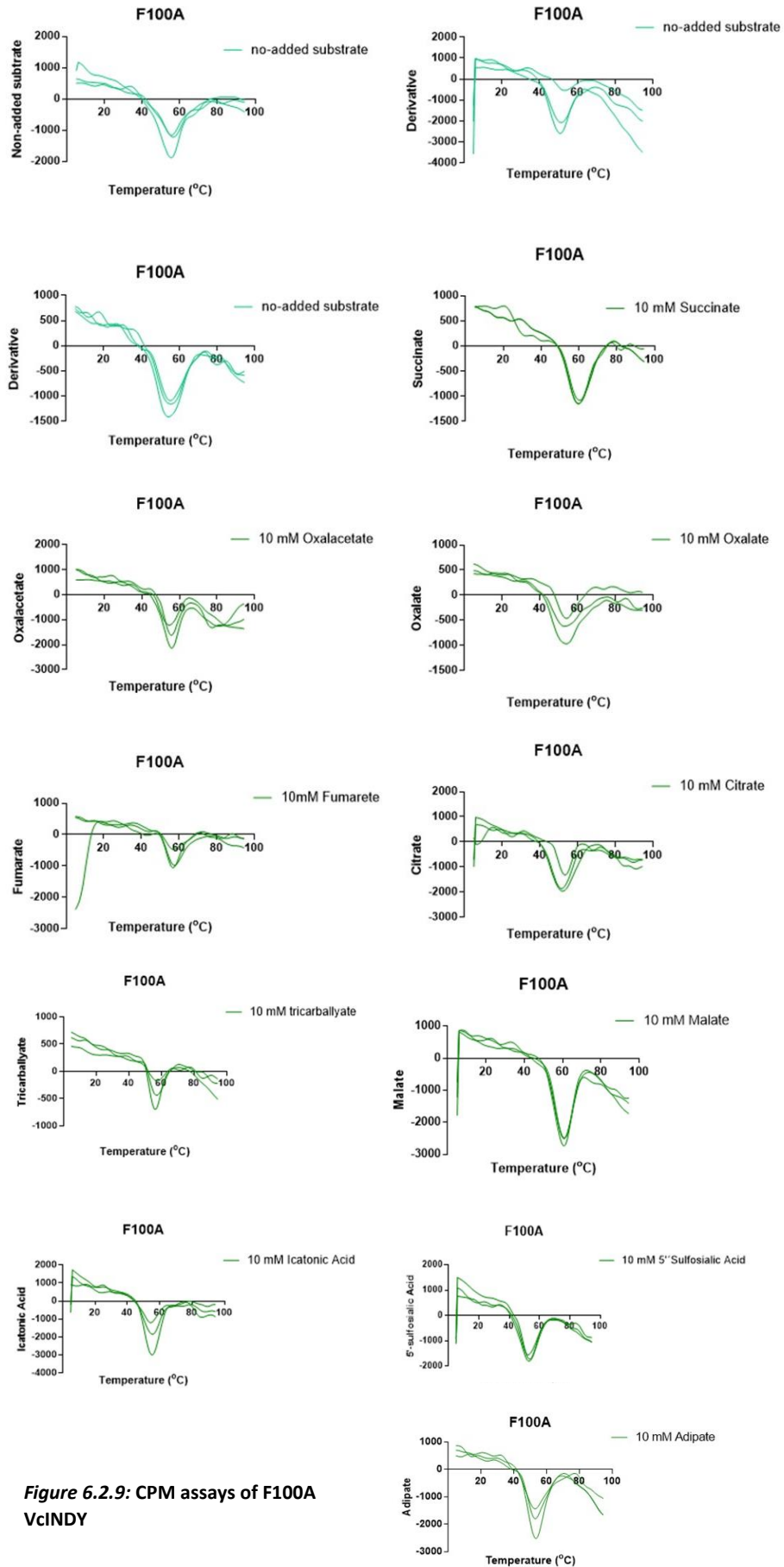
Figure 6.2.9: CPM assays of F100A VcINDY

XXIII
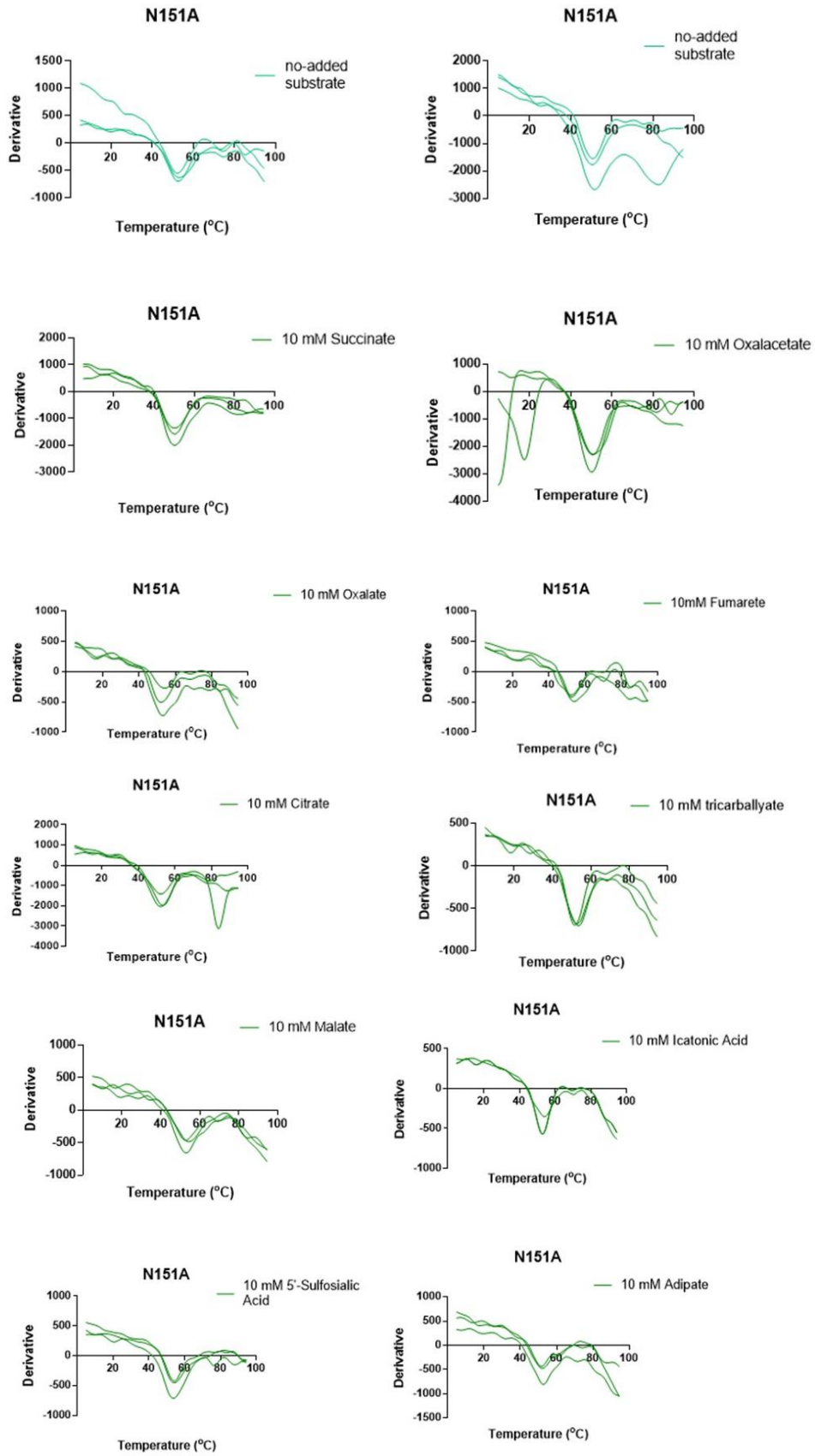
Figure 6.2.10: CPM assays of N151A VcINDY
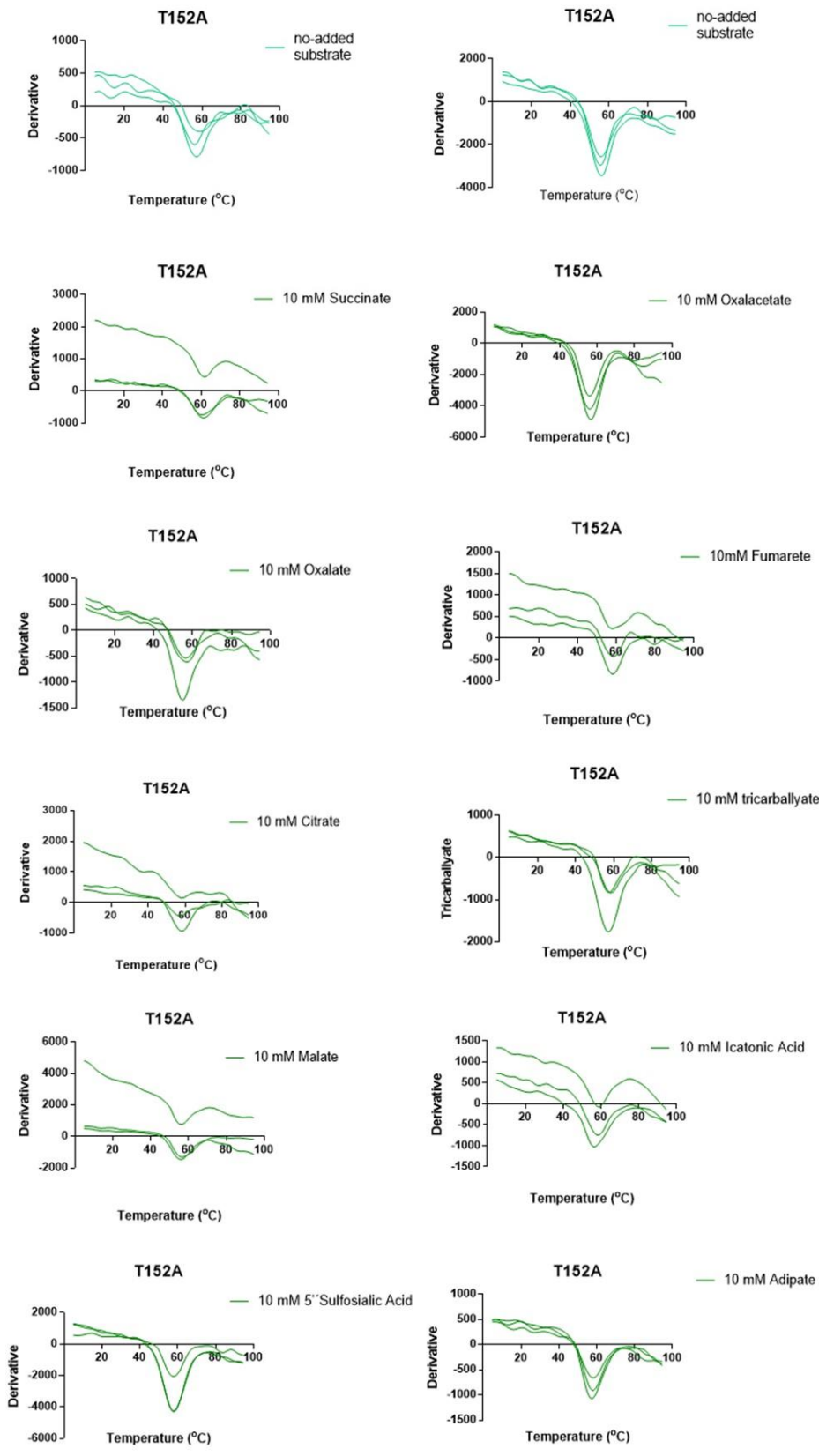
Figure 6.2.11: CPM assays of T152A VcINDY

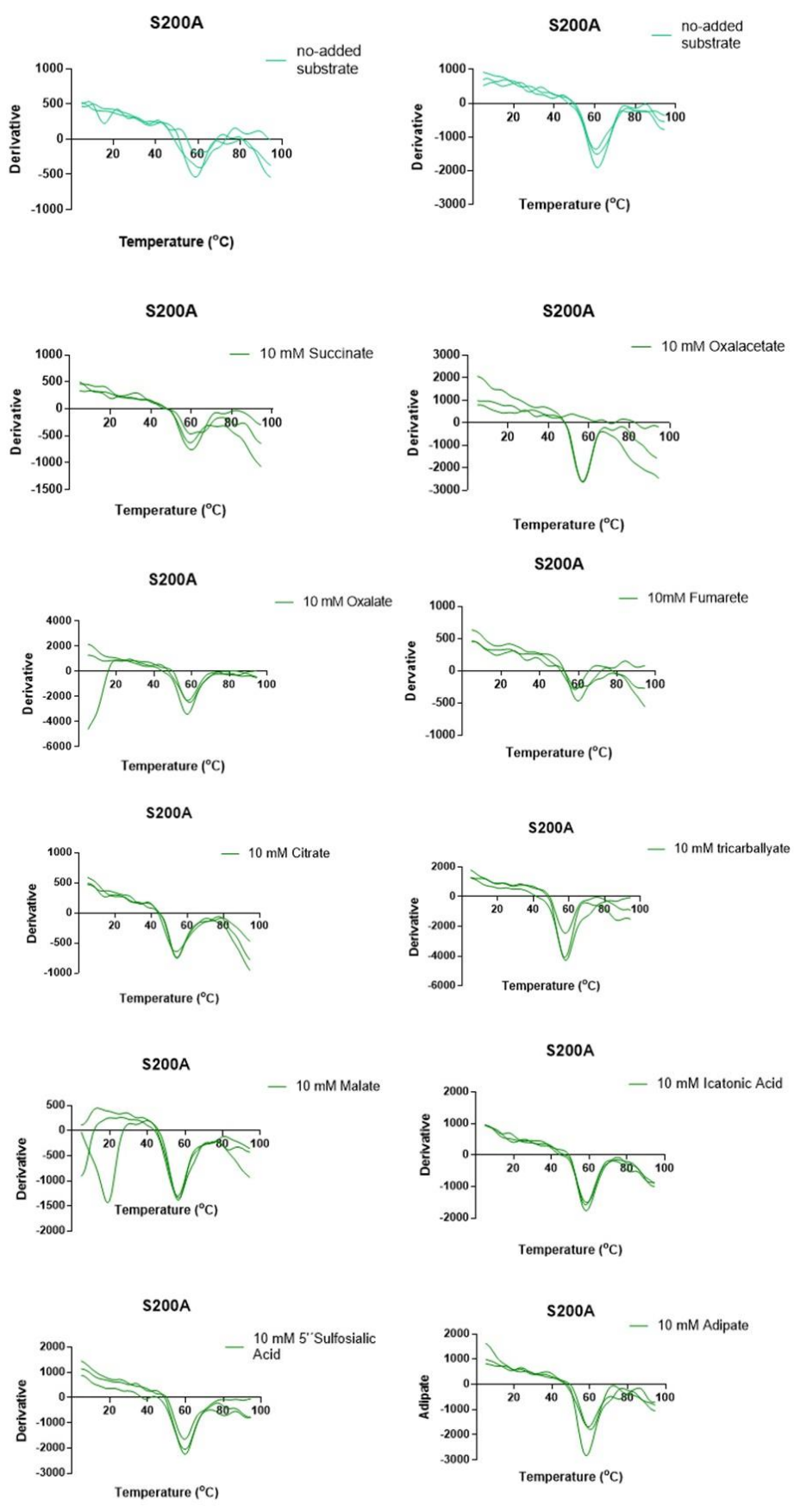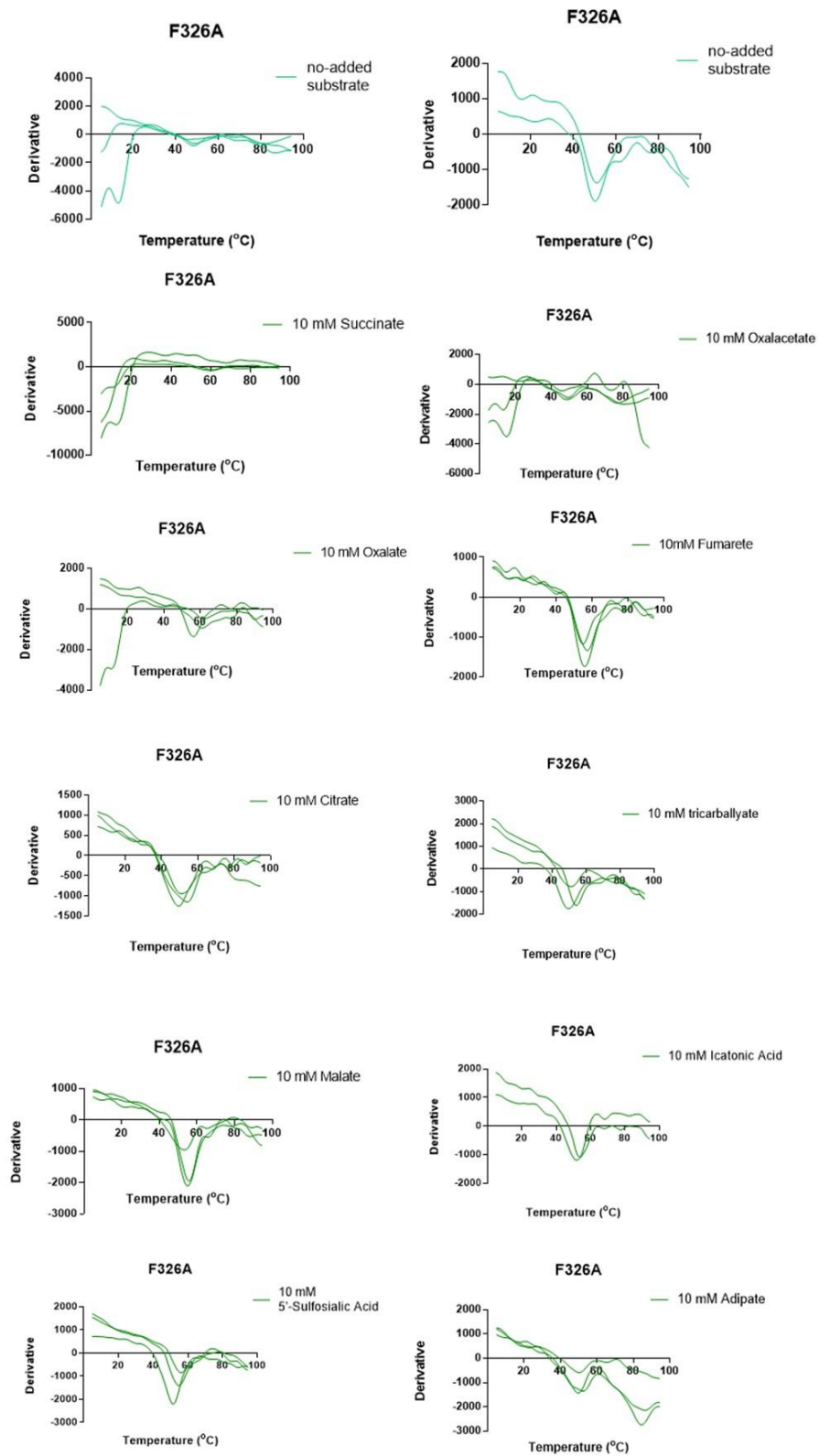**Figure 6.2.12:** CPM assays of S200A VcINDY

F326A graphs

Figure 6.2.13: CPM assays of F326A VcINDY
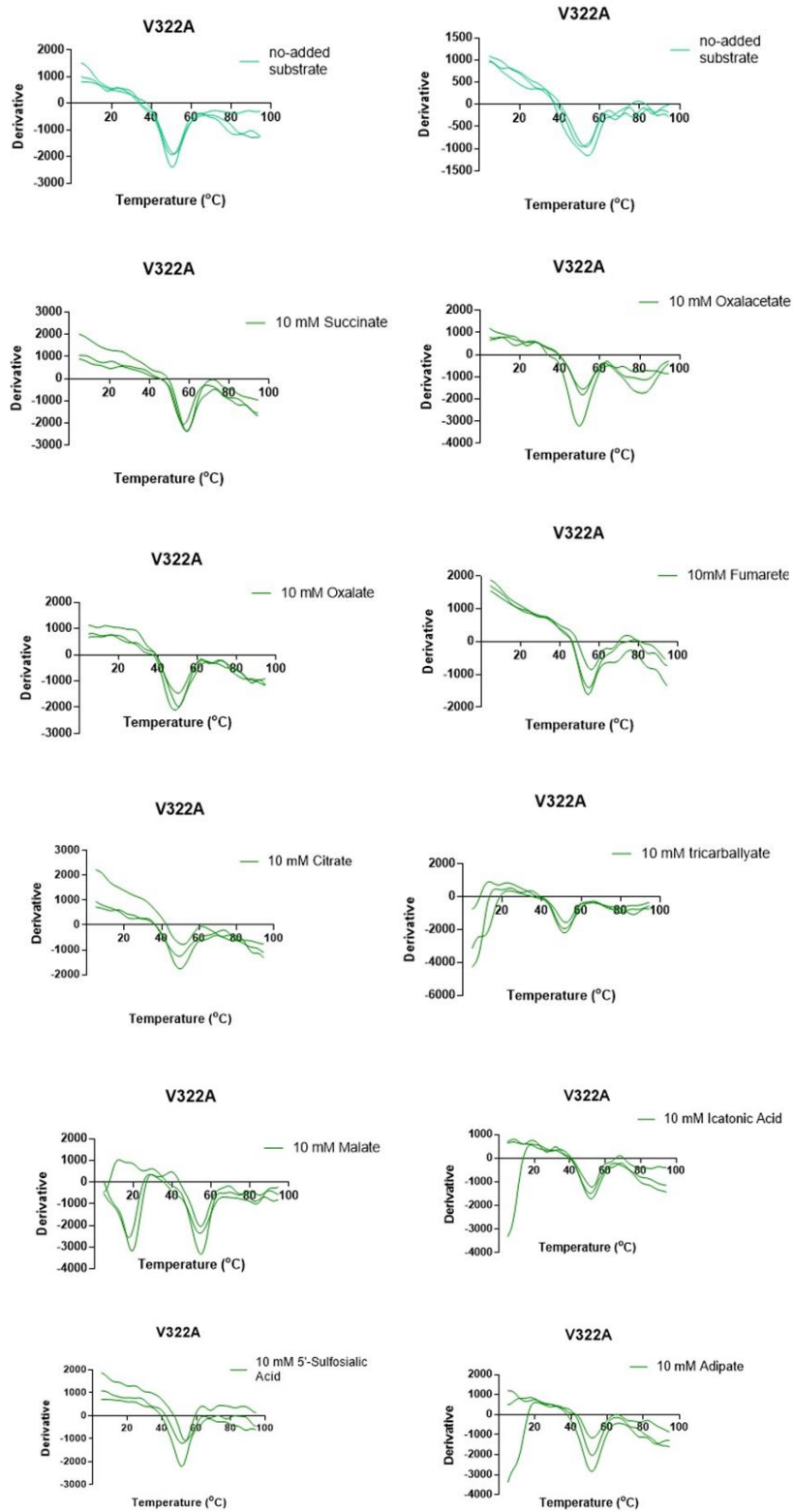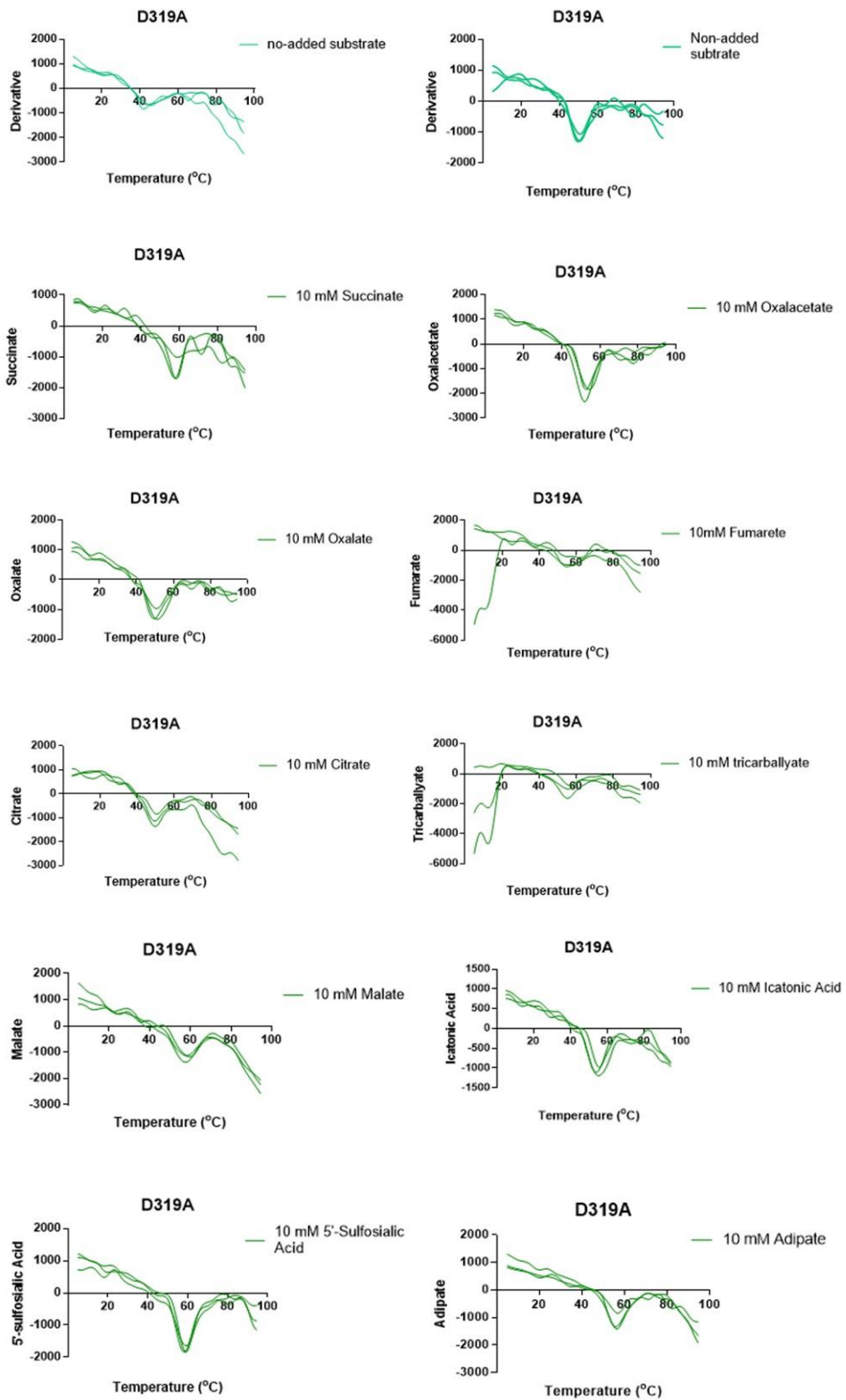
Figure 6.2.14: CPM assays of V322A VcINDY

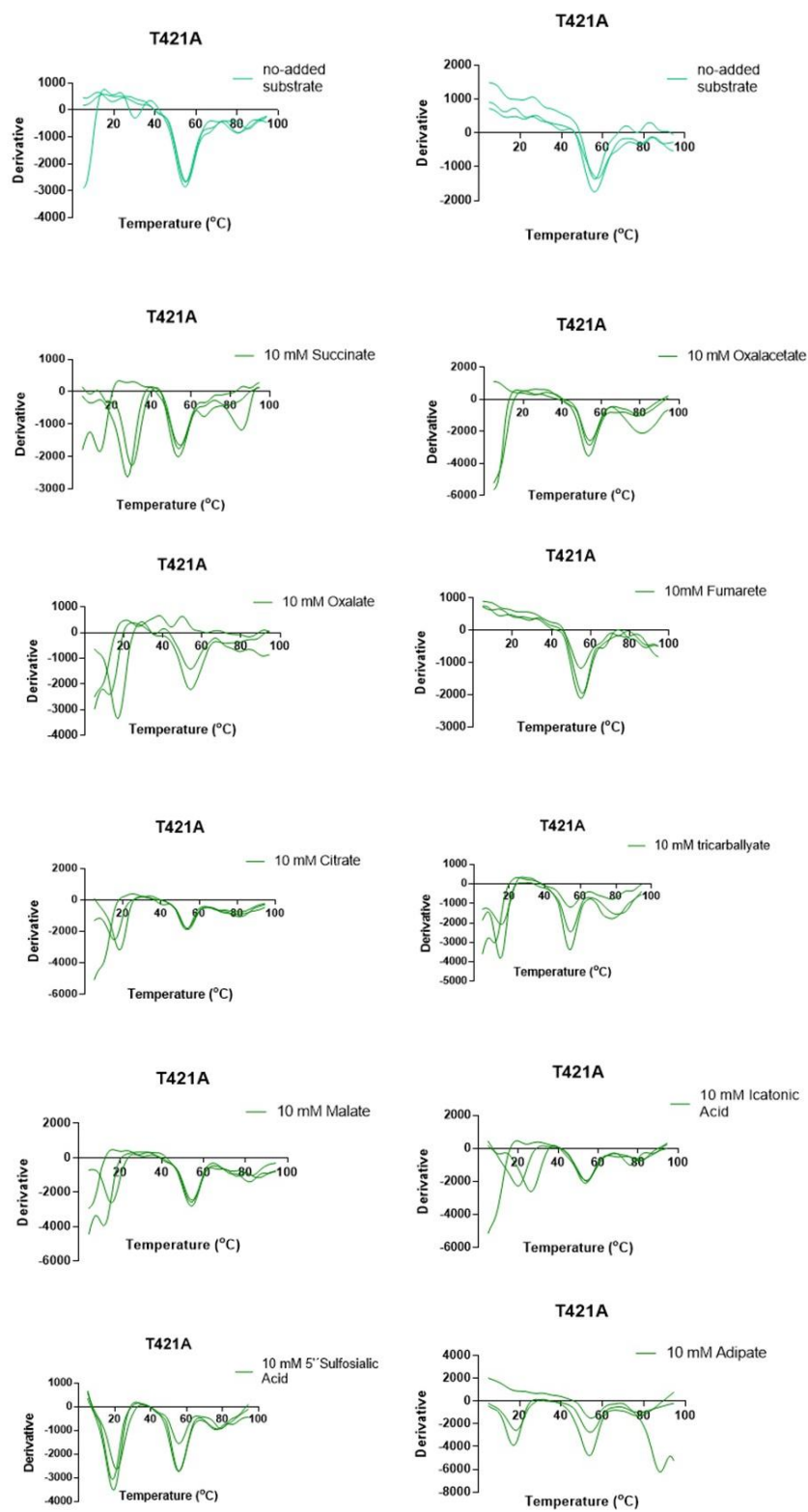*Figure 6.2.15:* CPM assays of D319A VcINDY

Figure 6.2.16: CPM assays of T421A VcINDY

The untouched charts from the derivative of the fluorescence read in CPM assays for each VcINDY transporter tested for lithium and potassium cation's effect would be displayed. Graphs would be always shown in the same format; *dark lines* are for readings with the substrate present, which would be specifically indicated in each graph, and *light lines* represent baselines (absence of substrate).
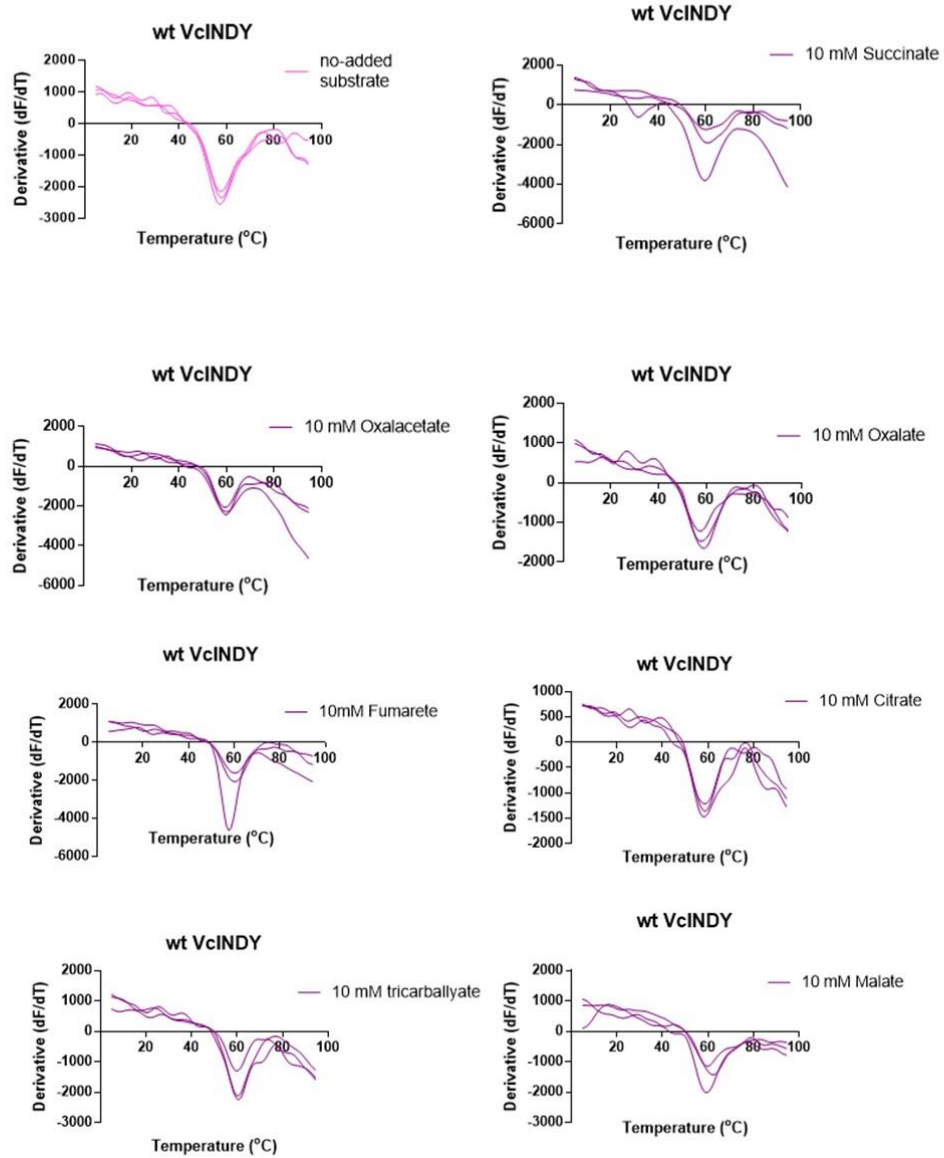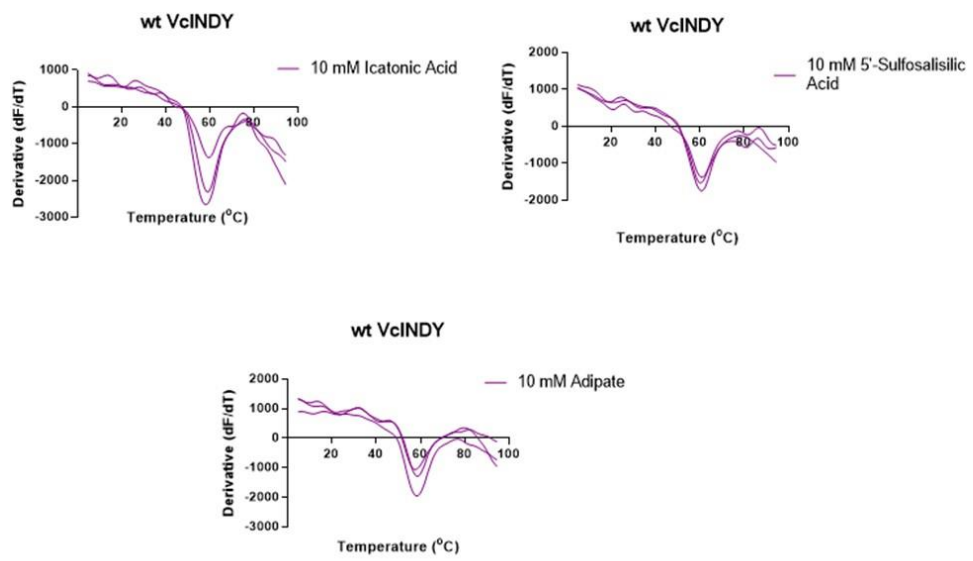

Figure 6.2.17: Continued

wt VcINDY — 10 mM Icatonic Acid

wt VcINDY — 10 mM 5'-Sulfosalisilic Acid

wt VcINDY — 10 mM Adipate

Figure 6.2.17: **CPM assays of wild-type VcINDY with Li$^+$**
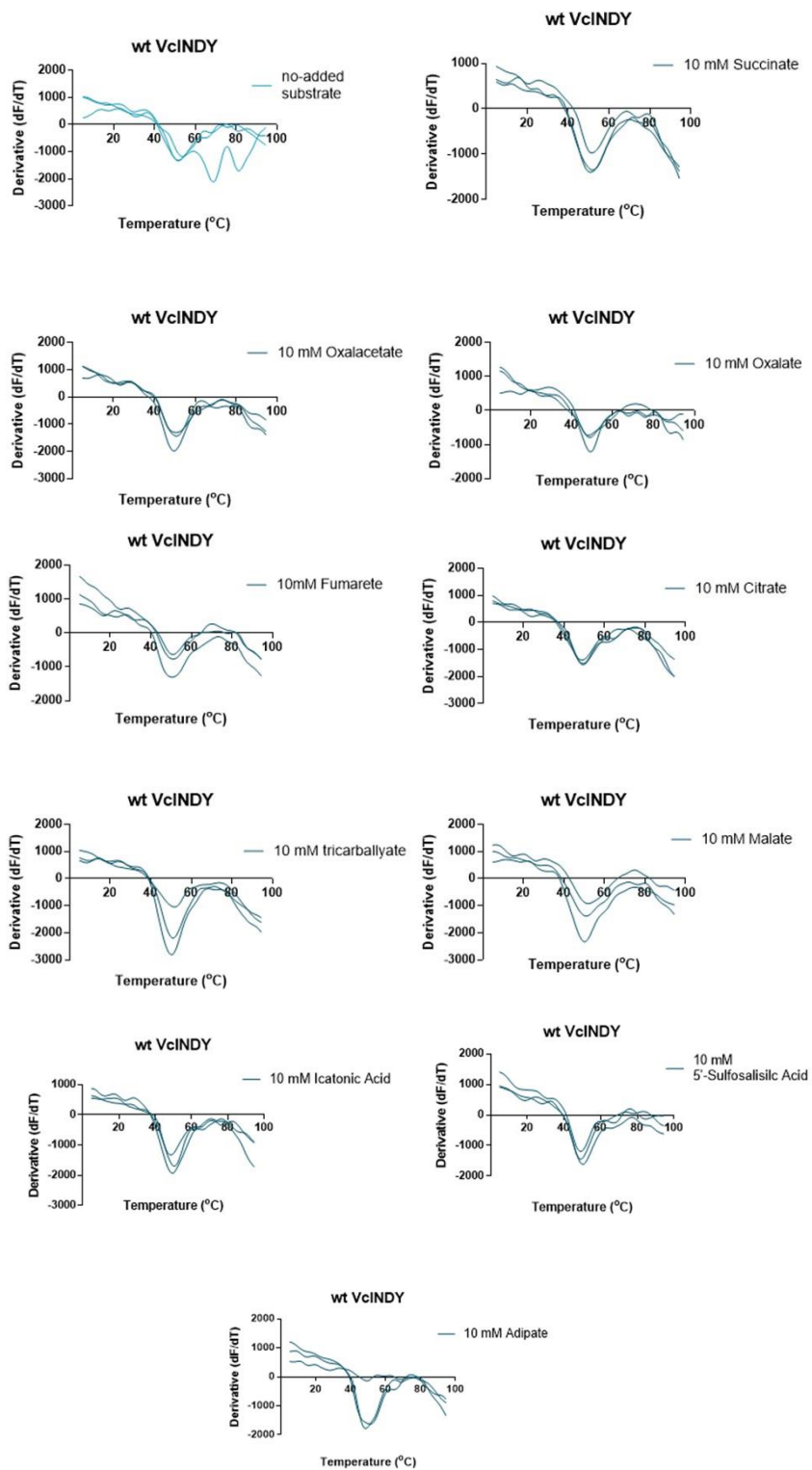
Figure 6.2.18: **CPM assays of wild-type VcINDY with K⁺**

Cation/ Substrate	Na⁺	Li⁺	K⁺
Alone	56,66 ± 0,81	57,66± 0	52,36 ± 0,93
Succinate	8± 0,00	2.7± 0,47	-1± 0,47
	P. Value: 0,000	P. Value: 0,001	P. Value: 0,251
Oxalacetate	1± 0,00	2 ± 0	-2± 0,47
	P. Value: 0,000	P. Value: 0,00	P. Value: 0,055
Oxalate	-1,3± 0,47	0.3± 0,47	-2,6± 0,81
	P. Value: 0,116	P. Value: 0,373	P. Value: 0,039
Fumarate	4± 0,81	2± 1.41	-1,6± 0
	P. Value: 0,008	P. Value: 0,116	P. Value: 0,067
Citrate	-0,6± 0,47	1± 0	-3 ± 0,47
	P. Value: 0,373	P. Value: 0,000	P. Value: 0,016
Tricarballylate	2,6± 0,47	2.7± 0,47	-1.3± 0,47
	P. Value: 0,016	P. Value: 0,001	P. Value: 0,148
Malate	4± 0,00	3± 1,40	-1.3± 0,47
	P. Value: 0,002	P. Value: 0,039	P. Value: 0,148
Icatonic Acid	1,3± 0,47	1.3± 0,47	-2.65± 0,81
	P. Value: 0,116	P. Value: 0,016	P. Value: 0,039
5'-Sulfosalicylic Acid	4± 0,81	3± 0	-2,98± 0,94
	P. Value: 0,013	P. Value: 0,000	P. Value: 0,033
Adipate	2,3± 0,47	0,6± 0,47	-2,98± 0,94
	P. Value: 0,025	P. Value: 0,116	P. Value: 0,003

Figure 6.2.19: **Melting temperature shift effect of VcINDY wild-type in the compounds of the study and presence of 50 mM Na⁺, Li⁺ or K⁺.**

Table representing the melting temperature shift (ΔTm) of VcINDY wild-type in the presence of 3 different cations. ΔTm is represented as a mean together with its standard deviation (blue squares). Below each condition and ΔTm, the p-value is noted. This statistical value was subtracted by comparing the triplicated results of VcINDY protein without substrate as a baseline and the protein with the corresponding ligand.
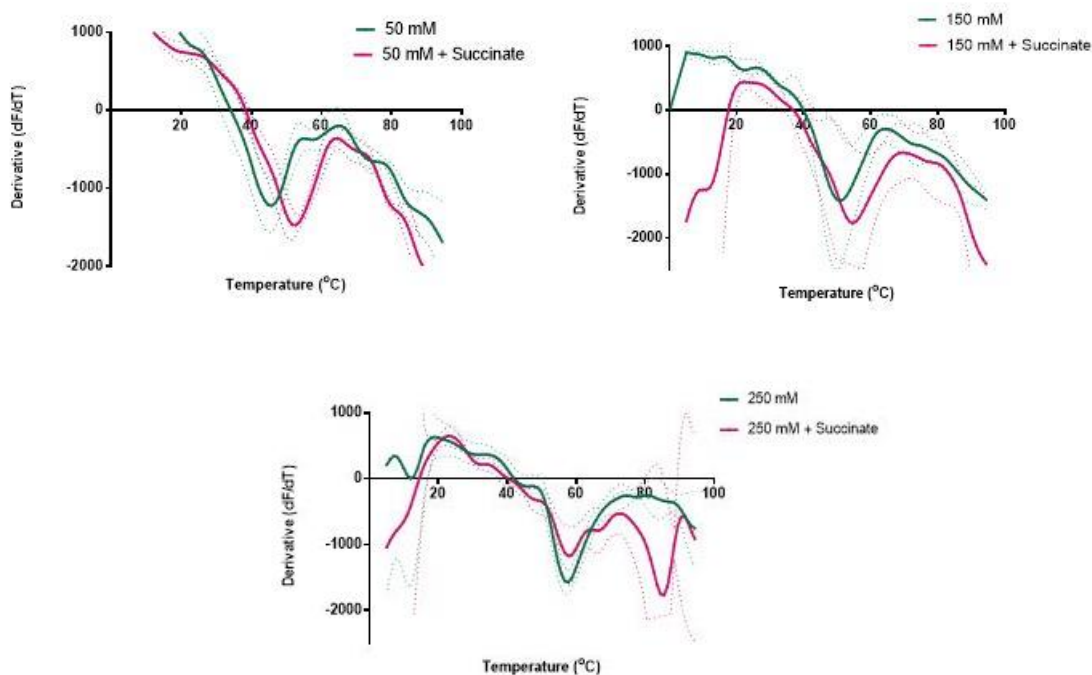
Figure 6.2.19: Sodium increased test for D319A.

Graphs represent the derivative curve in different conditions to evaluate the best sodium concentration for the unstable D319A mutant. Melting curves of this CPM test were conducted with the presence of the mutant, CPM dimer, absence or presence of substrate and different sodium concentration **A)** 50 mM Na$^+$ **B)** 150 mM Na$^+$ **C)** 250 mM Na$^+$. Hence, two main melting curves were obtained by each cation: protein thermostability baseline (purple), protein thermostability in the presence of 10 mM of succinate (green). Measures were taken as triplicates for sodium concentration and condition. Mean is represented as the ticker line.